Investigation of microstructural evolution by real-time SEM of high-temperature specimens.

FIELDEN, Iain M.

Fines are charged at £2 per day
No renewal

REFERENCE

INVESTIGATION OF MICROSTRUCTURAL EVOLUTION BY REAL-TIME SEM OF HIGH-TEMPERATURE SPECIMENS

IAIN MICHAEL FIELDEN

AUGUST 2005

A thesis submitted in partial fulfilment of
the requirements of Sheffield Hallam University
for the degree of Doctor of Philosophy

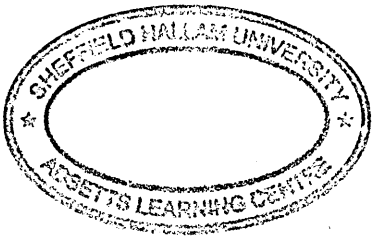

ABSTRACT & PREFACE

This thesis presents the results of a project to investigate the growth of grains and movement of grain boundaries in face centred cubic metals, using Environmental Scanning Electron Microscopy (ESEM).

The original aim proved impractical without considerable modification to the microscope technique. The result of this was an imaging technique suitable for "real-time" characterisation of dynamic microstructures, evolving as materials are heated, cooled or held at high temperatures in the SEM. The technique is adaptable to both conventional "high-vacuum" SEM and environmental SEM. The development of the technique is described, and its application to hot metal specimens.

The technique has been applied to various metals, but most notably to steel. The project has yielded probably the first "real-time" images of grain growth with time in steel, the first images of Austenite decomposition and phase change occurring in steel, the first images of grain growth in a bulk gold alloy and images of grain growth in an aluminium alloy.

It is shown that the motion of grain boundaries in polycrystalline metal bulks is discontinuous ("jerky") and that this jerky motion occurs independent of grain boundary grooving.

It is also shown that the first manifestation of austenite decomposition is an as-yet unexplained micron-scale "cellular" sub-structure within the austenite grain.

It is further shown that in cooling of steel at slow-to-moderate speeds, the first appearance of permanent non-austenite structure is the precipitation of relatively large carbides at surfaces. Unexpectedly, this observation is in a slightly hypo-eutectoid steel, in which a slight excess of ferrite would be expected, leading to the logical but erroneous expectation that pro-eutectoid ferrite should be the first phase to precipitate.

In slow-to-moderate cooling of near-eutectoid steel, it is shown that the number of nuclei initiating the austenite-to-pearlite transformation is small by comparison to the number of austenite grains present and that the austenite-to-pearlite transformation front sweeps from grain to grain with relative ease.

Some of the work on which this thesis is based has been published. Firstly at The Institute of Physics Electron Microscopy and Analysis Group bi-annual conference (EMAG) [Fielden et al. 2003] and subsequently at the Second Joint International Conference on Recrystallisation and Grain Growth (ReX-GG2) [Fielden & Rodenburg 2004] [Fielden 2004]. The "results" paper [Fielden 2004] was awarded the ReX-GG committee's "outstanding young scientist award". These papers are included as appendices to this thesis.

The technique and its results were published in brief as a short-listed entry in the 2004 UK National Measurement Awards (category 5, materials). The author was selected as the winner and presented with the 2004 NPL Materials Award, "acknowledging the development of new techniques for materials measurement and characterisation".

CONTENTS

APPENDICES

CHAPTER 1
INTRODUCTION

Mankind's initial discovery that heat fundamentally changes the properties of metals, often for the better, is lost in the mists of human pre-history. However, it seems safe to say that the initial discovery must have occurred around the beginning of the Copper Age, some 5,000 years ago, and was replicated in other metals as mankind progressed into the Bronze Age and Iron Age. In the era of written history, smiths were well aware that heat and temperature change had two distinct effects on metals. Heating the metal to some critical temperature and holding there, would render the metal soft and workable, it would also undo the hardening effects of previous working (annealing) while a rapid cooling (quenching) could sometimes harden iron, usually in the form of swords, to a "magical" degree.

The study of these phenomena and their many variants, the processes that underlie them, and the microstructures that they produce, still constitute a large proportion of the science of metallurgy.

Today, mankind's structural metals are produced by "thermo-mechanical processes", which, while they would be wondrous to the ancients in their scale and precision, would be quite familiar in concept. Literal "heating and beating" using charcoal furnaces, pumped by an apprentice, followed by the muscle-powered hammer and the smith's anvil, have gone. In their place are huge gas, oil or electric furnaces, feeding tons of metal to high-speed computer-controlled rolling mills. However, the underlying techniques and aims remain the same:- To heat the metal enough to soften it, but not over heat it, then deform it by compression from a thick lump of metal of limited usefulness and relatively poor properties into a much more useful long & thin shape, with improved properties. All but a tiny proportion of the metal produced each year is passed through at least one thermo-mechanical process, usually rolling, on the journey from freshly solidified to finished artefact. These processes, and often the manner and speed with which the metal is finally cooled, have a profound influence on the microstructure of the metal, both in terms of grain size & grain shape and the size, morphology & distribution of any second phases. These microstructures in turn influence and limit the fundamental properties of strength, ductility, toughness, creep resistance, fatigue resistance and in some cases even corrosion resistance and magnetic properties. Indeed relatively few important engineering properties of a metal are not dependant upon, or at least influenced by, the microstructure.

Accordingly, the study and ultimate understanding of these processes is of considerably more than academic interest. Improved understanding would logically be expected to lead to greater control of the processes and hence control of material microstructure and properties. Considerable advances have already been made in control of grain size, using the experience and knowledge already available. These advances have brought considerable advantages to those who have exploited them in metal manufacturing, those who have used the improved materials in their products, the end-users of the products and society generally. These efforts have, however, been hampered by the complexity of the phenomena at the heart of microstructural evolution and by the lack of experimental results in certain areas of the field, particularly the kinetics of microstructural evolution processes.

This lack of real experimental data is largely attributable to the great difficulties that are inevitably associated with studying phenomena that occur only under extreme conditions, i.e. high temperatures and, usually, large forces and rapid motion as well. To date most experimental results have come from materials one step removed from the actual phenomena of interest, i.e. "post-mortem" studies. In these studies, specimens are thoroughly characterised at room temperature for the properties and/or microstructural characteristics of interest, then heated (and/or deformed), then cooled back to room temperature and characterised again. This is repeated with specimens extracted from the process for cooling at various stages, and the remaining evidence of high temperature structures in the cooled samples is used to infer the high temperature behaviour and kinetics.

The current project was originally conceived as a means of using the much-vaunted high-temperature capabilities of the Environmental Scanning Electron Microscope (ESEM) to partially address the historical dearth of experimental results on grain growth and grain boundary movement, and particularly the kinetics of boundary movement. However, with the passage of time, the project evolved to encompass the development of electron microscopy techniques suited to generating the necessary results. Significant observations of phase transformations have also been made, which go beyond the original remit, which focussed on grain growth processes.

The original aim of the project was to investigate "Grain Growth And Grain Boundary Movement In The Gamma Phase Field". In other words to experimentally investigate grain growth and grain boundary movement kinetics in face-centred cubic metals, preferably steel in its high-temperature form (Austenite). The expectation was that the then new ESEM technology would be capable of this task and would be used for this project.

The initial aim proved to be impractical due to the limitations of the ESEM, and thus the eventual aim of the project became:

1. To devise a practical means by which (environmental) scanning electron microscopy can image material at high temperature and simultaneously discriminate between grains in a single-phase material.
2. To use this new technique to image evolving microstructures in some face-centred cubic metals (preferably including steel) at high temperature and to record their behaviour over time at high temperature and/or through some industrially-relevant heating and/or cooling regimes.

Clearly, the aim of (2) would be best served if the technique developed in (1) were capable of "real-time" imaging, to produce a moving image or video recording. However, given the dearth of "at-temperature" experimental results, a time-series of "snapshots" would also be a very worthwhile result.

CHAPTER 2
LITERATURE REVIEW

2.1 HISTORICAL

The scientific study of metal microstructures and the changes produced by different heating and cooling treatments dates from the seminal metallographic work of H. C. Sorby in the 1860s.

FIG 1. Henry Clifton Sorby, gentleman scientist. Sorby came from a respected Sheffield family, several of whom had been elected Master Cutler. He devoted his life to science in various forms, pioneering the use of microscopy first in geology, then in metallurgy and finally brought his energy to bear on research in natural history/biology and the promotion of scientific/technical education.

Pictured aboard his yacht-cum-research vessel.

Mankind became aware of grain boundaries as an immediate and inevitable consequence of Sorby's invention of metallography. However, while grain boundaries were the first lattice defect to be observed, they are far more complex than point defects, dislocations or stacking faults, and will be the last lattice defect to be fully understood. The scientific study of grain boundaries and their motion was started by C. S. Smith about the time of the Second World War; he divided the field into two subfields, recrystallisation and grain boundary motion (grain growth) and pointed out the importance of grain shape.

FIG 2. Cyril Stanley Smith, Director of the Institute for the Study of Metals at University of Chicago.

This was a de-militarised spin-off/continuation of the "University of Chicago Met Lab." project, which built the first nuclear reactor and produced the fissile metals for "The Manhattan Project". Smith is shown holding a glass capsule full of soap bubbles – an early analogue/model of metal grain growth.

Rightly, the full details of Smith's work in "The Manhattan Project" have not been published. However, the literature does not show any evidence of Smith having had a significant interest in recrystallisation and grain growth before the Second World War. At this time, he was working for the American Brass Company, on the electrical properties of brass and copper. His role in the Manhattan Project was to oversee and direct

the production and preparation of the fissile metals required. On his return to a civilian career, he appears to have had an intense interest in grain boundaries and some knowledge of the subject. These facts strongly suggest that the effectiveness of the most fearsome weapons of our time depend just as much on the control of their metal's microstructure as did the effectiveness of the swords used by our ancestors.

The field of grain growth study was given added impetus by the work of E.O. Hall (1951) and N.J Petch (1953). Hall and Petch independently demonstrated the first quantitative relationships between grain size and strength, Hall in ductile yield of steel and Petch in brittle cleavage fracture of steel. The relations were then combined as follows:

$$\sigma_{lyp} = \sigma' + \frac{k_H}{\sqrt{d}} \quad \text{(Hall)} \qquad \sigma_c = \sigma_0 + \frac{k_p}{\sqrt{l}} \quad \text{(Petch)} \qquad \sigma_y = \sigma_0 + \frac{K}{\sqrt{d}} \quad \text{(Hall-Petch)}$$

where σ_{lyp} is lower yield point strength, σ_c is brittle cleavage fracture strength, σ_y is yield strength, σ' is the yield strength of a single crystal, σ_0, k_H, k_p and K are constants, d is mean grain diameter and l is mean linear intercept (proportional to d). σ_0 is the "friction stress" or "dislocation friction" – increasing this term by alloying, second phases, precipitates, lattice distortion or creation of dislocation pile-ups is the other means of increasing material strength.

The Hall-Petch relationship was initially shown to be valid only for quite a narrow range of grain sizes, and only in steel, but was later shown to be valid in many other metals and shown to be valid over the full range of grain sizes in steel by W.B. Morrison (1966). This firmly established grain refinement not only as an important factor in commercial metals production, but also as a key research target for bringing improvement in materials technology.

2.2 MOTION OF GRAIN BOUNDARIES

2.2.1 FACTORS CONTROLLING GRAIN BOUNDARY MOVEMENT

It is now well known that grains grow in order to reach a low-energy equilibrium state, just as any other system in nature will develop towards the lowest feasible energy state. The balance between the surface energy and other energies associated with grain boundaries (e.g. mis-orientation energy, entropy) and the energy of the crystalline grain interior is such that the lowest energy state of a 3D grain network will be attained by the minimum number of grains. This implies maximum grain size, or minimum grain boundary area per unit volume, and that the shape of those grains should tend towards spherical. Clearly spherical grains imply small grains in the interstices, a situation that is not energetically favourable or implies gaps at the interstices, a situation that does

not fulfil the topological space-filling requirements of the grain network. Grains will grow and consume neighbouring grains in order to reach the stable low energy ideal, which is in practice attained with large grains each being (in 2 Dimensional section) hexagonal, i.e. with six nearest neighbours and in 3-D taking a form close to the "Kelvin tetrakaidecahedron", a curved face polygon whose closest plane-faced relative is the truncated octahedron, and having 14 nearest neighbours (Fig 3).

FIG 3. The Truncated Octahedron and its thre-dimensional tessellation.

Image from http://en.wikipedia.org/wiki/Truncated_octahedron Last accessed 11/06/05

The surface energy effect, normally referred to as surface tension, is the main driving force behind grain boundary motion. Indeed, in most laboratory cases it is the only driving force. In industrial metals processing, the metal is likely to be under stress or to have been deformed very recently. Thus, in industrial situations, externally applied and/or as-yet-unrelaxed internal stresses, along with distortions to non-equilibrium grain shapes/boundary curvatures and junction angles, would be expected to be significant additional drivers of boundary movement.

Opposing the net driving force are a large number of factors, many of which may interact. Mattisen et al. (2001) showed that at lower temperatures the mobility of triple junctions was lower than that of plane grain boundaries, and thus that grain boundary motion is retarded by the triple junctions present in the network. This work also showed boundaries and a triple point migrating at a steady rate in a high-purity aluminium tri-crystal. Estrin (2001) has shown that vacancies are generated in the freshly formed crystal left behind a moving grain boundary. These inevitably increase the energy of the freshly-formed crystal relative to the grain boundary energy, and thus would be expected to oppose the driving force by reducing the energetic "pay-back" of eliminating grain boundary area.

There is much work showing that the presence of solutes and/or segregates affects boundary motion, even at exceptionally low overall concentrations. Usually the effect is to retard motion, but occasionally motion is accelerated by the presence of impuri-

ties. However, the effect appears to depend upon many factors, such as velocity of boundary motion, temperature and the nature of the boundary and/or solute (Molodov et al, 1998). No clear pattern has yet emerged from this work. The effect of coherent and incoherent second phases or precipitates on boundary movement, Zener pinning or Zener drag (Zener 1948), is probably the most thoroughly investigated of the mechanisms of grain boundary retardation, and the most widely used means of grain refinement in industry.

2.2.2 THE NATURE OF GRAIN BOUNDARIES

To fully understand how some of these driving forces and retardation mechanisms might affect boundary motion would require a fairly detailed knowledge of the structure of grain boundaries. However, as Humphreys and Hatherley point out in their book (1995) *"...there is still a great deal of uncertainty about the structure and properties of boundaries. Most of the theoretical and experimental work has been carried out for static boundaries and there is even more uncertainty over the structure, properties and energy of migrating boundaries, which are unlikely to be similar [to static boundaries]."* Thus, it would appear unproductive to discuss the nature of boundaries in great detail here. It is proposed merely to outline the three main classes of boundary, namely low-angle, high-angle, and special.

Boundaries are described primarily by their angle, the minimum angle through which one crystal would have to be rotated in order to become continuous with the other, and if more detail is required, the crystallographic direction of the axis of that rotation is added. Special boundaries are also frequently described in terms of "Sigma" values, which correspond to certain specific misorientations. Due to the symmetry of cubic crystals the range of misorientation angles is limited, the maximum possible misorientation is 62.8° about <1,1, ((√2)-1)>, (i.e. 62.8° about <1,1,0.4142>). Values higher than this would be meaningless, as symmetry dictates that there would be a smaller angle rotation available about some other functionally identical axis.

Low-angle grain boundaries (LAGB) are largely self explanatory and are roughly defined as those having a misorientation of 10-15 degrees or less, i.e. boundaries in which the interface can be formed from simple, though large, arrays of dislocations and whose nature is thus dependant on the size of the misorientation angle, (Brandon, 1966). These low-angle boundaries are sometimes regarded as sub-grain boundaries, rather than "proper" grain boundaries and the behaviour of these boundaries (along with subgrain nucleation) are the main determinants of primary recrystallisation behaviour. High angle grain boundaries (HAGB) generally have properties and structures that are largely independent of their misorientation angle, the exception

being special grain boundaries, a subset of HAGB that do have structure and properties particular to their misorientation angle. Non-special HAGBs are often referred to as “random boundaries”.

Special HAGBs, “CSL’ boundaries or “high-sigma” boundaries are those which possess a “coincidence site lattice” (CSL), originally proposed by Kronberg and Wilson in 1949. The coincidence site lattice concept is discussed at length in Randle’s books (1993, 1996). In a CSL boundary, if one lattice is notionally projected into the other, some proportion of lattice sites in one lattice coincide with the notional sites of the other [fig 4]. Logically, this type of boundary has significantly less “free volume” at the interface than the “random” HAGB.

Free volume is the empty space between the mis-matched neighbouring lattices, in which segregate or impurity atoms can easily congregate. The interstices between the atoms of the main crystal lattice are only able to accommodate small atoms (e.g. carbon, nitrogen). Larger impurity atoms must either take the place of an atom in the lattice (“substitutional” alloying) or congregate (“segregate”) in the grain boundary free volume, where there is space to accommodate them.

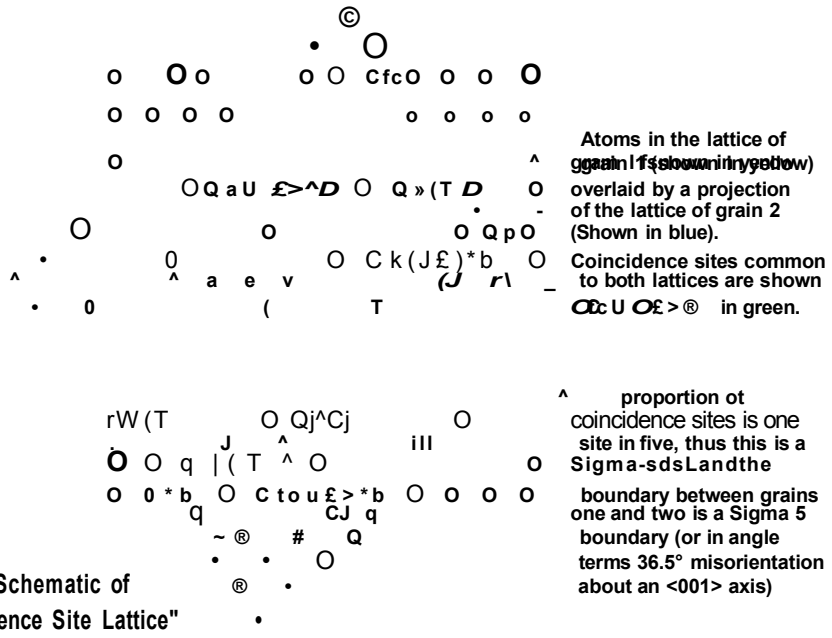

FIG. 4. Schematic of "Coincidence Site Lattice"

The “goodness of fit” between the two lattices is expressed as the sigma value (a concept proposed by Aust & Rutter in 1959), 2 being the reciprocal of the proportion of sites coinciding. Thus 23 is a close coincidence with one in three sites common to both lattices,while 229 has just one in twenty-nine of its sites coincident.A coincidence ofsites is similar to the situation that wouldbe found in a twin boundary, but these boundaries are assumed to have been formed conventionally and have migrated conventionally rather than forming by shear/distortion of an existing crystal. Therefore, special boundaries meet at a distinct boundary where all atoms, or at least most atoms,

are clearly allied to one crystal or the other, rather than both crystallites sharing a plane of atoms common to both, as in a twin. Unlike a twin boundary, there is free volume at a high-Σ CSL boundary, but less than at random boundaries. They would thus be expected to have significantly different physics and segregate chemistry and thus different properties when compared to both twin boundaries and the other classes of grain boundaries. The importance of the sigma value is assumed to be 1) that it gives some guide to the free volume at the interface and 2) the fact that when the boundary moves, a significant proportion of the atoms can "move" from one crystal to the other simply by changing their bonding allegiance, and without actually having to physically relocate in space. Thus high-Σ boundaries are expected to require less energy for grain boundary motion, or in other words to have a higher "mobility" – more movement for a given driving force.

Thus, it seems reasonable to expect three classes of behaviour from grain boundaries, corresponding to the three classes of boundary. There is much work to suggest that special boundaries, and certain low Σ values in particular, are more mobile than others as they tend to predominate in microstructures after certain more strenuous thermo-mechanical treatment regimes. For example, as shown by Aust & Rutter (1959), Randle (1996) and Molodov (2001). This predominance of high-Σ boundaries and the techniques for bringing it about are the basis of "Grain Boundary Engineering". There is also much work that suggests that low angle grain boundaries, often regarded as sub-grain boundaries, are also more mobile than the "average". However, moving sub-grain boundaries are principally associated with primary (initial) recrystallisation phenomena, rather than grain growth, and have not been investigated in this work.

In summary, it appears that the motion of any particular grain boundary potentially depends upon all of the following:

- Surface tension driving force, dependant upon:
  - Local grain boundary curvature
  - Grain radius
  - Grain shape
  - Co-ordination (number of nearest neighbours)
  - The balance of volumetric free energy -vs.- surface/boundary energy
  - Junction angles
- Opposing forces/factors, including:
  - Vacancy generation (Estrin, 2001)
  - Solute effects
  - Segregate effects (nature of segregate atom, boundary free volume)

- Triple junction drag (Shvindlerman et al. 2001, Mattisen et al, 2001)
- Material diffusion across the boundary (matrix and impurity)
- Misorientation angle
- Misorientation axis
- Velocity of boundary motion (instantaneous velocity)
- Temperature
- Surface interactions (Humphreys et al, 1996)
- Surface grooving (Mullins, 1958)
- Activation energy for motion
- Precipitates (Zener Pinning)
- Second phases
- Inclusions
- Interaction with dislocations (Molodov, 2001)

◆ Stresses

- Applied stresses (Winning, 2001)
- Residual stresses

Clearly, many of these factors are likely to interact with others. For example, the introduction of a segregate to a grain boundary would be expected to interfere with the transport of atoms across the boundary, but equally would be expected to alter the boundary surface energy – these could have synergistic or opposing effects. The exact behaviour of that segregate and the quantity that could segregate to the boundary would depend on the boundary free volume. The velocity of a boundary's motion will affect the amount of segregate that it can sweep with it, which would in turn be expected to affect boundary velocity. A change in misorientation will change a boundary's activation energy for movement, interaction with dislocations, thermal response, solute and segregate interactions and the boundary free volume (which might be expected to affect diffusion across the boundary and vacancy generation when in motion).

Logically, a high free volume boundary and/or a high velocity of motion, implies a relatively long journey for atoms moving across from one crystal to the other. This implies a higher probability that any given atom will fail to reach its "ideal" lattice site before the grain boundary as a whole moves on, leading to the generation and "freezing-in" of vacancies, as observed by Estrin.

The forces and factors opposing grain boundary motion are often lumped together under the heading "grain boundary mobility" – the response of a particular grain boundary to a particular driving force or surface tension. The term "mobility" to describe the

response of a boundary to a driving force is potentially misleading, as the phrase "high-mobility boundaries" evokes images of a class of boundaries moving much more rapidly than the rest. In fact, the high-mobility boundaries merely have the potential to move faster, if they are subject to the same driving force. Given the particular nature of high-Σ boundaries, this is a big assumption. It is quite possible that the surface energy liberated by the elimination of a given area of high-Σ boundary surface will be very different to that liberated by the elimination of the same area of random boundary. Logically it would be expected to be considerably smaller, given the reduced free volume and the coincidence of lattice sites. Thus it is probable that a high-Σ boundary will experience a different, and probably lower, surface-vs.-volume free energy balance component of the driving force, than would a random boundary under otherwise identical circumstances. It is therefore a dangerous assumption that "high-mobility" boundaries will necessarily move more rapidly in practice than will other boundaries.

In short, grain boundary motion is a complex phenomenon with a great many variables, some of which clearly are, and more of which may well be, inter-dependent. It is quite conceivable that conventional statistical techniques will prove to be of limited use in characterising grain boundary behaviour and that tools intended for "complex" or "chaotic" systems may be more successful if sufficient experimental data can be generated. Similarly, conventional experimental design is poorly equipped to cope with multiple inter-dependent variables, and a "Taguchi" experimental design scheme may prove more rewarding (Taguchi, 1987(1976)). The rather limited insight arising from the data currently available certainly implies that the problem is complex and resistant to analysis as well as lacking in experimental results.

2.2.3 INVESTIGATION OF MIGRATING BOUNDARIES

Due to the difficulties of working with materials at elevated temperature, the vast majority of the existing experimental work is based upon before-and-after studies, in which a grain structure is characterised, heated above its recrystallisation temperature for some time, then cooled and characterised again. Clearly, these "post-mortem" studies are generally unable to yield much meaningful information about the dynamics of grain boundaries (there are two specialised exceptions to this, i.e. the revealing of "ghost lines" by atomic force microscopy and segregate analysis). These before-and-after studies have reached only rather general conclusions about average grain sizes, a fact that adds weight to the suspicion that the motion of grain boundaries is a complex phenomenon that will not yield its secrets to such investigation techniques. Confusingly, many workers describe post-mortem experiments as "in-situ" if the sample area is rigorously controlled to be identical both before and after heating. For example, an experiment that images or maps the grains, then withdraws and/or

shields the detector while the sample is heated in place, then reintroduces the detector when the sample is once again cold may be referred to as "in-situ", but is clearly not the in-situ, in-real-time goal of this project.

There have been very few real time in-situ studies or studies with capability to detect or infer the position of a grain boundary at any point in time other than the beginning or end of the experimental run. With regard to "true" in-situ studies, Rabkin (2000), notes *"The experimental observations in this field are scarce"* and offers only two references, Abdou et al (1996) and Molodov et al. (1998). Rost et al. (2003) (working on grain growth in thin films) further comment that *"In situ bulk observation of the evolution (grain growth) of polycrystalline metals, especially during heat treatment, proves to be difficult."*. They cite Van Swygenhoven (2002) and Marguiles et al. (2001).

Those few experimental observations that are available divide broadly into three types: those that show discontinuous "jerky" boundary movement, those that show steady, continuous motion and those that either do not state any observed mode of motion or have insufficient time resolution to conclusively show either of the first two cases. The first are typified by Rabkin et al. (2000). and Abdou et al. (1996). The second type are typified by the work of Gottstein's Aachen group: Mattisen et al. (2001), Gottstein et al., (2001). A third group (e.g. Humphreys et al, 1996) give images of grain networks at various times but do not report the mode of boundary motion. Regrettably Abdou's most intriguing references are respectively "P.F. Schmidt, PhD thesis, University of Munster (1977)", "TH Chuang, unpublished work (1985)" and "G. Kiessler, unpublished work (1986)", none of which could be meaningfully consulted. In particular, Abdou et al. report that Schmidt's work showed discontinuous motion of a recrystallised grain growing into a copper single crystal matrix, with a maximum velocity about one order of magnitude higher than its average velocity. They also reproduce copies of two of Schmidt's Time-Distance graphs. On-line searching for other relevant published articles by these authors has proved unproductive.

The data are very scarce, but it is notable that those workers finding jerky motion are mostly those working with polycrystals, while those that observe continuous motion are working with bi- and tri-crystals. Another interesting point is that Rabkin, observing an area covering a few grains, shows dwell times (the time during which an intermittently mobile boundary remains stationary at any given position) in the order of minutes. By contrast, Abdou et al. (and some others cited by Abdou et al.) observe a small portion of a single grain boundary within a polycrystalline film and show dwell times in the order of seconds. These films are both artificially deposited thin films and Transmission Electron Microscope (TEM) specimens thinned down from bulk samples.

Much of the polycrystal research showing discontinuous motion has suffered from the fact that it is based on surface-imaging techniques. In all these cases, interaction with the specimen surface, and in particular with grain boundary grooves, will have influenced boundary motion and has raised the suspicion, from some quarters of the research community, that this surface effect is sufficient in itself to account for the discontinuous motion observed. This may be particularly true with thin film and TEM studies, where surface effects would be proportionately much larger than bulk effects.

Since the start of this project, data has been published by Fielden et al. (2003), Schmidt et al. (2004), Juul-Jensen et al. (2004), Poulsen et al. (2004), Anselmino et al. (2004 A & B) and Fielden (2004). These show discontinuous motion at a surface in the absence of grain boundary grooves (Fielden, Anselmino et al.) and discontinuous volume changes and/or discontinuous boundary motion of a crystal within an aluminium bulk (Schmidt et al. Juul-Jensen et al. Poulsen et al. – the Risø laboratory 3DXRD group).

The surface results of Fielden and Fielden et al. (this project) and those of Anselmino et al. show discontinuous motion both before and after the appearance of surface grooving. The in-bulk observations of the Risø group cannot be suspected of being subject to surface effects, but do suffer from very poor time resolution and the absence of any information on the context and/or neighbour grains of the growing grain/moving boundary. It is clear that discontinuous motion of grain boundaries in polycrystals occurs independent of interaction with the material surface. Most of these polycrystal studies use industrial materials, thus there still exists a possibility that ultra-high purity model materials may not exhibit discontinuous boundary motion in polycrystalline form, although Rabkin's high-purity Ni-Al evidence suggests against this.

Until and unless the evidence becomes conclusive, the discontinuous motion results are likely to remain contentious, as the current models and theories of grain growth (Miodownik, 2002) envisage a near-constant surface tension driving force acting upon boundaries of near-constant mobility, i.e. a constant opposing force. While these forces will vary greatly from boundary to boundary, depending on boundary character, neighbours, local topography, etc., for any given boundary moving from position A to position B, with no other radical changes in neighbouring grain network geometry, these forces should remain roughly constant or should at least not change radically. This means that boundary velocity will change when local geometry changes, such as when a neighbour grain is annihilated, but that between such events boundary motion, while somewhat variable, should not be discontinuous or subject to large, sharp changes and boundary motion should neither stagnate permanently, halt temporarily nor fail to start.

2.3 INVESTIGATION TECHNIQUES CONSIDERED FOR, OR SIGNIFICANT TO THIS PROJECT

The major techniques available to investigators are currently:

- Grain boundary etching/thermal etching techniques
  - Atomic Force Microscopy (AFM) techniques
  - Secondary electron SEM imaging
  - Optical microscopy
- Post-mortem metallography of segregate distribution
- X-Ray diffraction techniques
  - 3D-XRD microscopy (a synchrotron radiation X-Ray Diffraction technique)
  - X-Ray tracking of a single grain boundary
- Backscattered Electron techniques, composed of:
  - Electron imaging
  - Orientation mapping (EBSD)

2.3.1 GRAIN BOUNDARY ETCHING/THERMAL ETCHING TECHNIQUES

These techniques rely upon the phenomenon of etching of grain boundaries. This induces a topographic feature on the specimen surface at the grain boundary position, thus allowing topographic imaging techniques such as optical microscopy, secondary electron scanning electron microscopy or atomic force microscopy to detect the boundaries indirectly, via the etched features.

There are two means of etching, chemical and thermal. In chemical etching, material is removed from the specimen by exposing it to a moderately corrosive chemical mix, usually for a brief time. The etchant is carefully selected such that it will be incapable of significantly affecting the bulk of the crystal grains of the material, but will remove material from the grain boundary, which is more chemically active due to the disrupted crystal lattice that is the boundary. Electro-chemical or electrolytic etching can also be employed, but is functionally the same. Both techniques are widely used in conventional optical metallography.

In thermal "etching" (or grain boundary ditching) [fig.5] no material is removed. Material is transported by surface diffusion from the grain boundary and deposited on the adjacent surface of a grain. This process can only occur at temperatures relatively close to the melting point (Mullins, 1957).

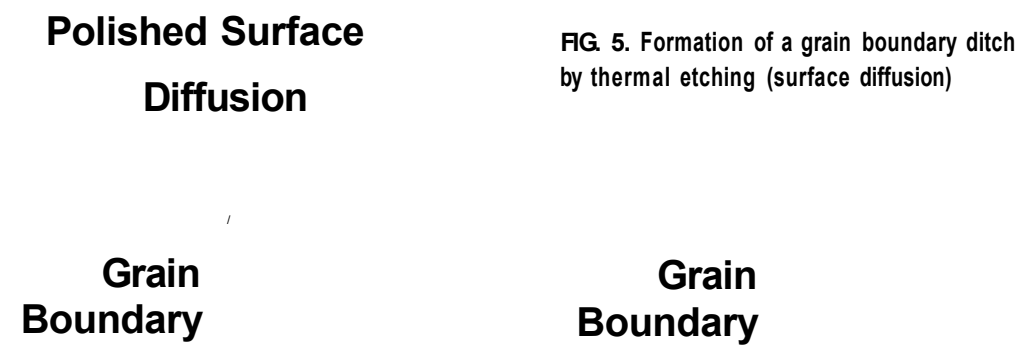

FIG. 5. Formation of a grain boundary ditch by thermal etching (surface diffusion)

The driving force for thermal etching is surface tension. A sharp corner on a grain (shown in the "as polished" case above) is energetically unfavourable - the "ideal" low-energy configuration for the triple junction between three grains is three angles of 120° each. The equilibrium angle between two grains and the surface will not be 120°, but is highly unlikely to be 180°, as in the "before" diagram of fig 5. Thus, material will diffuse away, bringing the surface-grain-grain junction angles closer to equilibrium, once the temperature becomes sufficient to activate surface diffusion in the material. This diffusion is time and temperature dependent.

2.3.1.1 LIMITATIONS OF ETCHING TECHNIQUES

Because diffusion is time dependent, a ditch will not appear instantly when a grain boundary moves to a new position. Neither will an existing ditch disappear when the grain boundary that caused it moves away. Thus, if the boundaries are moving at any speed, thermal etching techniques could easily give a misleading impression of the instantaneous position of the boundaries.

With chemically etched specimens not only will the prior surface topography not vanish, but new topography will not appear at the new boundary positions until and unless the specimen is re-exposed to an etchant.

Finally, all techniques that induce surface topography will suffer from the suspicion that the topography generated will probably influence the motion of grain boundaries that intersect the surface [Fig. 6] (Mullins, 1958).

FIG. 6. Grain boundary pinned by surface groove, then breaking away

2.3.1.2 Optical Microscopy and Secondary Electron Techniques

As noted above, these techniques rely upon induced surface topography in order to indirectly detect the position of a grain boundary. There are however two "special circumstances" exceptions to this.

1) Zinc has optical properties which are anisotropic with crystal orientation, thus grains of zinc can be imaged optically without etching (e.g. Shvindlerman et al. 2001). Unfortunately, zinc has hexagonal close-packed crystallography, and may therefore reveal relatively little about the behaviour of the metals with face-centred cubic crystals that are this project's primary focus.
2) Secondary electron emission from a specimen is generated by the passage of high-energy electrons either into ***or out of*** the specimen surface. Thus, a proportion of the secondary electron signal corresponds to the backscattered electrons leaving the specimen. If the (topography dependent) contrast in the beam-induced secondary signal is practically non-existent (high quality flat polished specimen) then a very weak contrast may be observed between crystals using secondary electron imaging. This is an indirect use of backscattered electron imaging, which is discussed in more detail in that section (2.3.3).

2.3.1.3 Atomic Force Microscopy techniques

Atomic force microscopy "images" surface topography by physically scanning it in a raster pattern with a nano-scale stylus, but in addition it measures the surface features that it encounters. This technique has been used by Rabkin et al. (2000) and Rabkin & Klinger (2001) to investigate the movement of grain boundaries in a polycrystalline Ni-Al intermetallic compound at high temperature.

A knowledge of surface diffusion rates for the material of interest at the temperature of interest is necessary. Given this knowledge, and the depth of a grain boundary ditch as measured by the AFM, it is possible to calculate the time over which the ditch forming diffusion mechanism was in operation. This time will correspond to the time at temperature for a stationary grain boundary, or would be the time spent dwelling at a position for a mobile boundary. Rabkin's work shows some grain boundaries remaining stationary throughout his experiment while others move in a discontinuous fashion, leaving behind them telltale trails of partially formed ditches or "ghost lines", indicating the positions at which the boundary stopped and the approximate duration of the stationary dwell.

2.3.1.4 THE POST-MORTEM METALLOGRAPHY TECHNIQUE

Rabkin (2001) refers in passing to ghost lines revealed by metallography and appropriate etching to reveal segregates. Chongmo and Hillert (1982) used the technique to investigate diffusion induced boundary migration. Moving grain boundaries tend to sweep segregate, impurity or alloy elements with them, but, when moving rapidly, the quantity of segregate that can be carried is reduced. Thus, if a boundary moves in a discontinuous manner, segregates will be found at higher concentrations where the boundary has stopped, as they were unable to follow the boundary when it re-commenced movement and accelerated away. The increased concentrations of segregates at these positions can be etched for and imaged. However, these are highly specialised and problematic techniques. Spatial resolution will be much reduced by the fact that, once free of the boundary, segregates will tend to diffuse away during the remainder of the heating time, "smearing" the position indication. This makes the segregate concentration more difficult to detect, and, in the case of brief dwells, erases the segregate concentration evidence by reducing it to a level indistinguishable from the background. No evidence was found in the literature for the use of this technique to study boundary motion in single-phase materials, however the technique is used to determine positions of prior austenite grain boundaries in cooled and transformed steel specimens.

Sensitive microanalysis techniques such as Secondary Ion Mass Spectroscopy (SIMS) have the potential to directly map segregate concentrations. However, no reference has been found to their use for this purpose, and they would be subject to many of the same problems.

2.3.2 X-RAY DIFFRACTION TECHNIQUES

These techniques rely on diffraction of X-Rays passing through the crystal lattice and either the disturbance of this diffraction by the grain boundary or the difference in diffraction generated by some differently oriented crystal. The simplest of these techniques is grain boundary tracking by X-Ray.

2.3.2.1 GRAIN BOUNDARY TRACKING BY X-RAY

In this technique, an X-Ray beam is directed onto a polished specimen such that the diffraction process reflects the beam to a detector, as illustrated below [fig 7]. The intensity of the reflected beam will be different for the two differently oriented crystals, and different again where the beam falls on the grain boundary and straddles the two crystals. By calibrating the system with the boundary reflection intensity, a logic controller can be set up to hunt for that intensity and thus track the position of the grain boundary. The system was developed by Gottstein's Aachen group (Czubayko et al., 1995) and is heavily used by them.

FIG 7. "XCITD" X-Ray
Continuous Interface
Tracking Device schematic

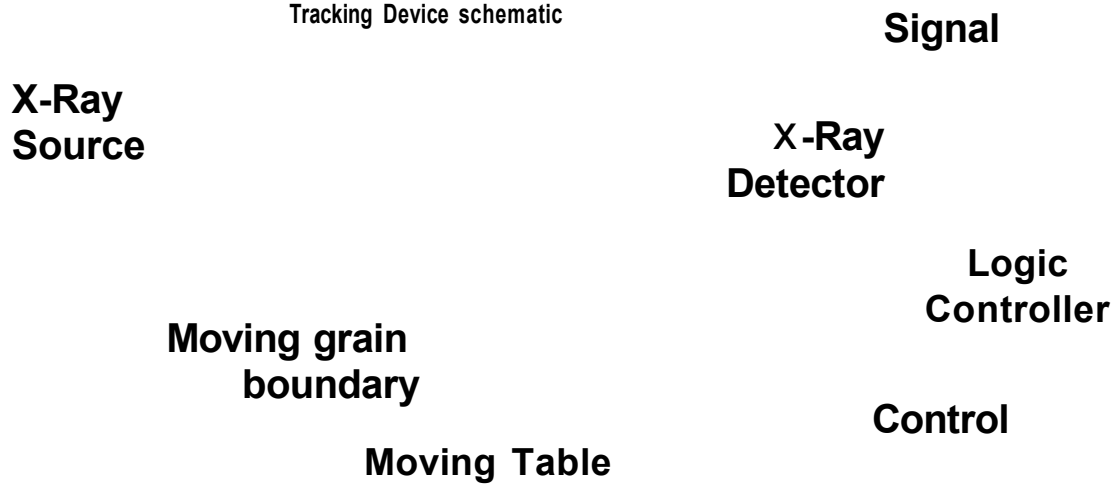

The system that this author has seen maintains the X-Ray beam source and detector stationary and moves the specimen stage such as to keep the grain boundary at the point where the beam hits the specimen. Clearly the system is limited in that the stage is only capable of one dimensional movement, though 2-D motion is theoretically possible. Also the logic processing and X-Ray optics are greatly simplified by a knowledge of which direction the boundary will move in. Two dimensional motion could be tracked, but would probably entail a much reduced response time.

Current boundary tracking systems use artificial bi-crystals, and occasionally tri-crystals as specimens, and often apply a magnetic field to drive grain boundary motion, as the form of a bi-crystal dictates little or no surface tension driving force (Gottstein, 2001 B).

A further limitation is the fineness of the X-Ray beam. If the technique were applied to a polycrystal, the beam would have to be small with respect to the grain size present in order to avoid detection of more than one boundary simultaneously. Similarly the beam would have to be large with respect to the "X-Ray visible" boundary width, in order to produce a clear and repeatable target intensity. Given the technical difficulties of producing finely collimated X-Ray beams of relatively high intensity this technique seems likely to remain limited to studies of model systems.

2.3.2.2 "3-D XRD" Microscopy

3-D X-Ray Diffraction microscopy is an extremely expensive technique is based upon high power synchrotron X-Ray beams, the instrument is usually installed for just a few weeks of the year at the E5RF (European Synchrotron Radiation Facility) at Grenoble or at DESY (Deutsches Electronen SYnchrotron) in Hamburg. A similar instrument is under development at Argonne National Laboratory, near Chicago in the USA.

A high-brightness X-ray beam, typically of 40keV energy, is passed through a specimen and diffracted to an annular detector. A thick metal shielding mask is placed in front of the detector. This contains very narrow slots, machined and aligned in the form of part of a cone, such that only diffracted rays originating from a small target volume at the apex of the cone (the gauge volume) can pass through to the detector. This gauge volume is presently at best about 1 micron x 1 micron x 20 microns. The specimen is mounted on a 3-D movable stage, such that the gauge volume can effectively be scanned around the specimen' s volume (actually the specimen is scanned through the gauge volume) and diffraction data is captured to form a 3-D map. Alternatively, the diffracted signal from one crystal can be monitored and the specimen either scanned, to build a 3D topography map of just that crystal or monitored for its intensity with the specimen stationary. This latter yields a measure of the volume of a grain, but not its shape, location or context (Juul-Jensen (2001), Lauridsen (2003), Poulsen et al. (2004)). The specimen can be heated, or strained during X-Ray examination. This system was successfully used by Lauridsen et al (2001), to monitor the volume of a growing grain of known orientation in a bulk of 1050 Aluminium and later by Schmidt et al. (2004) to sequentially map the 3 dimensional shape of a growing grain over time. There are several major limitations to the technique:

- In order to monitor a particular grain it is necessary to forgo capturing any information on its neighbours or the context surrounding it
- Spatial resolution is poor by comparison to most other techniques
- Time resolution is very poor, as each full volume scan takes a considerable time to complete, particularly if more than one crystal is being monitored or if crystal shape is being mapped rather than simple volume being monitored.

2.3.3 BACKSCATTERED ELECTRON TECHNIQUES (INCLUDING "FORWARD" SCATTERED ELECTRONS)

These techniques rely upon two phenomena. Firstly, the partially directional scattering of backscattered electrons, a proportion of which are diffracted and/or channelled to form Kikuchi or Electron BackScatter Patterns (EBSP). Secondly, the small changes that occur in overall backscattered electron signal (i.e. changes in absorption or backscattering coefficient) with changing electron probe/crystal lattice geometries, due to channelling and consequent preferential absorption.

2.3.3.1 MECHANISMS OF ELECTRON BACKSCATTERING

The electrons of the microscope beam (primary electrons) penetrate the specimen material (in the context of this project, a metal crystal). The electrons very rarely strike or interact with the surface atoms, but once inside the specimen, can interact with

the electrons and atoms of the material in a variety of ways and hence ultimately suffer a variety of fates. The electrons of interest in the context of this project are among those that are "backscattered". In the near-surface bulk of the specimen, these electrons undergo a number of elastic and/or inelastic collisions/interactions with atoms and their nuclei. Ultimately they escape from the material surface with a relatively large fraction of their initial energy remaining, albeit with the vector of their velocities deviated through a large angle. Most electron-specimen interactions can be relatively simply explained in terms of particle interactions (collisions) despite the fact that moving electrons have both wave character and particle character.

Backscattered electrons will have undergone one or more scattering encounters (possibly several) prior to exiting the specimen. These encounters will be a mixture of inelastic and elastic collisions, thus the exit energy of the electron will generally be inversely dependent upon the number of scattering encounters it has undergone, exit energy being lower if the number of collisions is high. Repeated collisions may send the electrons on a journey analogous to a 3-D random walk, biased by the uniform initial velocity of the electrons and the probability that the angle of scattering in any one encounter will be relatively low (see Reimer, chapter 3). By implication the lower energy backscattered electrons, having undergone a larger number of small-deviation collisions (i.e. having taken a longer random walk), are likely to exit the specimen further from the beam entry point than will the Low-Loss backscattered Electrons (LLE), that have suffered one or very few large-deviation collisions. This accounts for the relatively low resolution of backscattered electron imaging compared to the more frequently used secondary electron imaging in conventional scanning electron microscopy. Secondary electrons (which give higher resolution images) are ejected by the passage of the incident electrons (SE1 secondary electrons) and also by the passage of low-loss backscattered electrons exiting the specimen from a relatively compact area around the beam entry point (SE2 secondary electrons). The higher-loss backscattered electrons exiting the specimen more distant from the beam entry point generate fewer SE2 electrons and thus make a progressively smaller contribution to the overall SE image. By contrast, the common backscatter electron detectors are designed to respond almost equally to backscattered electrons across a fairly wide range of energies, thus the high-loss BSE make a proportionally larger contribution to the image and limit the available resolution. For more detail on any of the foregoing, Reimer's book (1998) is recommended.

By convention, "backscattered" electrons are defined as being those that escape the specimen with an energy in excess of 50 eV (from a primary beam energy of typically 20 KeV). This definition is convenient because it reflects the range of electron energies likely to be detected by "backscattered" and "secondary" electron detectors respective-

ly. However, it is not wholly accurate, nor is it particularly convenient in the context of this project. As noted below, this broad definition of backscattered electrons includes "channelled" or diffracted low-loss electrons carrying valuable information on crystal structure as well as a large number of "ordinary" backscattered electrons, which can provide a strong and unhelpful background signal.

2.3.3.2 IMAGING CRYSTALS VIA BACKSCATTERED ELECTRONS

Crystal Orientation Imaging/Electron Back-Scatter Diffraction (EBSD) mapping techniques rely upon the fact that the intensity (number) of backscattered electrons arriving at any given point on some detector area (usually a phosphor screen) will vary with varying crystal orientations relative to the detector. This geometry dependent variation of intensity is due to channelling and/or diffraction of the electrons escaping from the specimen.

A proportion of the incident electrons, having been scattered by encounters with the specimen atoms/electrons, will ultimately be sufficiently deviated from their original direction as to be moving back towards the material surface. If the number of scattering interactions was low and/or their nature mostly elastic then the backscattered electron will retain a high fraction of its initial energy (have a short equivalent wavelength) and thus may usefully interact with the specimen on its journey back to, and exit from, the (crystalline) material surface. The nature of these interactions can be simplistically explained by diffraction of the electrons, which have wave character, by the regular network of the crystal atoms. This model is analogous to the simplest models of transmission electron microscopy, the backscattered electrons appearing to come from some virtual electron source within the material, albeit a very poorly collimated and polychromatic source.

The electron backscattering patterns are often referred to as "Kikuchi" patterns from the diffraction phenomenon that produces them. Some of the electrons travelling (in many directions) towards the surface will be diffracted by passing between the atoms of the lattice. Because the electrons are travelling in a variety of directions, the diffraction does not produce a spot pattern (as would be expected from a single beam), but a line pattern resulting from conical families of diffracted beams. The lines from one diffraction are overlaid by the lines resulting from diffraction from the lattice's other directions of symmetry, producing a characteristic pattern of lines and nodes [fig 8] on a screen [fig 9]. To maximise pattern clarity, the specimen is tilted at 70° to the beam in order to maximise backscattered electron yield and the centre of the detector/phosphor screen is similarly at 70° to the specimen (140° to the beam) to maximise electron capture.

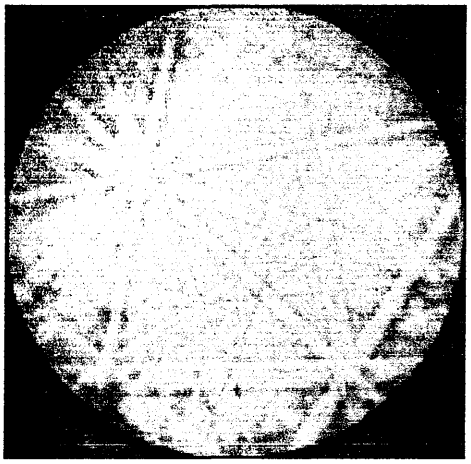

FIG. 8. A typical high-quality Electron Back-Scatter Pattern.

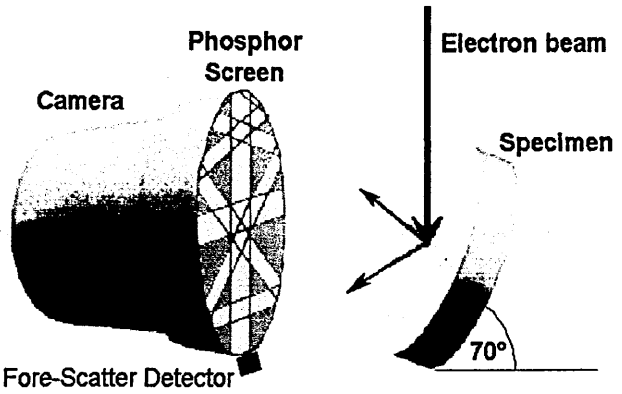

FIG. 9. Schematic of EBSD system

More sophisticated models of this interaction consider the phenomenon of "Channelling", which is discussed further below. In summary, due to the regular stacking of the crystal lattice, there are certain directions in which it is easier for the electron to pass through the crystal (or put another way, directions in which the electron is likely to travel further before being deflected or absorbed).

This effectively increased "transparency" to electrons travelling in certain specific directions would account for some of the directional nature of backscattering and for orientation-dependent preferential absorption of some incident electrons. For example, if the incident electrons happen to coincide with a channelling direction leading into the crystal they are likely to scatter at a greater depth and thus are less likely to exit the specimen before being absorbed. In a backscattered electron image, such a crystallite would appear slightly darker than some randomly oriented crystallite.

Thus the journey of an electron [fig. 10], which was earlier referred to as analogous to a biased random walk could be better modelled as a three-dimensional game of snakes and ladders. Conventional electron-specimen collision interactions are the steps along the main random-walk path, but with the electron likely to lose energy at each collision the number of "dice-rolls" available to it is limited and only those few that roll consistently high will reach the end of the game and exit the surface. Most will run out of energy and be absorbed. However, a proportion will encounter a channel – a snake or a ladder – moving the electron a relatively great distance, perhaps even to the surface, for little or no energy loss. Not all channels lead to the surface. Like the snakes in the game, some channels lead even deeper into the specimen, from where the electron is even less likely to escape.

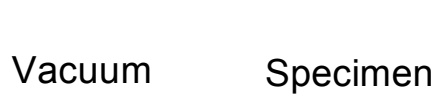

FIG. 10. A typical "Monte Carlo" simulation of electron-specimen interaction

The diffracted and/or channelled backscattered electrons leave the specimen in families of preferred directions. The conventionally backscattered electrons are emitted in a much more nearly omni-directional fashion and may well have lower energies (as channelled electrons have effectively taken a “short cut"), although the overlap is large. These conventional backscattered electrons provide a large background signal, which degrades the contrast that ought to be available in the diffracted/channelled portion of the low-loss backscatter signal (which carries the orientation information).

Electron Backscatter Diffraction (EBSD) captures a large portion of the structured backscatter pattern across a large detector area [fig 9] and exploits image processing and computing technology to determine what crystal orientation is most likely to be responsible for producing the observed pattern (Randle’s book, 1993, gives a good overview).

2.3.3.3 ORIENTATION CONTRAST IMAGING

Orientation Contrast Backscattered/fore-scattered electron imaging follows one of two possible strategies.

The more common approach, often referred to as “forward scatter electron imaging”, or “fore-scatter imaging” is usually done in the same “forward scatter” geometry used by EBSD and is often carried out in conjunction with EBSD [fig 9], This captures a backscattered electron flux falling on one or more relatively small detectors, and generates image contrast from the geometry dependent changes in that flux, i.e. changes in the diffracted/channelled contribution (dependent upon detector-crystal geometry).

The detector lies in a small part of the electron backscatter pattern cast by the subject crystal, and as the pattern will change when the beam moves on to a differently oriented crystal, the flux falling on the detector is likely to change as well. However, as this change is likely to be very subtle, fore-scatter detectors are often deployed in arrays of up to six elements, with sum or difference signal imaging options in order to enhance contrast for any given specimen. A further problem with detectors deployed with an EBSD system is that the ideal location for detectors (70° to the specimen, 140° to the beam) is already occupied by the EBSD detector screen, and thus the fore-scatter detectors are usually at a very oblique angle to the specimen, nearly 90°. This reduces the signal strength and greatly exaggerates topographic contrast. Even in "flat polished specimens", such as those produced by electropolishing, the greatly exaggerated topography contrast can easily overwhelm or mask the orientation contrast (Seward 2003, Reimer 1998 p 224).

The less common approach, usually referred to as Electron-Channelling Contrast Imaging (ECCI) or simply as Orientation Contrast (OC), can be done at the 70° position and the zero-tilt position. It employs a large detector area, capturing an averaged signal to detect changes in overall backscattered electron flux, i.e. changes in backscattering coefficient, η, due to the differential absorption due to channelling (dependent upon beam-crystal geometry), see Simkin 2001. The set up used for this imaging mode is identical to that used for producing channelling patterns in the SEM, however it is unnecessary to rock the beam, as the desired beam/crystal angle changes are provided naturally by multiple differently oriented crystallites.

Backscattered Electron imaging techniques are limited by the detectors available and the low contrast/weak signal both of electrons backscattered to form a channelling or Kikuchi pattern and of the generally very small differences in backscatter co-efficient between crystals oriented for maximum channelling compared to those oriented for minimum channelling. This latter contrast, the maximum ratio of $\Delta\eta/\eta$, is shown by Reimer (p358 and fig 9.17) to be in the order of 1-5%, for most materials.

2.3.3.4 BACKSCATTERED ELECTRON DETECTOR TECHNOLOGY

There are currently two major classes of readily available detector for backscattered electron imaging: semi-conductor diode detectors and scintillation detectors (based on the Everhart-Thornley secondary electron detector, including the Robinson detector). Also available are microchannel plate detectors, these tend to be restricted to specialised low beam energy applications and are very expensive. The diode detector is by far the most common of these types, and all of the recent published data on SEM imaging of grain structures appears to have been generated by workers using diode detectors. The limitations of the various detectors are discussed below.

2.3.3.4.1 Limitations of Techniques Based on Diode Detectors

The Diode detectors are sensitive to light and Infra-Red (IR) photons, one or both of which will be emitted from any hot specimen – depending upon just how hot it is. This is an extremely serious limitation, as both the industrial and model materials of most interest for investigation undergo grain growth at relatively high temperatures, at which significant photon fluxes will be emitted. For example: aluminium – in the order of 300°C and upwards, steels in the order of 700°C upwards, gold & copper in the order of 500°C and upwards. Signal contrast from the detector decreases as photon radiation increases until the point where the major workers using this technique report that there is no usable image contrast when specimen temperature exceeds about 400°C or 450°C (Humphreys, 2001; Mattisen 2001). Attempts have been made to screen the detectors from the hot sample and stage, however as both the undesired photons and the desired backscattered electrons follow line-of-sight paths, success has necessarily been limited (Anselmino (2005), Mattisen (2001)). Both Anselmino and Mattisen's information is with regard to partially successful screening by apertures and shields to restrict the IR reaching the detector to only that which emanates from the area of interest, not the rest of the sample or the hot stage as a whole. There does not appear to have been any investigation of the relative effects of number of photons hitting the detector versus the energy of those photons, but the reported benefits of reducing photon number suggest that number may be more important than wavelength/energy.

Further (but less serious) limitations of diode detectors include their inferior amplification capability and higher noise characteristics (compared to scintillator-photomultiplier types), and their relatively slow electronic response (due to their capacitance). This dictates that fast scan rates (particularly TV rate) cannot practically be employed with diode detectors. Image contrast in electron backscatter patterns is intrinsically poor, due to the diffracted electrons constituting only a small proportion of the overall backscattered signal, and scan speed must therefore be further sacrificed in order to retain usable contrast. Thus, all types of diode detectors would be limited in their usefulness for observation of very rapid movements of grain boundaries.

Diode detectors tend to be supplied in two forms, depending upon whether they are intended for placement and use as conventional backscatter detectors or as "forward-scatter" detectors (used in conjunction with an EBSD system). The conventional detectors are supplied in the form of a disc intended to be placed on the microscope pole-piece, having an annular detection area, subdivided into two or four segments [fig. 11].

FIG. 11A.
Typical BSE diode detector

piece

Detector jy

FIG. 11B.
Detector/Specimen geometry

Specimen

FIG. 11C.
2-segment iayout

FIG. 11D.
4-segment layout

These segments (A & B or A, B, C & D) produce a single summed signal in which each segment's contribution can be positive (+) , negative (-) (i.e. out of phase - producing a "negative" image), or zero. This arrangement has been developed to allow optimisation of topographical and/or atomic number (Z) contrast in conventional backscattered electron imaging, by far the most common application of this most common detector type. The shape and placement of the detector, when considered relative to the likely shapes/angular distributions of the electron backscatter patterns (EBSP) is not likely to produce strong image contrast [fig 12].

The "forward" scatter detectors are semiconductor diodes as described previously, in the form of circular or rectangular single active elements, typically around one square centimetre in area, designed for use with highly tilted specimens. Though the Sheffield

FIG. 12A. Example EBSP with schematic of typical BSE detector superimposed.

FIG. 12B. Some example Electron Backscatter Diffraction Patterns

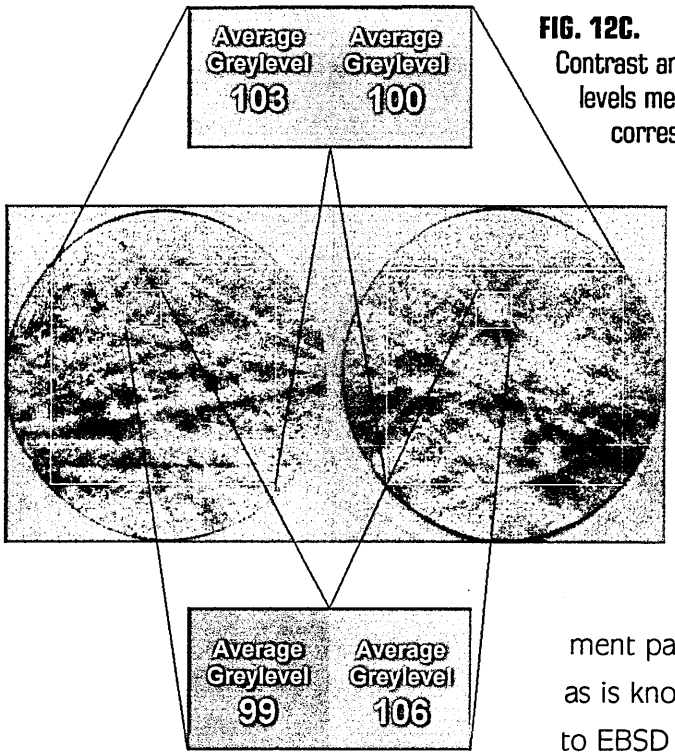

FIG. 12C.
Contrast and detector area. Averaged grey levels measured from areas of a real EBSP, corresponding to differing detector areas.

Hallam University (SHU) equipment features a single element, they are in use in arrays of up to six elements (connected as two pairs and two single elements producing a summed signal with contributions of +/-/zero from each element or element pair). This type of detector is (as far as is known) always installed as an adjunct to EBSD techniques for determining; (and usually mapping) crystal orientations. Their limitations in terms of infra-red sensitivity and detector capacitance are the same as apply to these.

These detectors have the advantage that they allow the specimen to be at, or close to, the optimum 70° sample tilt required to maximise backscattered electron yield generally and electron backscatter patterns specifically. They further have the advantage of small size (i.e. small angle of acceptance), which would tend to increase contrast between different backscatter patterns when the detector is placed at some arbitrary position in the pattern. They have the disadvantages that their placement is non-optimum in terms of received signal strength, due to the physical presence of the EBSD equipment, and that this very high angle placement exaggerates topography, frequently to the extent of obscuring the orientation contrast as reported by Seward (2003) and shown in the micrographs of Anselmino et al. (2004 A & B).

As can be seen from fig. 12, the overall flux of electrons falling upon the detector (or any one segment of the detector) is unlikely to be substantially different between the different patterns, giving very little image contrast between crystals. The example patterns shown here were produced by EBSD equipment manufacturers, using model materials, samples tilted to 70° and sophisticated video and digital contrast enhancements, such as background subtraction. Further, being free from the time constraints of practical orientation mapping, these EBSP images have been gathered with long image integration times to improve contrast and minimise noise. In practical microscopy the structure of the patterns could be considerably less marked.

The poor contrast in the signal is exacerbated by the fact that in the zero tilt sample geometry, backscattered electron yield is at its lowest. Contrast is also reduced by plastic deformation or residual stress in the sample, surface contamination, and higher scanning speeds. Other workers in this field report that great patience is required to produce good orientation contrast images of hot samples, even when the specimen is a purposely-grown artificial bi- or tri-crystal (Humphreys et al, 1996; Humphreys, 2001; Mattisen 2001 B). It was also reported that four segment detectors were greatly superior to two segment (Mattissen, 2001B), information which agrees with the author's difficulties in producing orientation contrast images from SHU's conventional two segment detector system, when using conventional working distances (i.e. only a modest detector angle).

2.3.3.4.2 Limitations of Scintillation Detectors

Scintillation detectors such as the Robinson detector rely upon a photomultiplier and are thus inherently light sensitive. In addition to this, all of the designs that the author is aware of are intended to be placed in very close proximity to the specimen and utilise a transparent plastic light-guide/scintillator support. Such a detector seems highly unlikely to survive use with a specimen at 400°C or more and would probably be an expensive loss. Thus, this technology has not been considered as a serious alternative backscattered electron detection technique.

2.3.3.4.3 Limitations of EBSD Techniques

EBSD or orientation mapping (also rather misleadingly termed "orientation imaging microscopy" by the equipment manufacturer TSL/EDAX) involves the capture of the EBSP (as illustrated above) on a phosphor screen, which is monitored by an electronic camera. Normally, this camera is actively cooled below room temperature in order to achieve a useable signal-to-noise ratio. The camera integrates the faint image from the phosphor for a user-selectable period, typically several hundred milliseconds, though occasionally in excess of a second is necessary to produce a good image of the pattern. Some manufacturers claim integration periods of tens of milliseconds to be practical with the most recent equipment.

The image from the camera is digitally transferred to a computer for processing. A software algorithm based on a Hough transform (Hough, 1959), identifies lines in the image and the computer then compares the lines and intersections to a database of patterns for the selected material in order to determine the probable orientation of the crystal responsible for the pattern in question (Oxford Instruments, 1995; Randle, 1993). This processing occurs concurrently with camera integration for the next pattern and on SHU's Oxford (INCA-OPAL) equipment (as of 2000-2004), takes around 500 milliseconds, though equipment now exists capable of "solving" patterns in around 25 milliseconds.

The technique can be used in two ways. Most simply the electron beam can be left to dwell on a point on a grain of interest, and the resulting pattern can be solved. More usefully the beam can be indexed across an area of interest, dwelling at each point for as long as necessary to integrate the camera image or solve the pattern (whichever is longer), thus building up a pixelated map of crystal orientations.

This process is time consuming. On the SHU equipment a typical "presentation-quality" map from a typical aluminium specimen prepared for orientation contrast imaging in this project, requires some 9 hours from start to finish, plus post-processing. If the manufacturer's claims are to be believed then the very latest equipment should be capable of producing a similar map in some 30-60 minutes.

In either case, this time to scan one frame is far too long to capture any but the most sluggish of dynamic events. Further, the pace of development in equipment speed, while impressive, does not appear likely to yield equipment capable of capturing dynamic events in the foreseeable future.

The EBSD technique, although reported to be largely insensitive to the effects of temperature (Humphreys et al, 1996, Seward et al. 2002), appears inappropriate to the needs of this project for characterisation of a dynamically evolving microstructure.

2.4 CLOSING SUMMARY

Much of this literature search was conducted in parallel with the early stages of technique development, described in chapter 3, and was directed by the results and non-results of that work. Thus, this literature search has a very heavy emphasis on imaging and characterisation techniques, as these were soon found to be a fundamental problem that had to be solved before any investigation of microstructure could be undertaken.

In summary, the literature search showed very little prior work on direct measurement or characterisation of grain boundary kinetics, and that what little did exist was inconclusive and, in some aspects, contradictory. It further showed that grain growth phenomena in the "real world" are governed by a great many factors, many of which are likely to interact in complex ways.

Finally, the literature search showed that imaging/characterisation techniques based on the fundamental properties of crystals (diffraction, channelling etc.) were more likely to give satisfactory results than those relying on secondary phenomena (boundary etching, etc.)

CHAPTER 3
TECHNIQUE DEVELOPMENT

3.1 INTRODUCTION

This chapter describes the development of a successful and award-winning technique for imaging microstructural evolution in-situ, at temperature and in real time. It covers the theory and practice of forming orientation contrast images in the SEM, the various problems caused by hot specimens and the development of approaches to resolve or work around those problems. It also describes the particular requirements of, and constraints imposed by, the specimen and hot stage, and how these were resolved.

3.1.1 SUMMARY OF POSITION AT START OF EXPERIMENTATION

Early attempts to image the microstructures of aluminium and copper in the ESEM, using the manufacturer's recommended techniques, gave no useful results, or even encouraging results, at either room temperature or elevated temperature.

The literature survey (see Chapter 2) was then focussed on imaging and characterisation techniques, and showed that, given the available equipment, the only promising technique for detecting and/or imaging grains or phases in situ, at temperature and in real time was electron channelling orientation contrast – a reflected (backscattered/ forescattered) electron technique. It further showed that this was almost certainly impossible in a conventionally-configured ESEM.

As described in detail in Chapter 2, the available "imaging" detectors for reflected electrons are fundamentally incompatible with hot specimens. This is due to their inherent sensitivity to light and vulnerability to heat damage. The available "mapping" technique – EBSD – was unacceptably slow and of unproven capability at temperatures much in excess of 500°C. Thus, a different detector strategy had to be developed.

3.2 SEM TECHNIQUE DEVELOPMENT

Several detector strategies thought potentially compatible with hot specimens were considered, and these were trialled, largely in tandem with an evolving knowledge of orientation contrast beam-specimen-detector geometries. Development and proving trials were conducted at room temperature, mostly using one specimen of commercially pure (1050) aluminium, which had given good EBSD results, and was thus known to give an acceptable level of electron channelling/backscatter phenomena with which to work.

3.3 ESEM TECHNOLOGY

The ESEM, or high-pressure SEM was developed by workers in Australia (Robinson 1975, Moncrieff et al. 1978, Moncrieff et al. 1979). The ESEM, as marketed by Electroscan inc., Philips Electron Optics B.V. and ultimately FEI Company inc., came into being in 1983 with Danilatos' invention of the "Gaseous Detector Device" (GDD) – a secondary electron detector capable of operating in the ESEM's gas atmosphere (Danilatos 1983). This was a highly desirable development, as the Everhart-Thornley SE detector used in all conventional SEMs requires a reasonable vacuum in order to operate – the previous generation ESEM (never made commercially available) was therefore restricted to backscatter electron imaging only. Backscatter electron imaging gives useful results, but secondary electron imaging gives better resolution and clearer topographic contrast.

The ESEM functions by maintaining the electron gun and electron optics column at high vacuum. These are separated from the chamber, in which there is a low-pressure gas atmosphere, by a system of Pressure Limiting Apertures (PLA) and an independently pumped intermediate vacuum zone (schematic, fig. 13).

The significance of the ESEM for high-temperature materials research is its alternative scheme for detecting secondary electrons. In this, the gas atmosphere is made to function as the detector, in a way analogous to the operation of a Geiger-Muller tube.

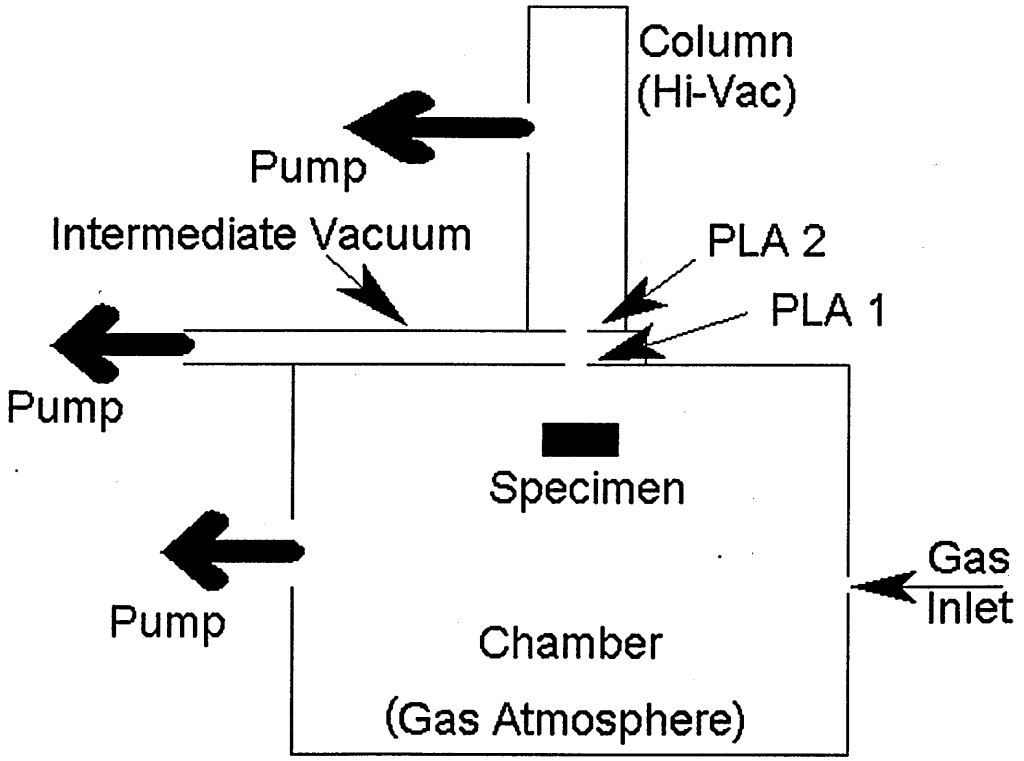

FIG.13. Schematic of ESEM vacuum system

An SE leaving the specimen is attracted towards a biased electrode, and accelerates. The bias used is typically up to 500V. The distance and gas pressure are selected such that the electron's mean free path is small by comparison to the distance to be travelled, so the electron will collide with a gas molecule long before reaching the electrode. Collision with a gas molecule will ionise that molecule, resulting in two free electrons now travelling towards the electrode. The process repeats and a "cascade" of ionisations rapidly builds up, giving significant amplification to the signal. In the Electroscan/Phillips/FEI ESEM the electron current arriving at the electrode is used as the imaging signal (Danilatos' original GDD). In the Zeiss XVP-SEM, the emission of light from the ionisation events is detected by the "Variable Pressure Secondary Electron" (VPSE) detector, and used as the imaging signal. Both of these configurations are illustrated in, fig. 14, though no instrument exists combining these two techniques as the patents are held by rival companies and it would be an unnecessary duplication of capabilities.

A by-product of the secondary electron cascade is the production of positive ions in the gas. These are free to move to the specimen and will neutralise any charge build-up if, for example, the specimen is non-conducting. In the context of this project, all the specimens are conducting and thus this key ability of the ESEM is irrelevant.

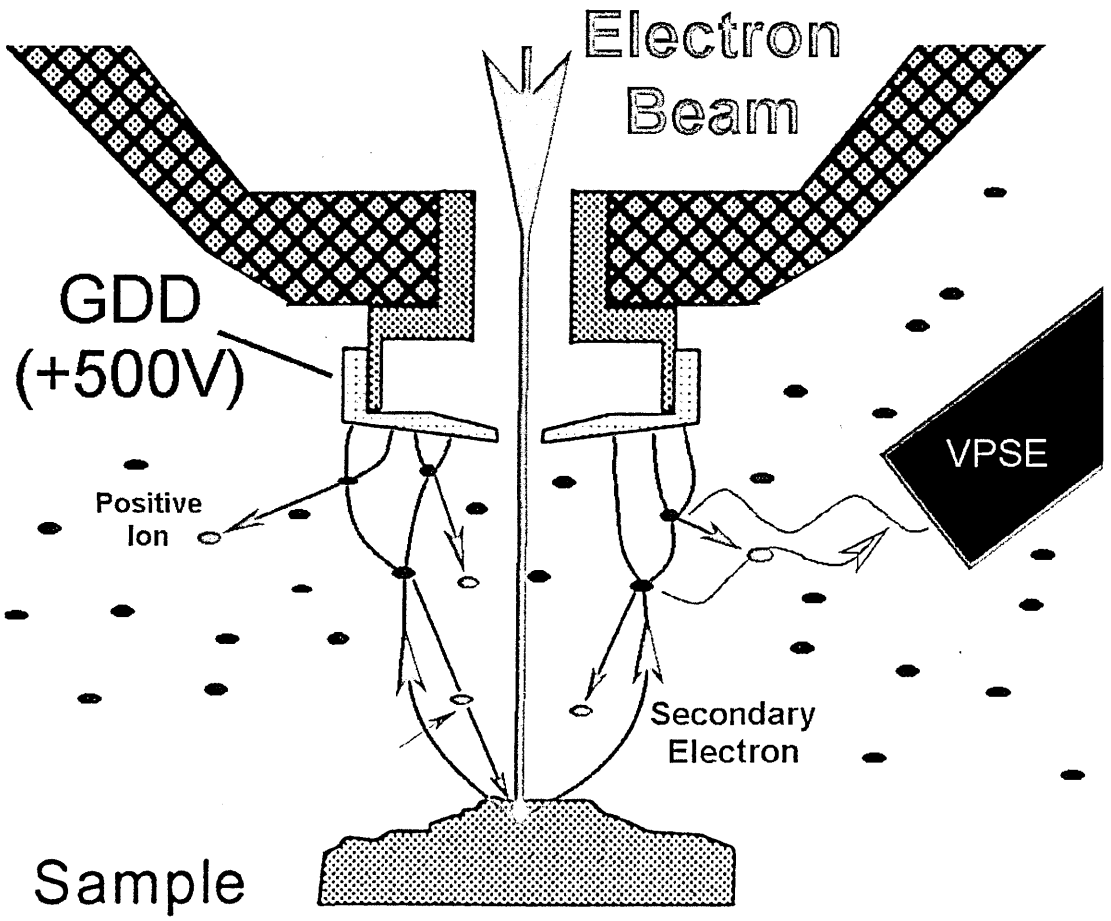

FIG.14. Schematic of ESEM (GDD) and XVP-SEM (VPSE) secondary electron detection modes

The electron cascade process is unaffected by light, unlike the Everhart-Thornley detector and the Robinson (scintillator-photomultiplier) backscatter detector. Both of these are inherently liable to be light sensitive, as they incorporate a photo-multiplier. The semiconductor diode backscatter detector is also light sensitive, as discussed in the literature review. The XVP-SEM VPSE detector will also be inherently sensitive to light, being similar to a cathodo-luminescence detector. Thus, the ESEM GDD seems to offer the only means of detecting either SE or BSE electrons, free from light interference. In other words, the GDD is expected to be the only detector that will function adequately with a specimen emitting significant infra-red or visible radiation (i.e. over 350-400°C), Hence this project was intended to use the ESEM from the outset.

3.4 TECHNIQUE DEVELOPMENT

Unfortunately, early experiments in imaging metal specimens in the GDD-ESEM mode clearly showed that the predominantly SE imaging signal used by the ESEM is unable to give adequate contrast between the grains of a flat-polished single phase metal specimen.

Therefore, some new scheme was required – either to make the grains/boundaries detectable by SE imaging, or to image by some other means or using some other signal.

3.4.1 APPROACHES CONSIDERED

Continuous exposure of the specimen to an etching atmosphere within the ESEM was considered, as this would etch a topographic feature at the grain boundary, thus revealing its position in the SE image. However there are many difficulties likely with such an approach, including:

- Etching must be either continuous or frequently repeated, otherwise grain boundaries that have moved will not be revealed promptly in their new positions.
- Etched positions no longer occupied by grain boundaries would retain their etched topography, leading to difficulty in interpreting the images.
- Handling of corrosive gasses in ESEM is possible, but highly problematic.
- A suitable etching atmosphere is very unlikely to be an efficient imaging gas.
- The development of a suitable gaseous etchant mix would be time consuming, particularly given that changes in specimen temperature will cause changes in etchant effect, potentially demanding a range of different mixes during just one experiment.
- Continuous exposure to an etchant would probably lead to an invidious choice of allowing excessive attack at stationary or slowly moving boundaries or tolerating only minimal attack on the most mobile boundaries.
- Undesirable pitting attack on the grain bulk is also possible.

- Unless the reaction product of the gas and the specimen is also gaseous, the surface is likely to become progressively obscured by deposits of corrosion product.

The above properties are highly unlikely to be available from any non-toxic gas, therefore, this approach was thus "put on the back burner".

The classical method of revealing grains in the SEM is by backscattered electron channelling contrast imaging (as discussed in the literature review, Chapter 2). Therefore, it was decided to either develop some means of protecting the backscatter detector from photon radiation or develop some different means of detecting backscattered electrons. This process is described in detail below.

Imaging of grains by Focussed Ion Beam channelling contrast was also considered. A "FIB" instrument is analogous to an SEM, but the electron beam is replaced by a beam of positive ions, usually Gallium. The images produced show very strong channelling contrast, probably due to the difference in ease of passage of the ions with changing angle of incidence to the crystal lattice, relative to the ease of passage of an electron in a channelling/non-channelling situation. Electrons pass easily through an atomic lattice, even when it is oriented for minimum channelling, thus when they are travelling in a channelling direction their even easier passage makes relatively little difference. However, ions (e.g. Ga+) are much larger and will not pass so easily through a given lattice, thus a change in angle of incidence to a channelling direction will probably have a much more profound effect on the ease of passage of the ions. This would profoundly affect their depth of penetration and hence the detectable emitted species (principally SE in the case of incident ions).

This strong channelling contrast makes FIB instruments extremely attractive for grain network imaging applications, and they are indeed in active use for such investigations (Fibics Incorporated, 2001, Blamire et al. 2001). However, the fact that the channelling contrast information in a FIB instrument is primarily carried by secondary electrons means that, at and above temperatures at which thermionic emission of electrons of similar energy to SE is common, it will be impossible to discriminate between SE and thermionically emitted electrons. Imaging will rapidly become problematic as the detector starts to flood with the rapidly growing thermionic electron signal. Thus, while FIB instruments are (notwithstanding their high cost) highly attractive for the investigation of grain networks, their operation is likely to be limited to materials having a temperature range of interest below the thermionic emission level. In practice this level would be around 1000°C, and thus the lighter, lower melting point metals (which are the least promising in channelling/backscattered electron mode) would be the most attractive for hotstage FIB investigation. However, in the context of this project no FIB instrument was available, as they are costly. Thus, the combination of FIB and hot stage is as yet untried.

Returning to the backscattered electron development option, a parallel 2-pronged experimental approach was taken, with one series of experiments attempting to determine the ideal detector and microscope geometry to maximise grain-to-grain contrast and another attempting to develop a shielding or "light-proofing" technique.

3.4.2 BACKSCATTERED DETECTOR GEOMETRY AND SIZE

A conventional two-segment annular, polepiece-mounting backscattered electron detector (diode type) was mounted either in the "forward scatter" detector position, normally occupied by the EBSD camera or in its conventional zero-tilt position on the microscope polepiece.

3.4.2.1 DETECTOR IN "FORWARD SCATTER" POSITION

The forward scatter position was achieved very simply by temporarily mounting the detector on the "lens cap" of the EBSD, and driving the EBSD in towards the specimen. In this forescatter geometry, the detector was tried in two placements, approximately 100mm from the specimen and approximately 35mm from the specimen. Both were at the same take-off angle, of approximately 70° to the sample normal, and 140° to the incident beam. In the 35mm position the detector was also tried as-is and with a thick aluminium foil mask cutting the effective detector area by a factor of about eight. The detector was also rotated such that elements A+B lay vertically above one another or were horizontally positioned either side of the microscope axis. In all of the configurations used, the detector was tried with one and both elements active, and with both sum (A+B) and difference (A-B) signals used for imaging. Finally, a variety of scan speeds were trialled, as was averaging of 4 frames for the fastest scan rate.

The 70° tilted results showed that the detector at a 35mm distance, gave the best results in all modes and that the difference signal (A-B) mode gave marginally the best results. Of the single active element modes, the best results were generated from the masked detector, 35mm from the specimen i.e. a small-angle detector. This configuration is very similar to the fore-scatter detectors used in combination with many EBSD systems, which utilise relatively small detector areas (typically squares or circles about 1cm across), placed at the edge of the EBSD screen, i.e. in close proximity to the specimen and at about 85° to the specimen. No difference was found between the geometries "A+B vertically one above the other" and "A+B horizontally positioned either side of the microscope axis".

The key results of these trials are illustrated on the following pages, in figures 15-18 (detector 100mm from specimen), figures 19-22 (detector 35mm from specimen) and figures 23-26 (small detector 35mm from specimen). Fig. 27(a) shows the experimental setup within the microscope chamber, and figs. 27(b) and (c) show the detector (large area and small area respectively). All geometry trials were undertaken in high-vacuum mode, for simplicity, repeatability and speed.

70° Tilt, 100mm Detector-to-Specimen

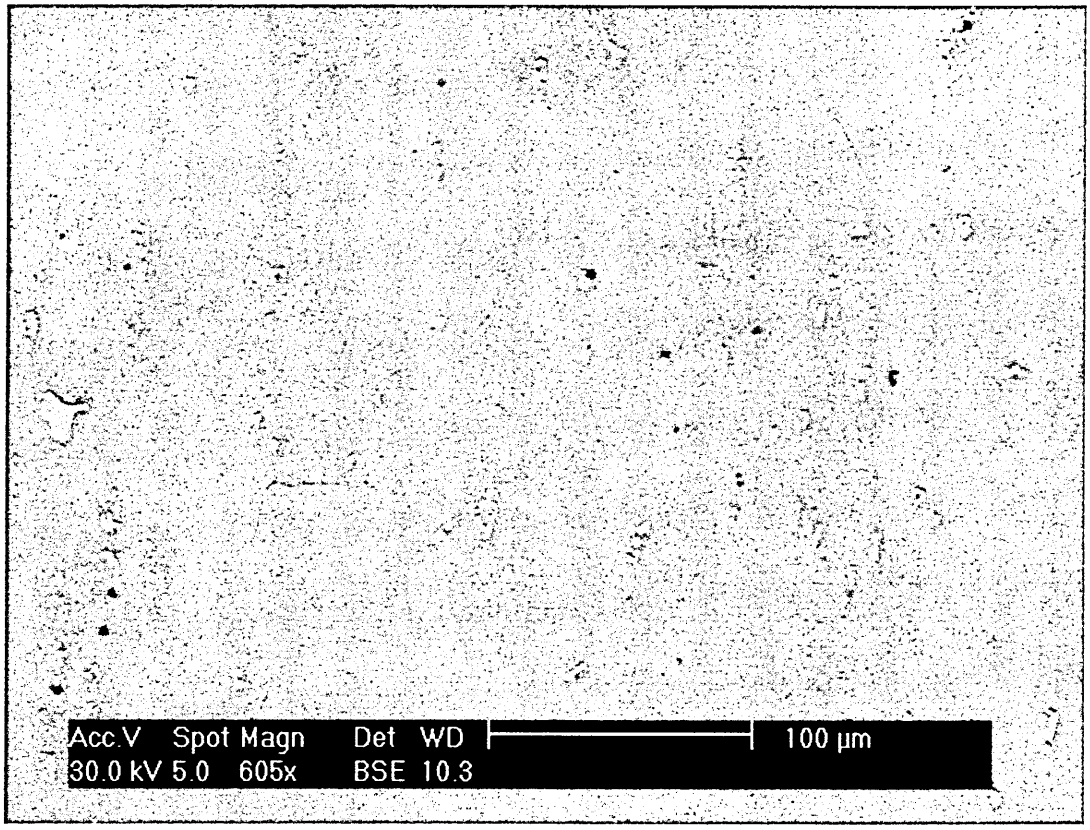

FIG. 15. Polished 1050 aluminium specimen tilted to 70°, imaged with BSE detector at 140°, 100mm from specimen, signal from segment A only.

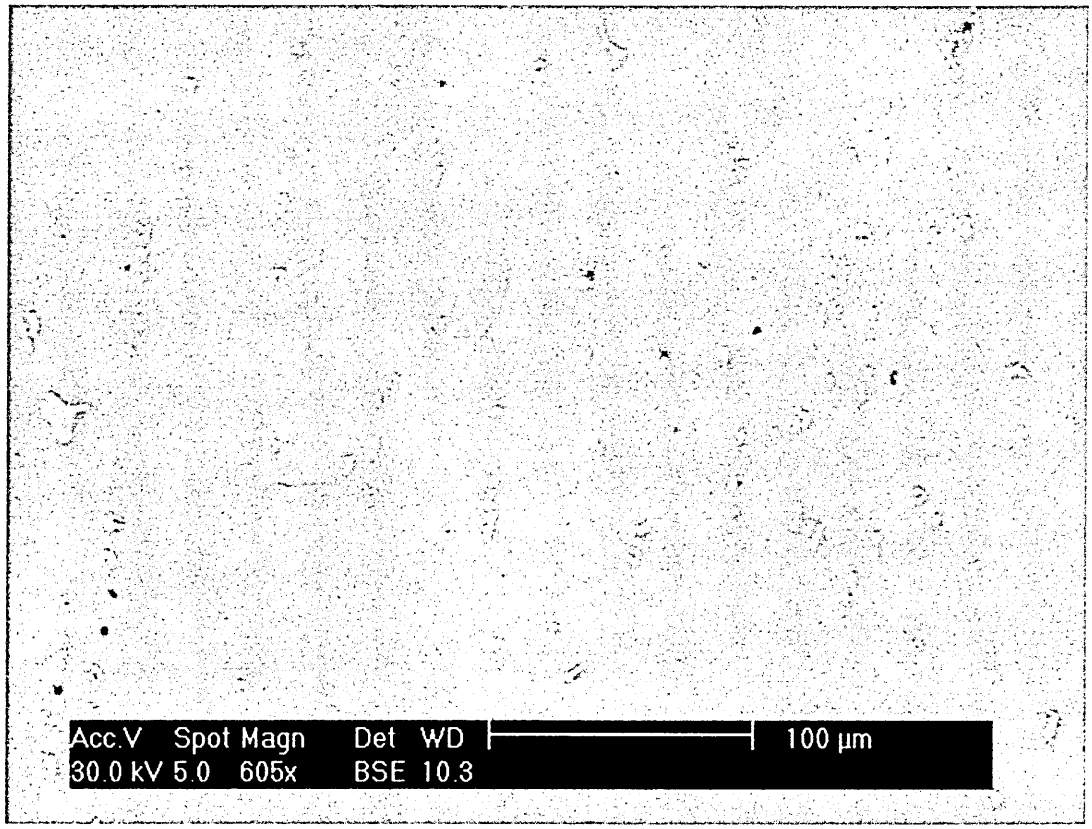

FIG. 16. Polished 1050 aluminium specimen tilted to 70°, imaged with BSE detector at 140°, 100mm from specimen, signal from segment B only.

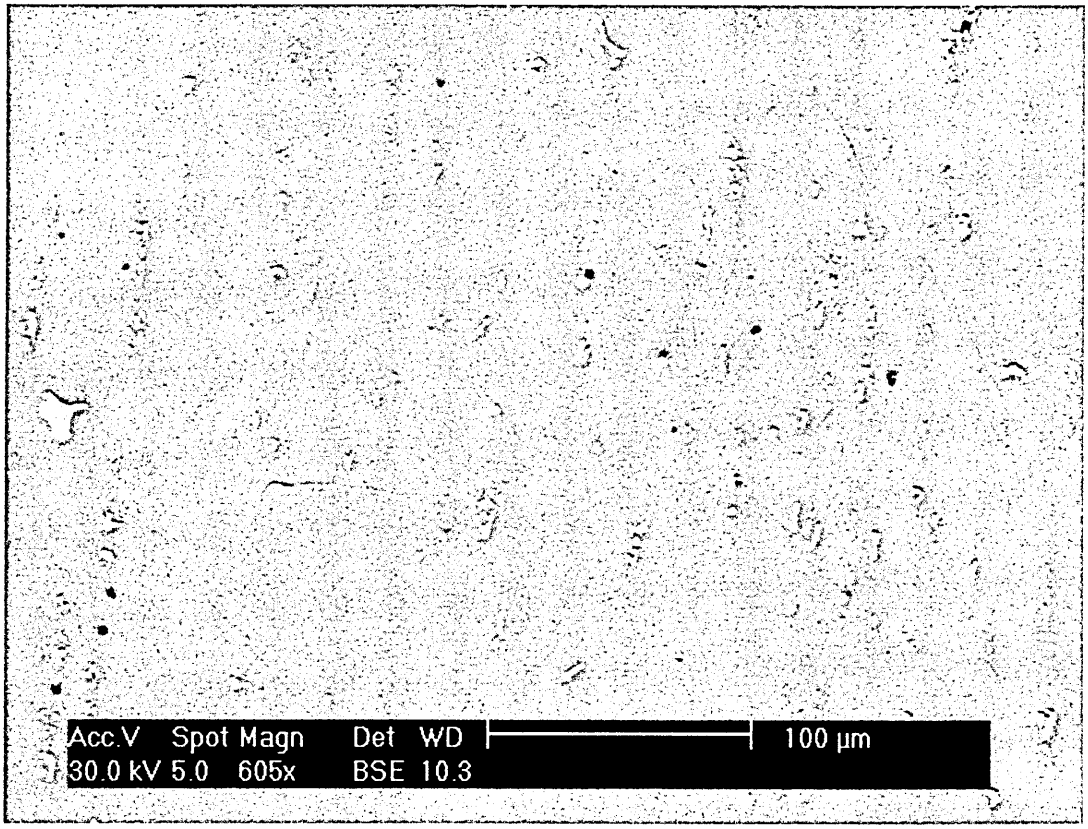

FIG. 17. Polished 1050 aluminium specimen tilted to 70°, imaged with BSE detector at 140°, 100mm from specimen, summed signal from segments A+B.

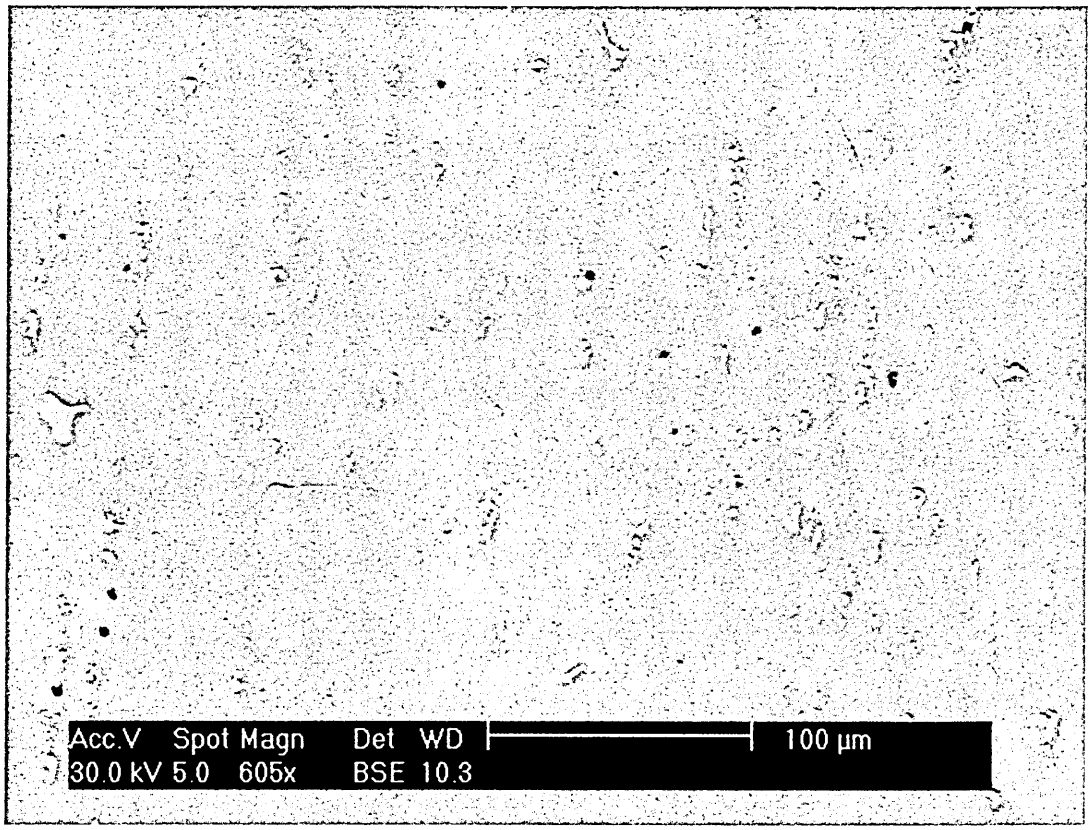

FIG. 18. Polished 1050 aluminium specimen tilted to 70°, imaged with BSE detector at 140°, 100mm from specimen, difference signal from segments A-B.

70° Tilt, 35mm Detector-to-Specimen

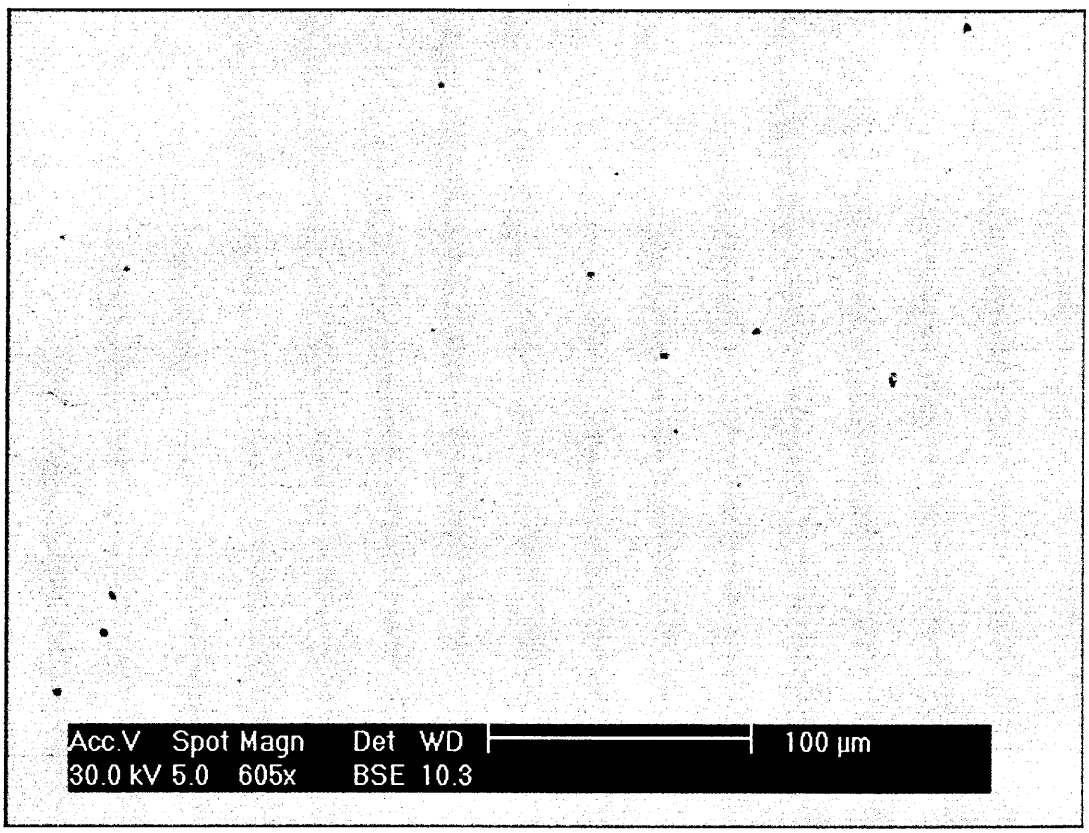

FIG. 19. Polished 1050 aluminium specimen tilted to 70°, imaged with BSE detector at 140°, 35 mm from specimen, signal from segment A only.

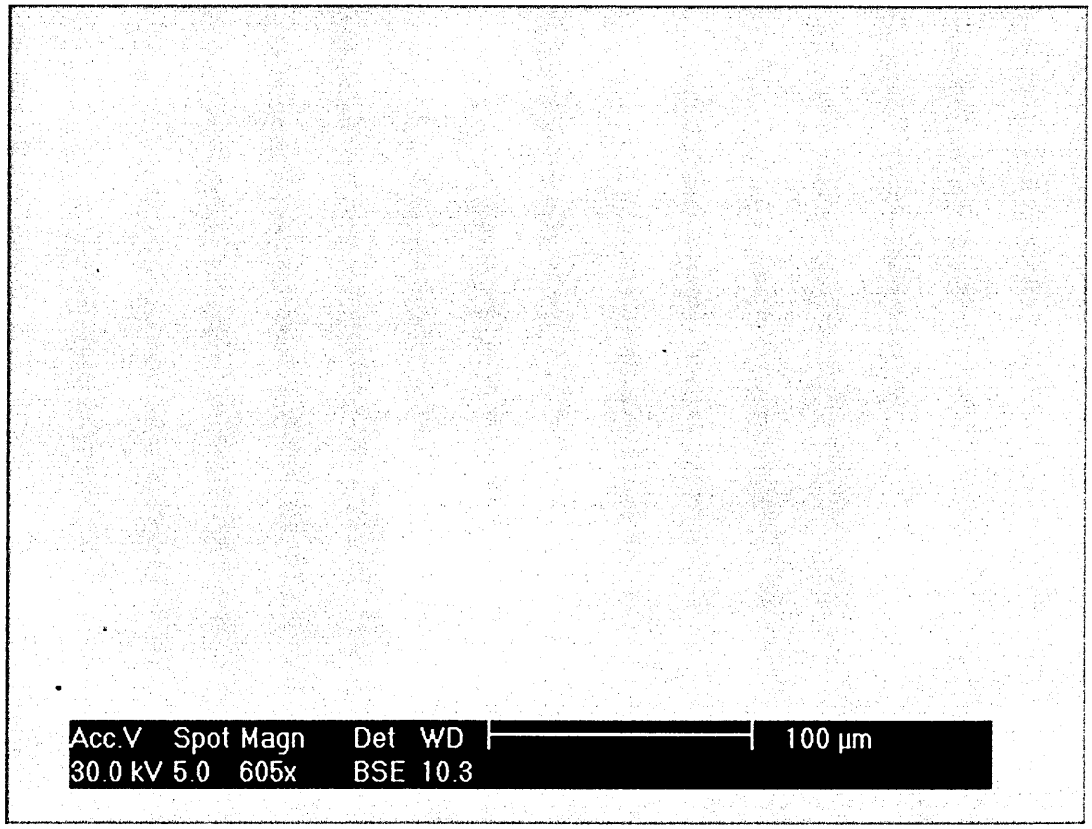

FIG. 20. Polished 1050 aluminium specimen tilted to 70°, imaged with BSE detector at 140°, 35 mm from specimen, signal from segment B only.

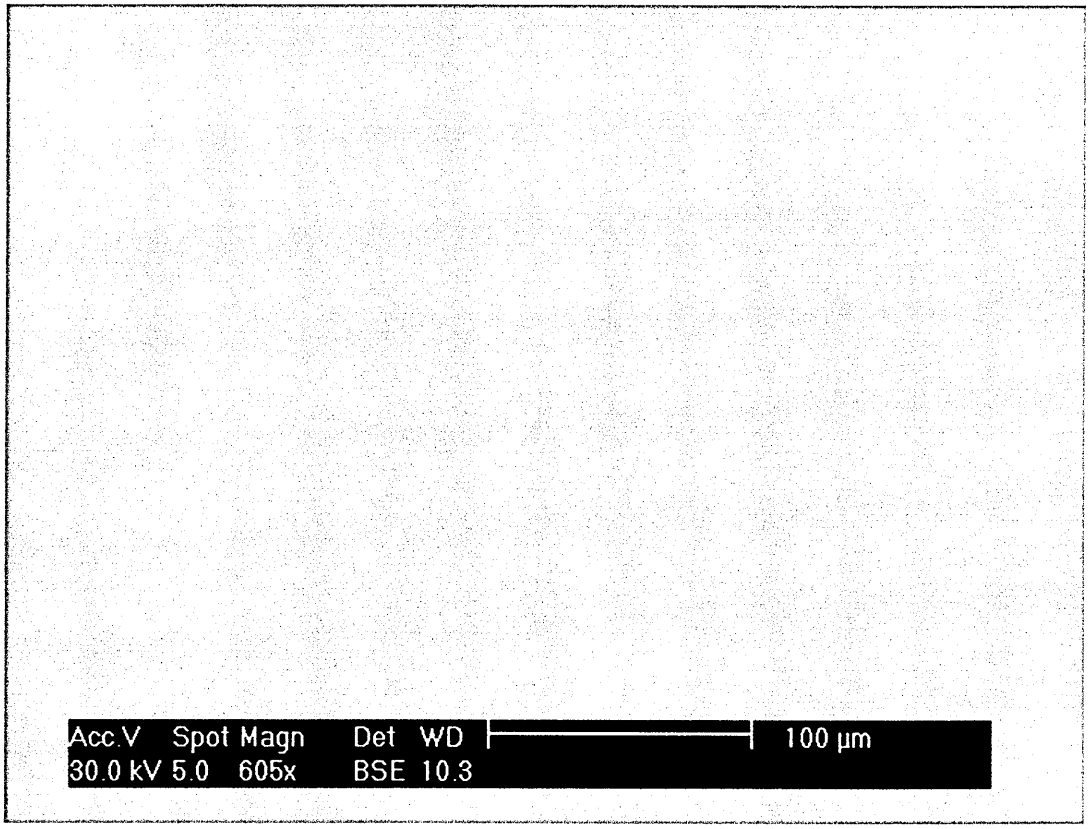

FIG. 21. Polished 1050 aluminium specimen tilted to 70°, imaged with BSE detector at 140°, 35 mm from specimen, summed signal from segments A+B.

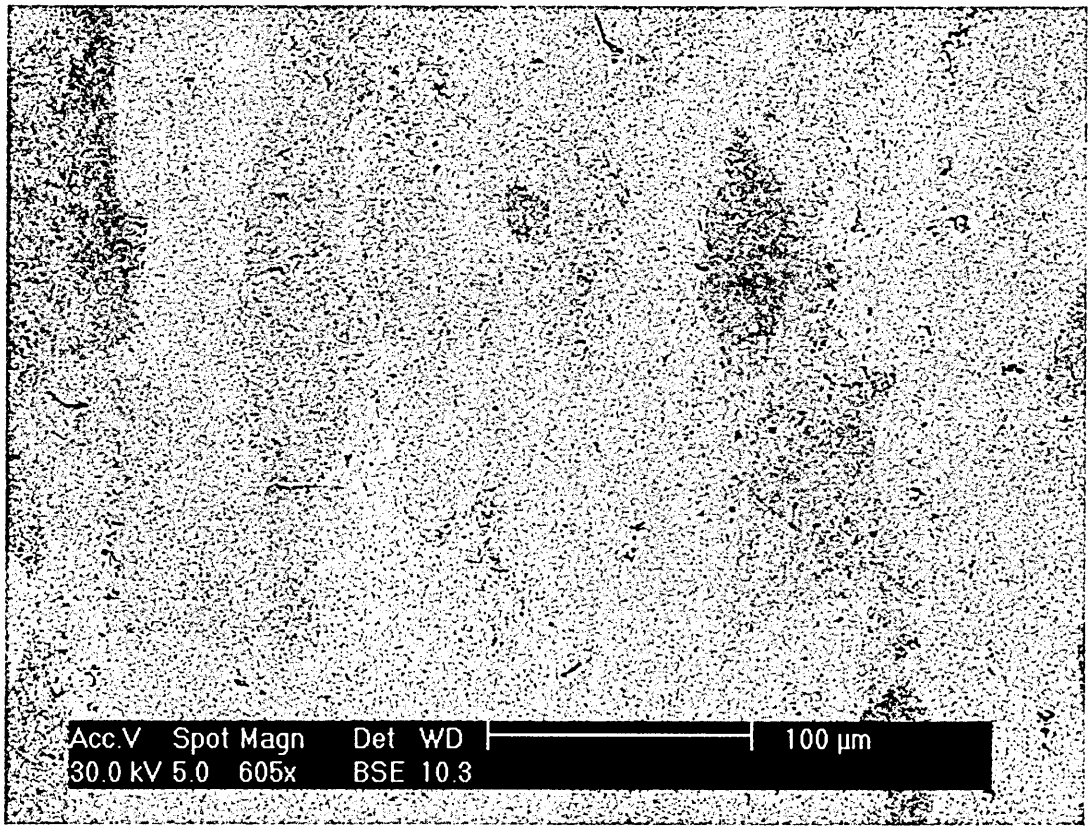

FIG. 22. Polished 1050 aluminium specimen tilted to 70°, imaged with BSE detector at 140°, 35 mm from specimen, difference signal from segments A-B.

70° Tilt, 35mm Detector-to-Specimen, Reduced Detector Area

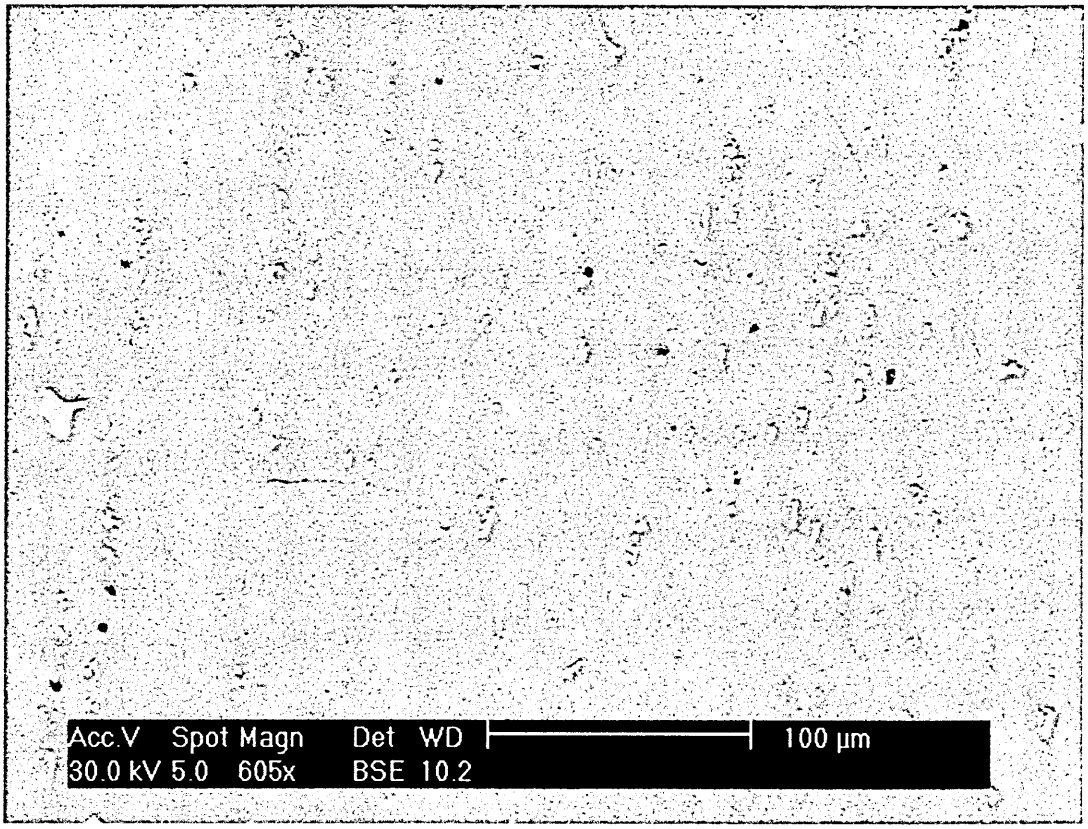

FIG. 23. Polished 1050 aluminium specimen tilted to 70°, imaged with masked BSE detector at 140°, 35 mm from specimen, signal from segment A only.

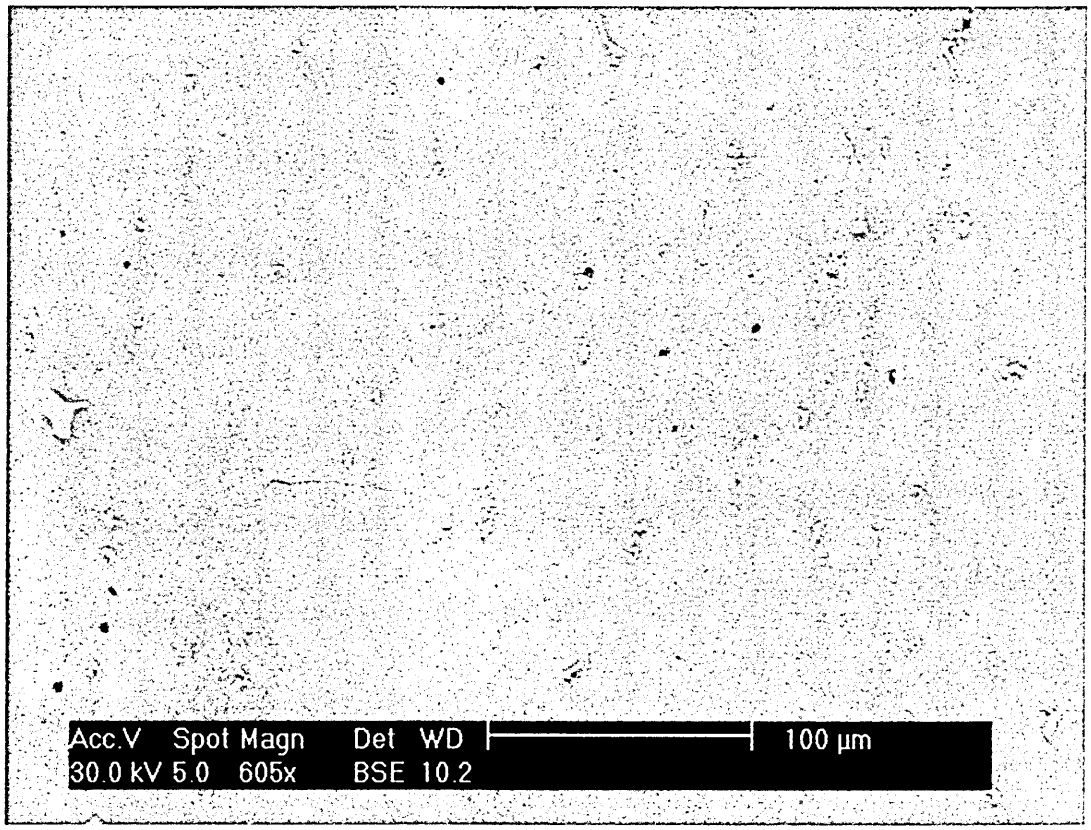

FIG. 24. Polished 1050 aluminium specimen tilted to 70°, imaged with masked BSE detector at 140°, 35 mm from specimen, signal from segment B only.

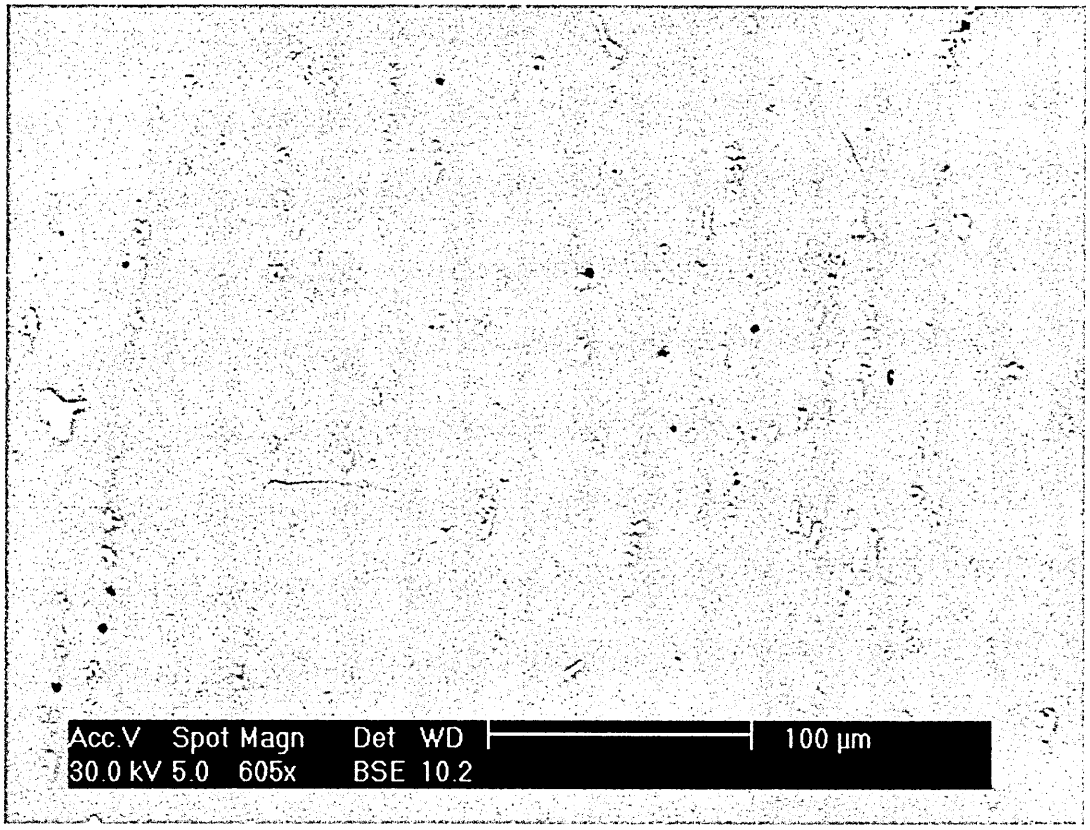

FIG. 25. Polished 1050 aluminium specimen tilted to 70°, imaged with masked BSE detector at 140°, 35 mm from specimen, summed signal from segments A+B.

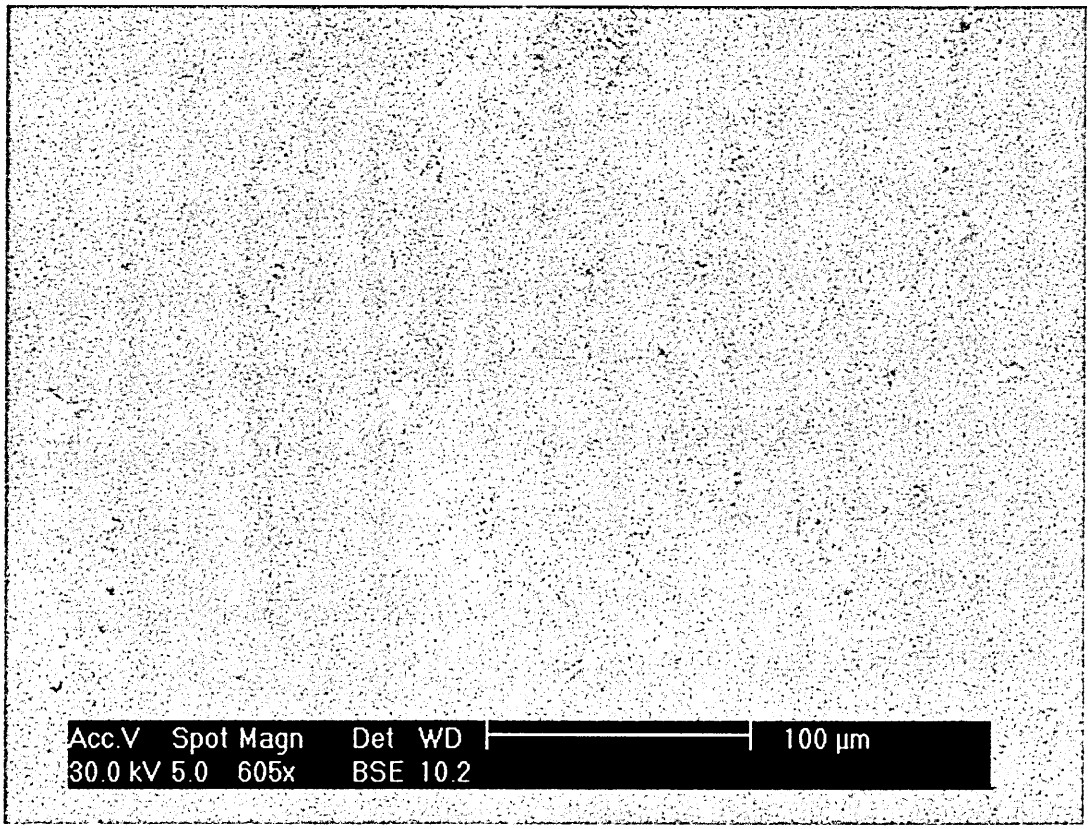

FIG. 26. Polished 1050 aluminium specimen tilted to 70°, imaged with masked BSE detector at 140°, 35 mm from specimen, difference signal from segments A-B.

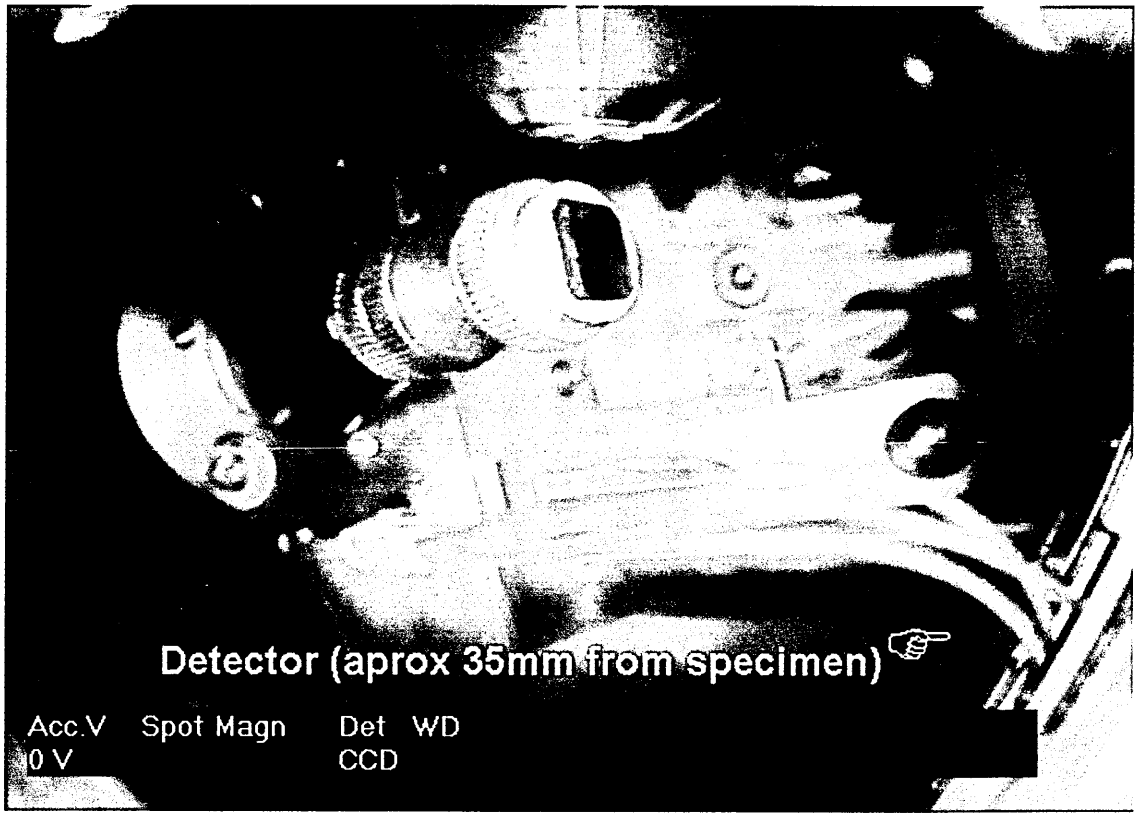

FIG. 27 A. Chamberscope image of sample and detector in 70° geometry set up.

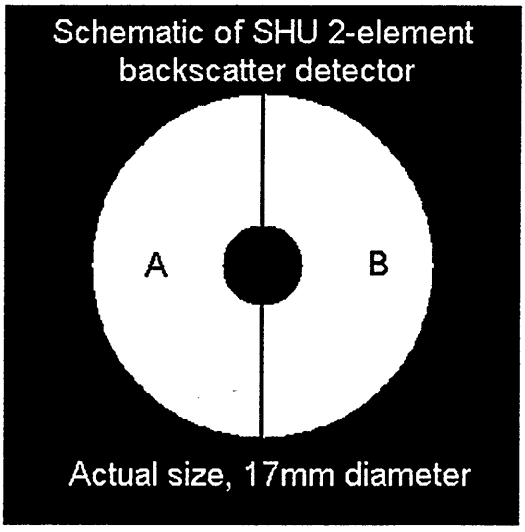

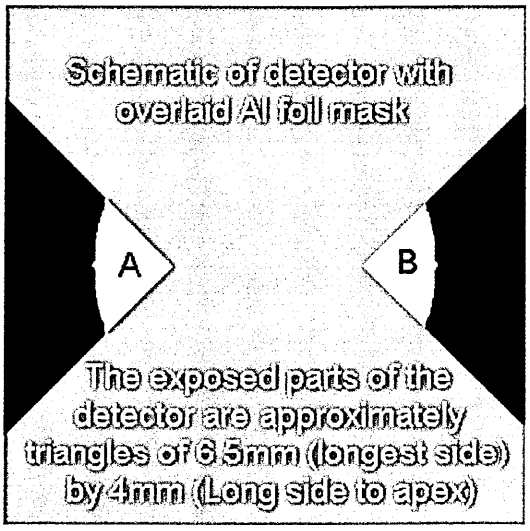

FIG. 27 B & 27 C. Detector schematics: b) unmasked and c) masked

The detector used was a two-segment annular detector of 17mm diameter, approximately 106mm^2 per segment [fig. 27]. At 100mm from the specimen, the full 212mm^2 area would correspond to a solid angle of about 10°, half of it about 5°. At 35mm from the specimen, the full area would correspond to about 25°. Each 6.5X4mm element of the masked detector at 35mm would correspond to about 8°.

Comparison of figs 15, 16, 19, 20, 23 & 24 suggests that the single active element at 100mm (approximately equal to 5° solid angle) is simply receiving too little signal to

be useful. Comparison of Figs 17 (100mm A+B) and 21 (35mm A+B) shows the loss of contrast that can occur with increasing detector area from a small solid angle to a modest solid angle.

Comparison of 22 (35mm A-B) with 26 (35mm masked A-B) shows the change in "difference" contrast between a pair of relatively large area detectors and a pair of relatively small area detectors. Fig. 22 shows a greater range between light and dark, while 26 seems to show slightly less noise and slightly more detail in some grey areas that appear uniform in fig. 22. Both images show some crystallites that are not visible, or are very difficult to discriminate in the other.

3.4.2.2 Detector in Zero-Tilt Position

These experiments were done in order to give some comparison of available image contrast between the 70° tilt position and the zero-tilt position and to investigate the effect of changing detector-specimen distance (i.e. changing solid angle). Again the "A+B" result was compared against the "A-B" result and the "A only" and "B only" results. "Masked" small detector areas were not tried in this configuration.

The same polished 1050 aluminium specimen was used, with the same accelerating voltage, aperture and "spot size". Again, the work was done in high-vacuum mode, for simplicity, repeatability and speed.

The configuration used for the 5mm specimen-detector test is shown as fig. 28. The key results are shown as figs. 29-42.

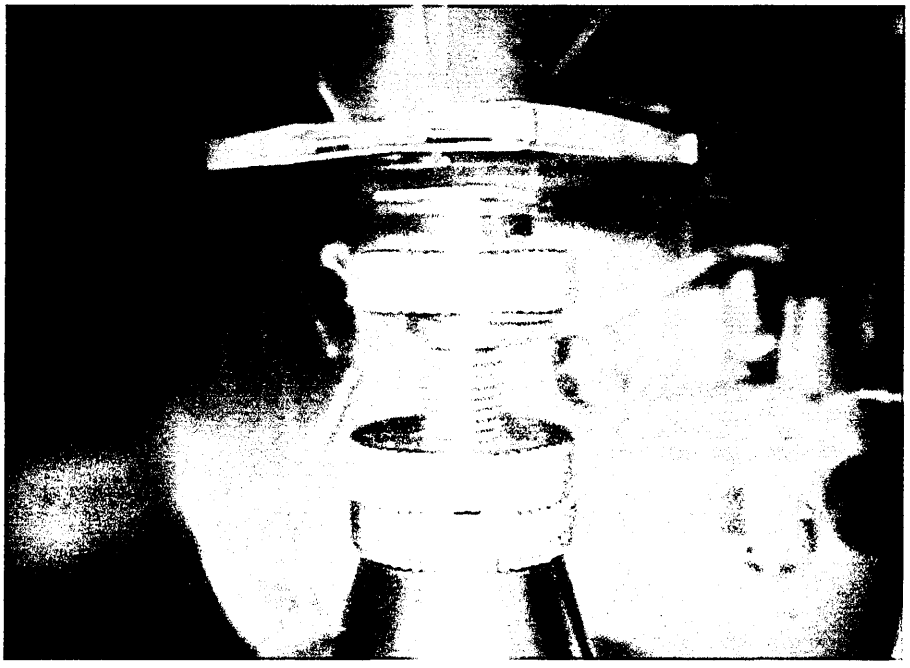

FIG. 28. Chamberscope image showing set-up for close-in zero-tilt tests

Polished 1050 Aluminium Specimen, imaged at 0° Tilt, Full Detector Area

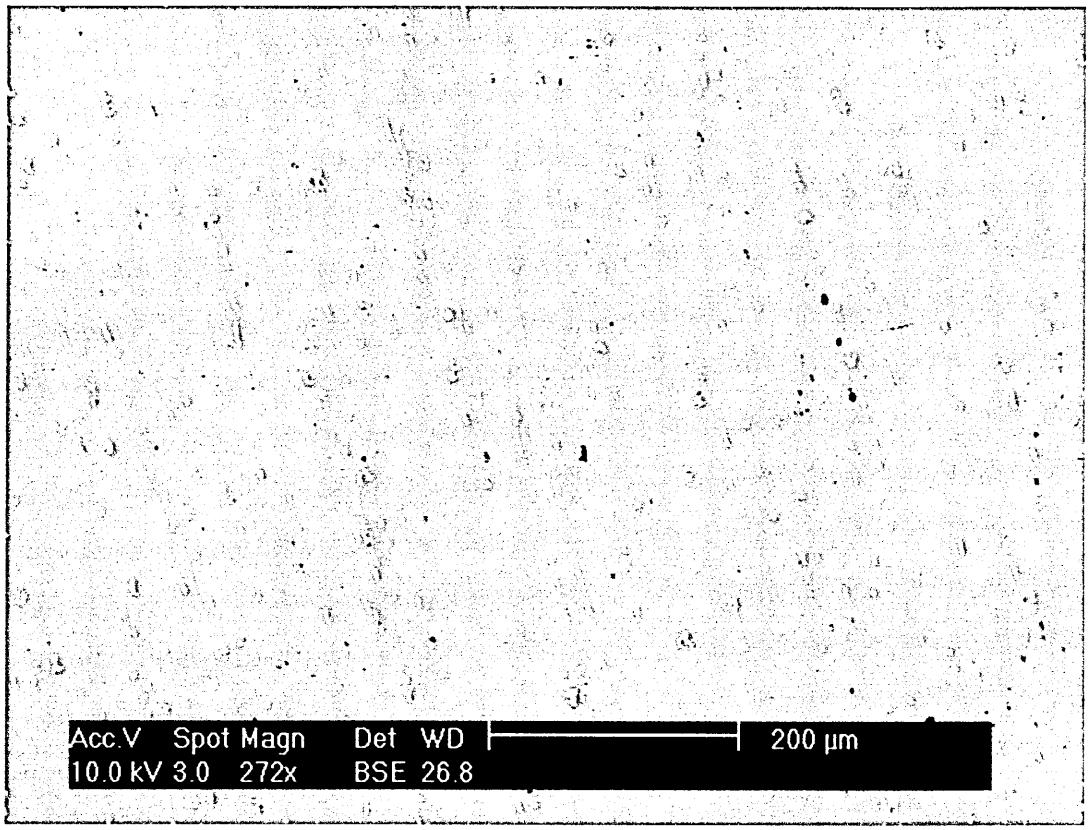

FIG. 29. Zero-tilt, 27mm specimen-to-detector, signal from segment A only.

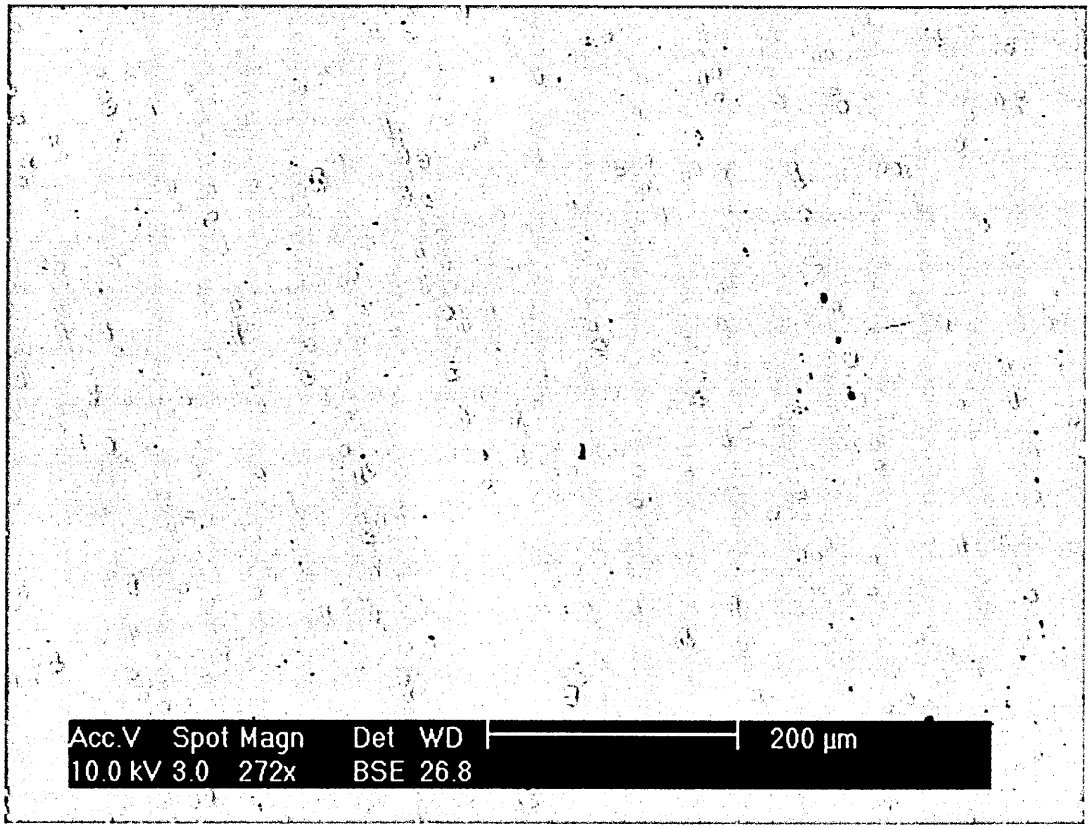

FIG. 30. Zero-tilt, 27mm specimen-to-detector, signal from segment B only.

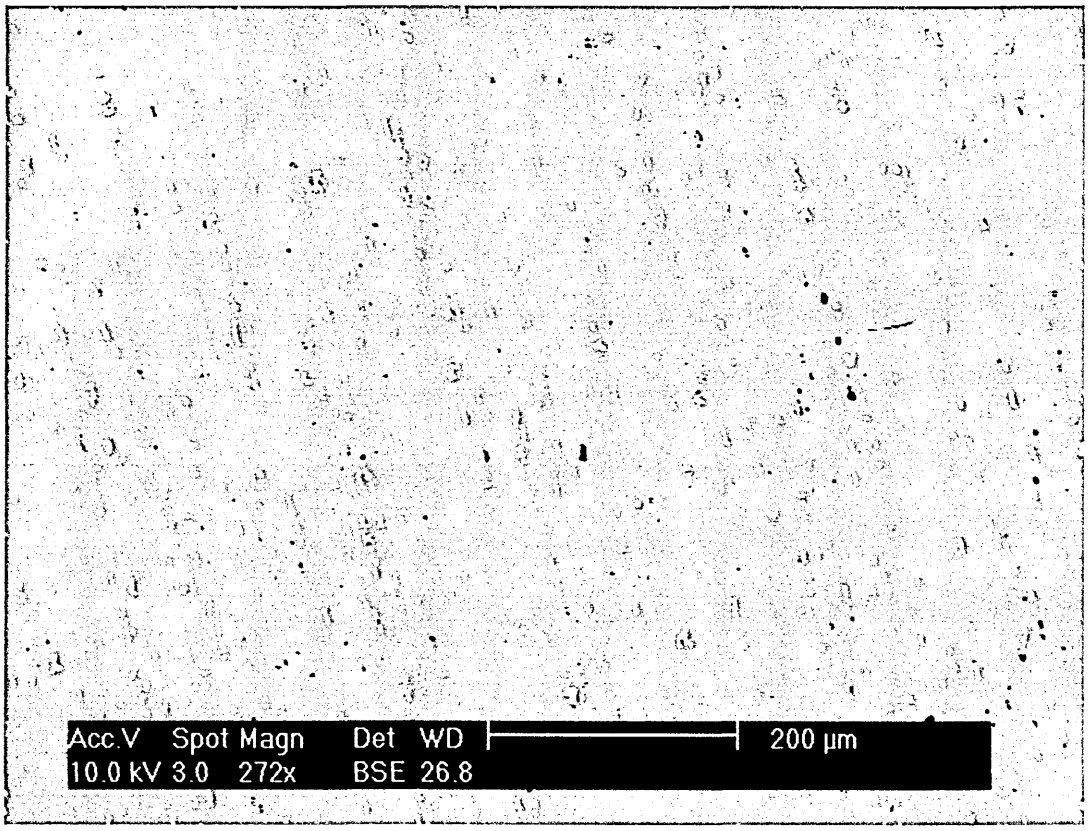

FIG. 31. Zero-tilt, 27mm specimen-to-detector, summed signal from segments A+B.

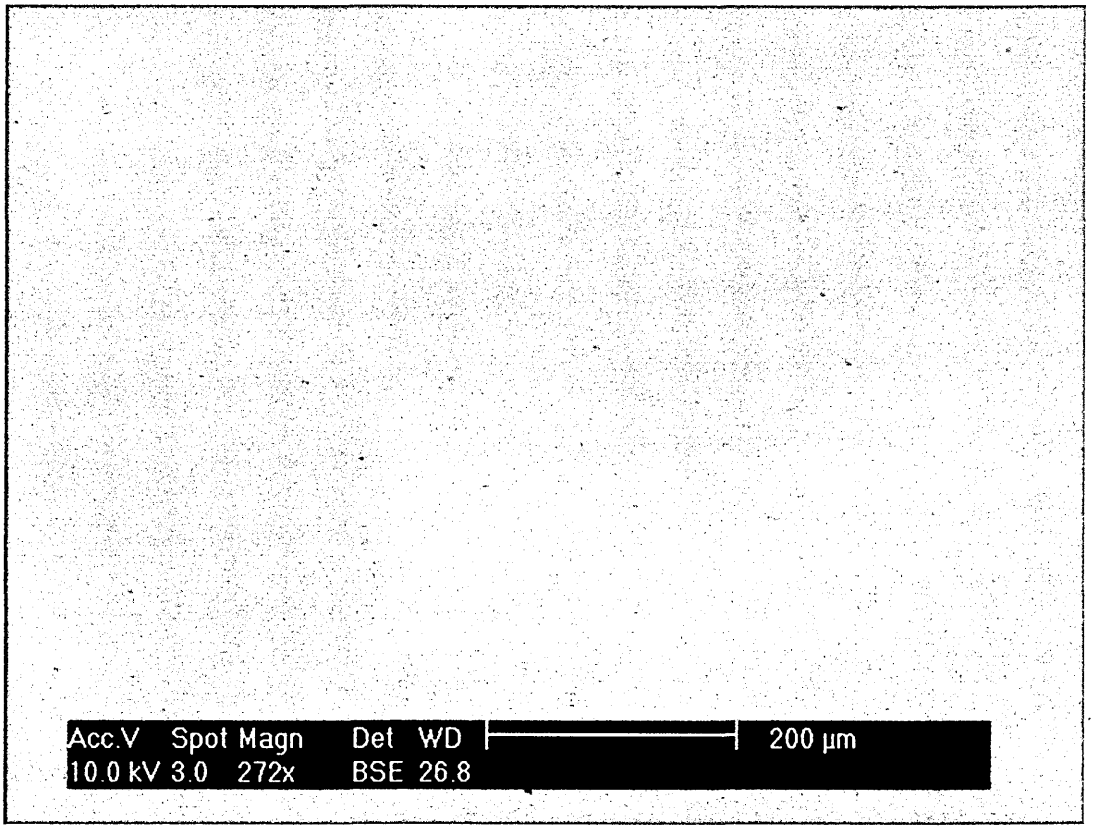

FIG. 32. Zero-tilt, 27mm specimen-to-detector, difference signal from segments A-B.

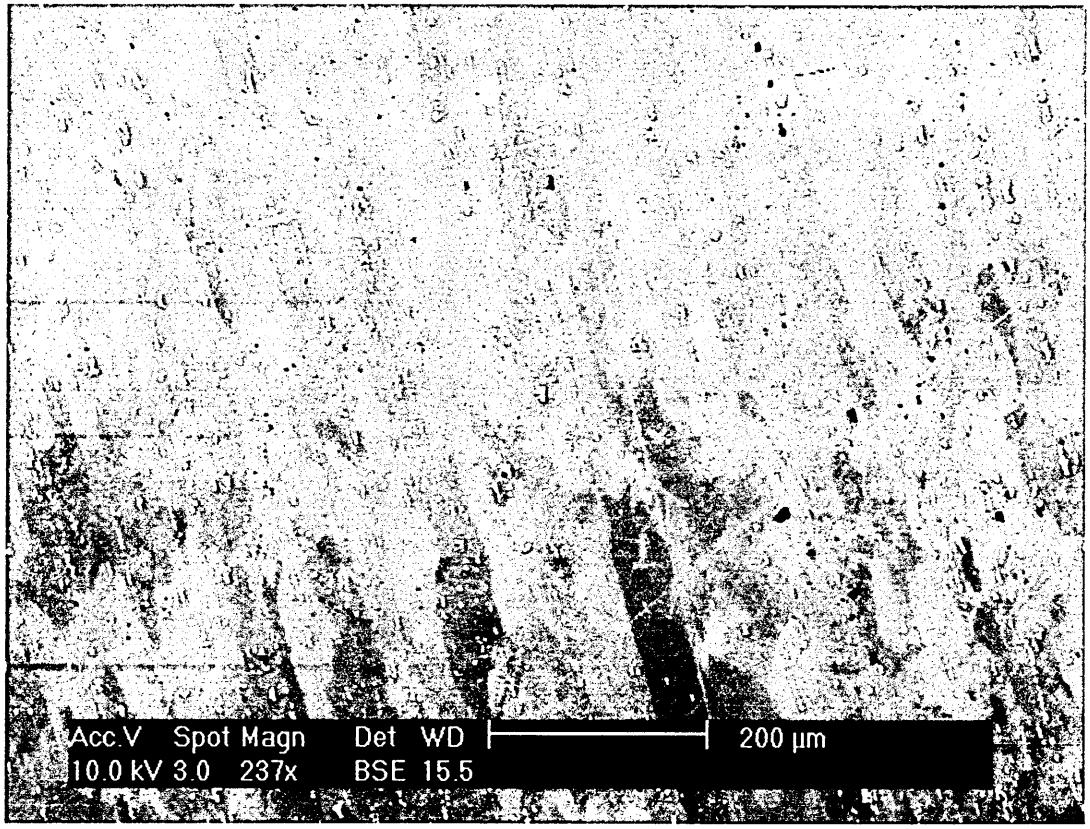

FIG. 33. Zero-tilt, 15mm specimen-to-detector, signal from segment A only.

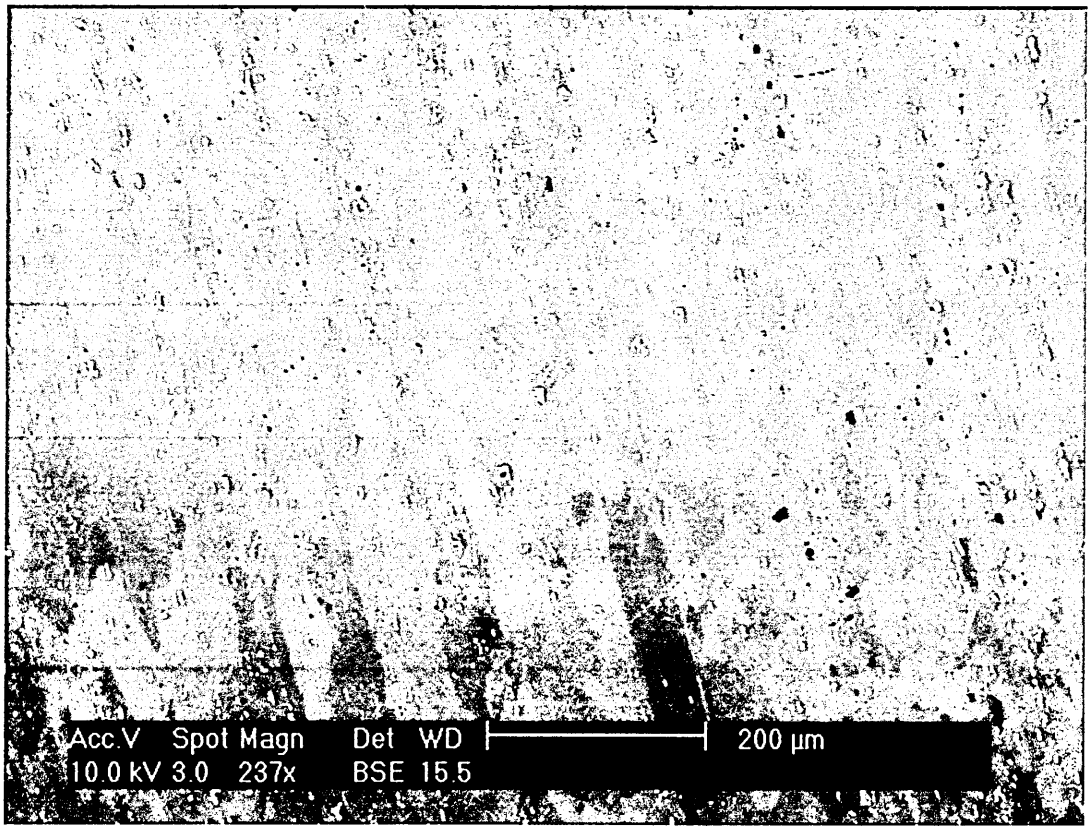

FIG. 34. Zero-tilt, 15mm specimen-to-detector, signal from segment B only.

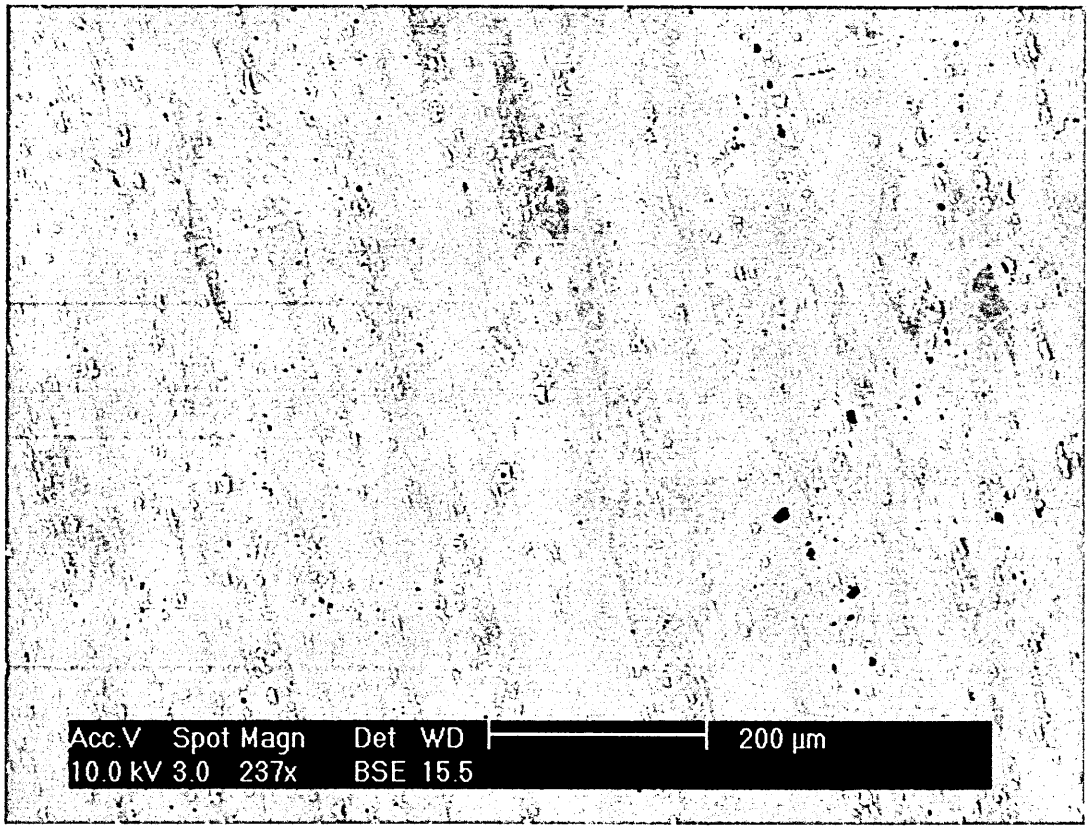

FIG. 35. Zero-tilt, 15mm specimen-to-detector, summed signal from segments A+B.

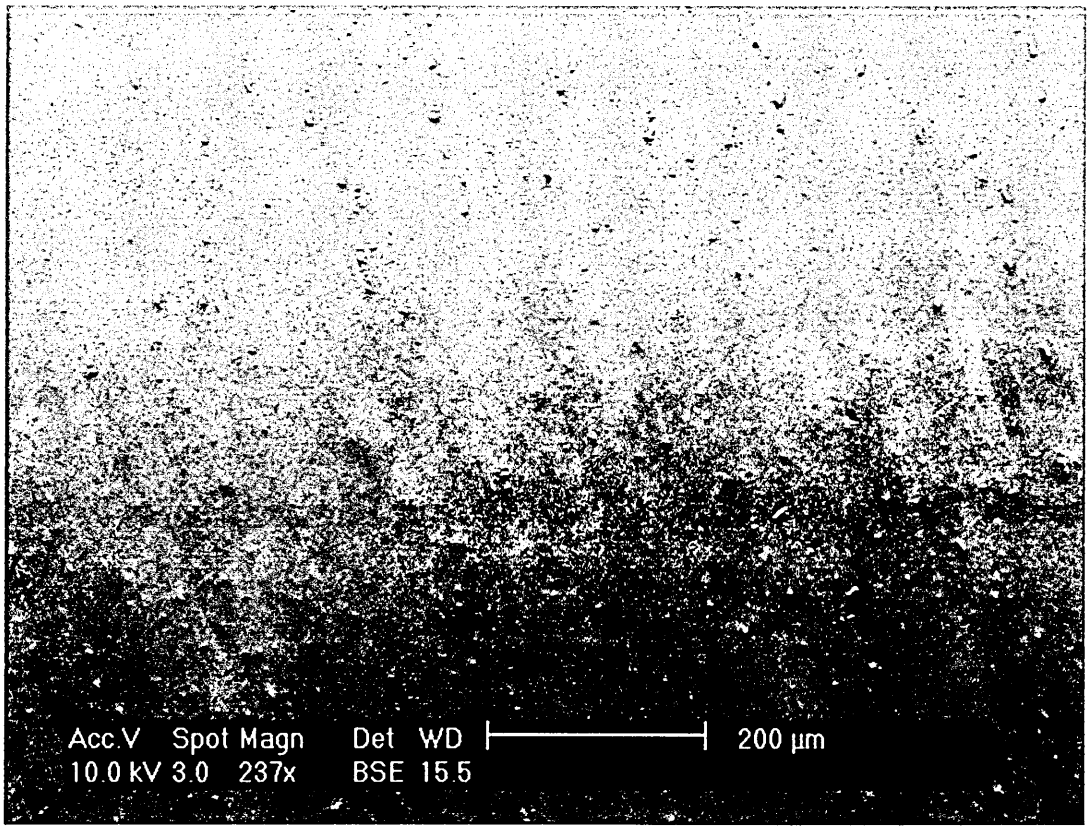

FIG. 36. Zero-tilt, 15mm specimen-to-detector, difference signal from segments A-B.

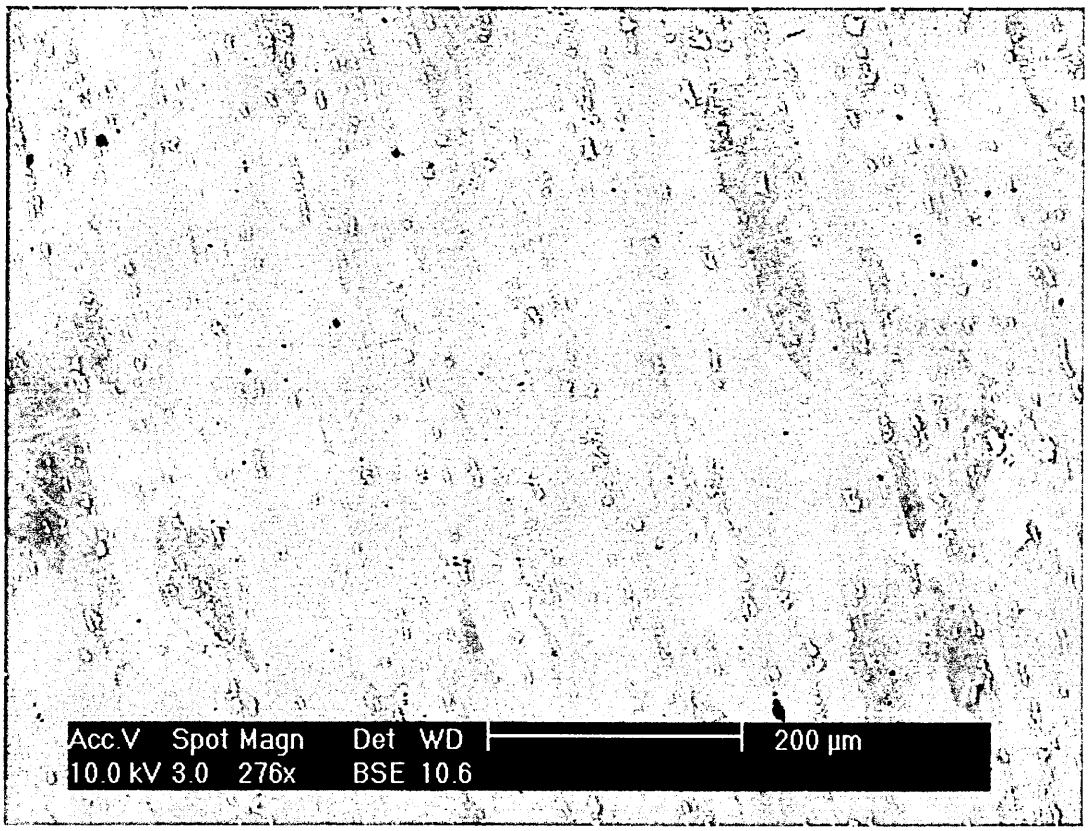

FIG. 37. Zero-tilt, 10mm specimen-to-detector, summed signal from segments A+B.

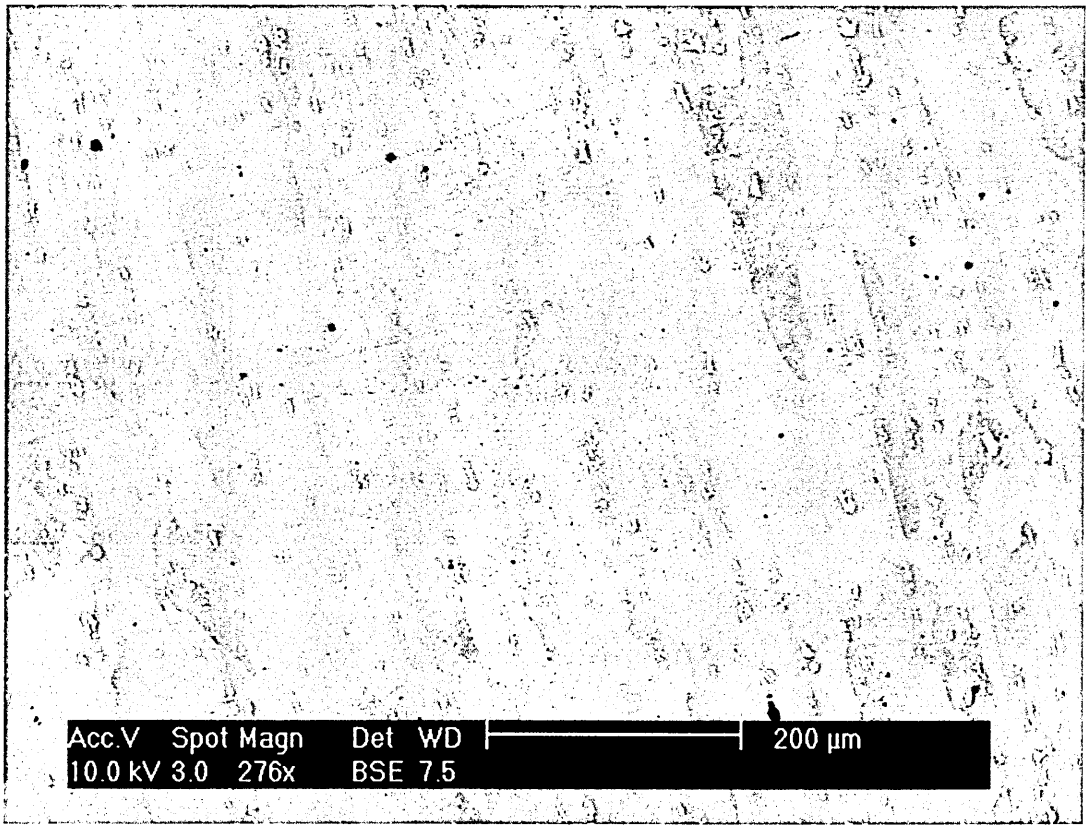

FIG. 38. Zero-tilt, 7.5mm specimen-to-detector, summed signal from segments A+B.

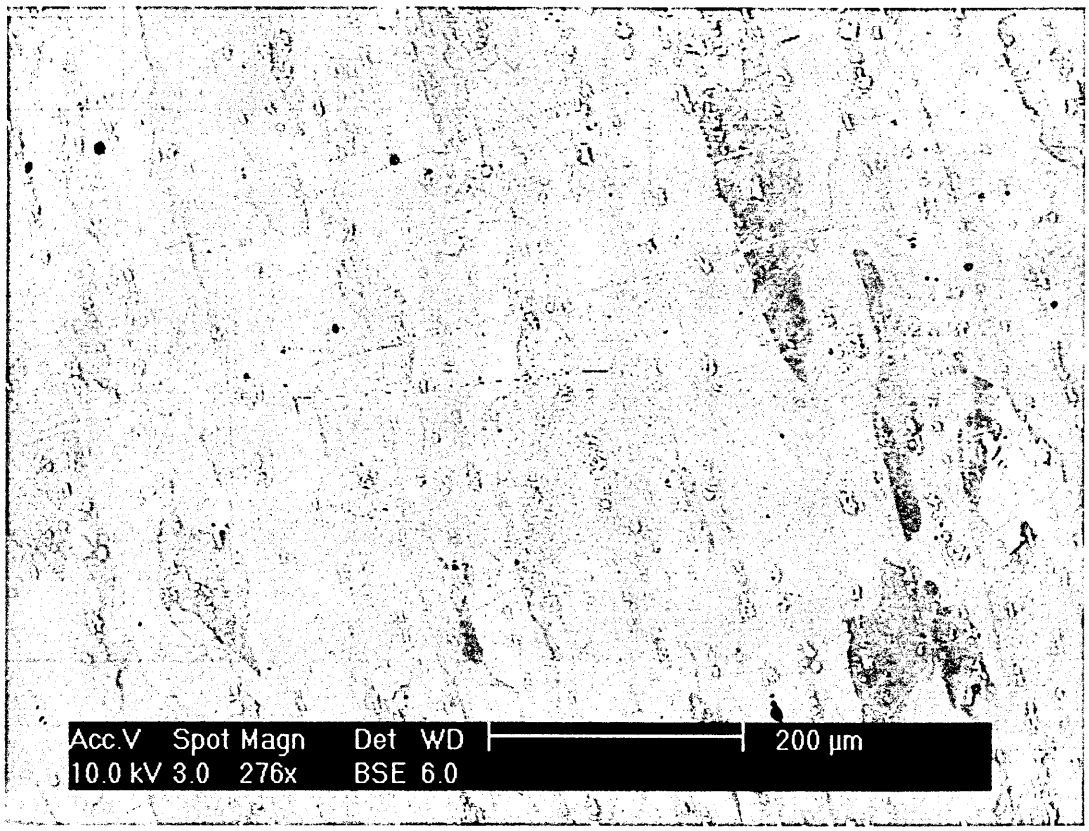

FIG. 39. Zero-tilt, 6mm specimen-to-detector, summed signal from segments A+B.

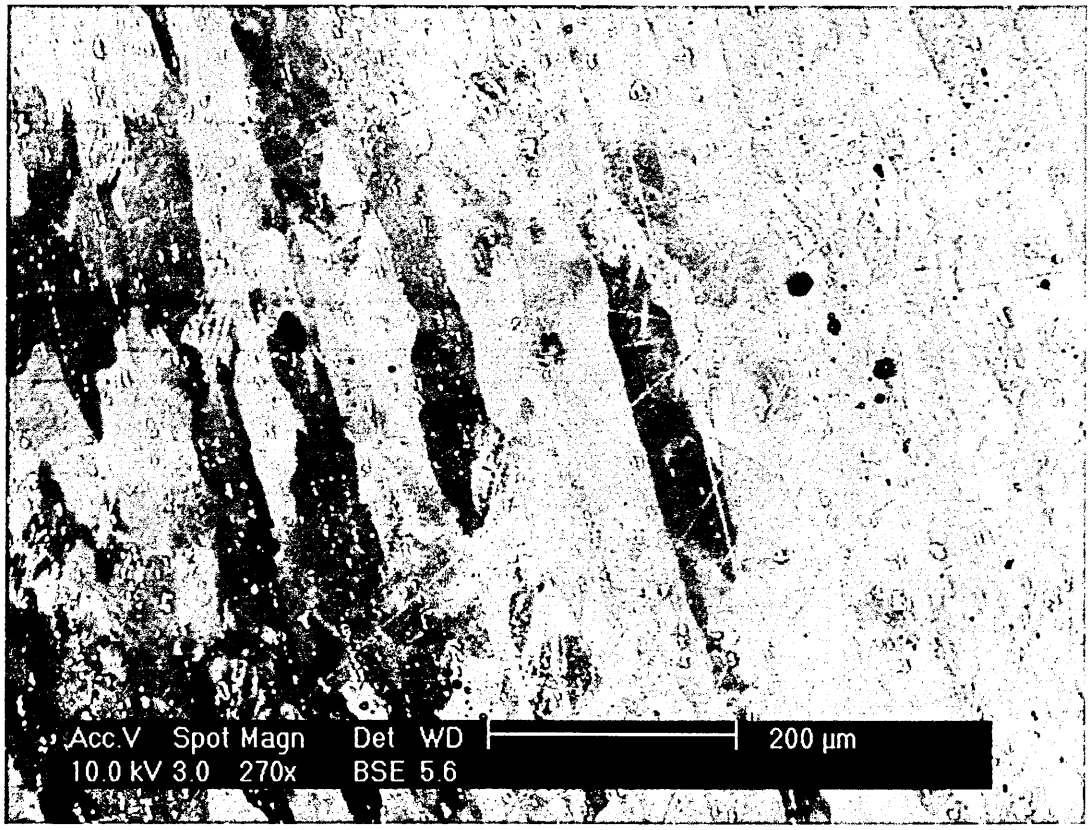

FIG. 40. Zero-tilt, 5mm specimen-to-detector, summed signal from segments A+B.

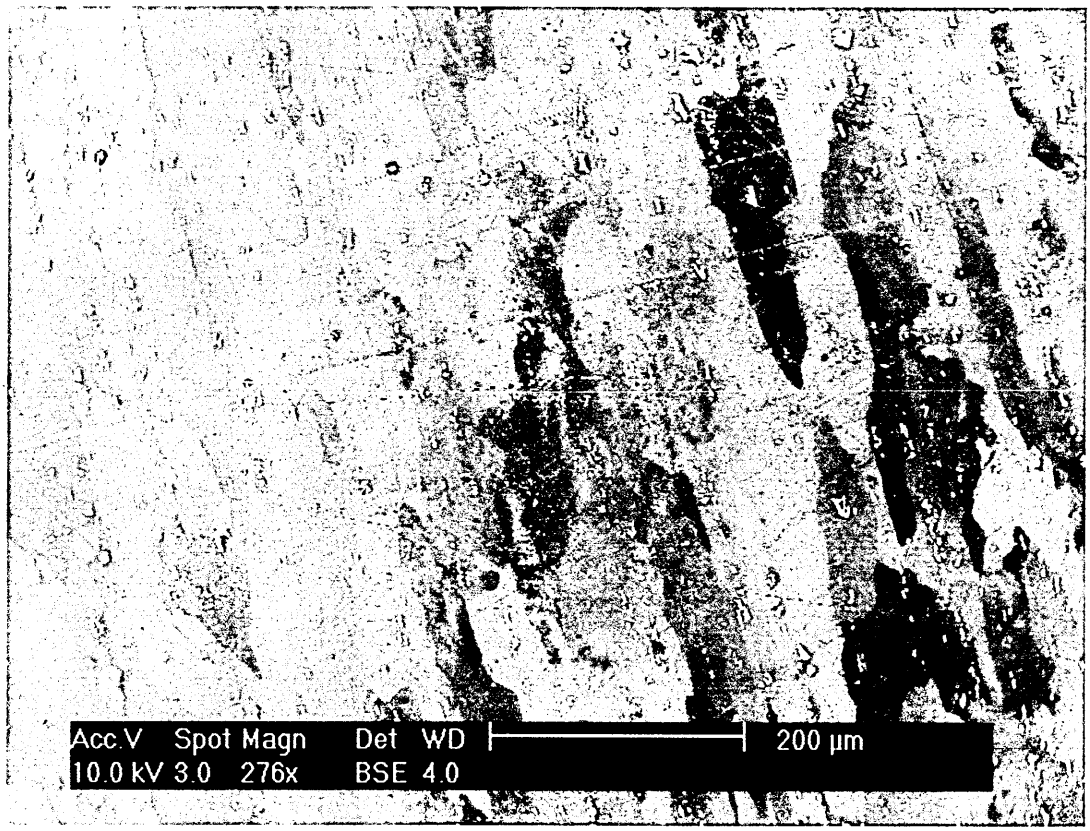

FIG. 41. Zero-tilt, 4mm specimen-to-detector, summed signal from segments A+B.

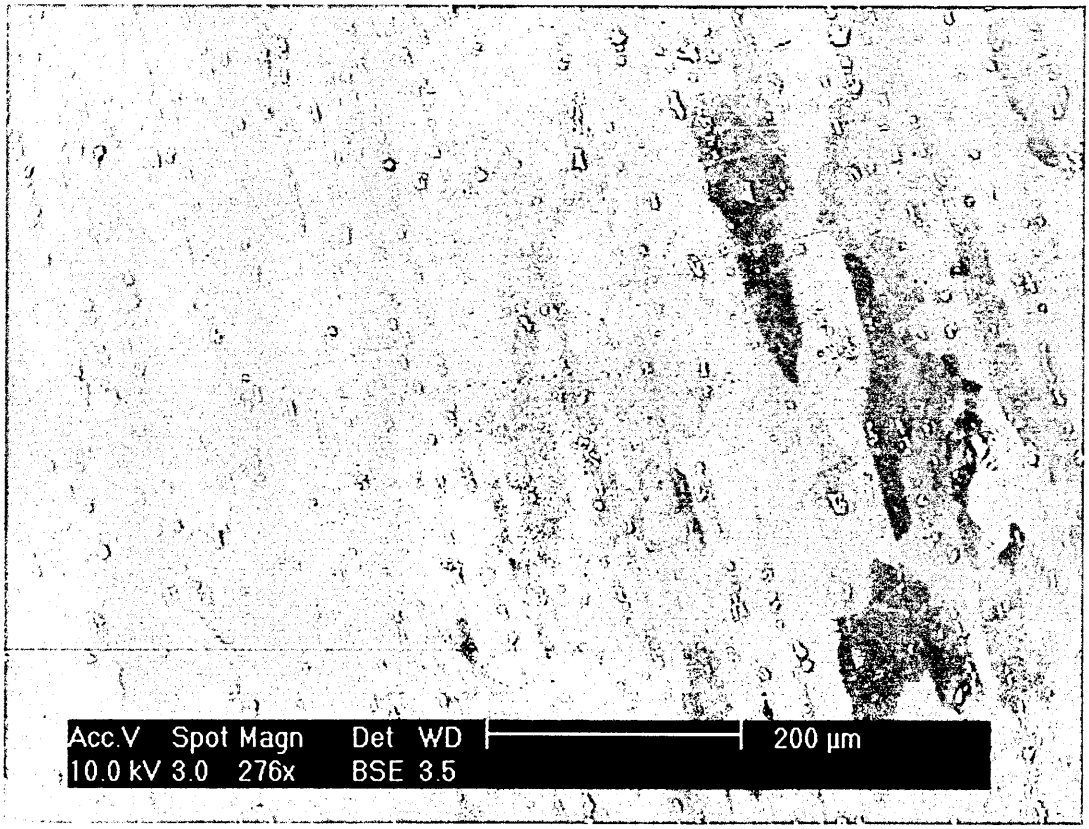

FIG. 42. Zero-tilt, 3.5mm specimen-to-detector, summed signal from segments A+B.

Clearly, the images taken at 27mm and 15mm specimen-to-detector distance show that the best results in this geometry are obtained from the A+B configuration – i.e. the largest possible effective detector area. Subsequent images show only the A+B result and show that contrast improves down to about 5mm and then degrades slightly. It is likely that below 5mm the proportion of BSE electrons passing through the hole in the middle of the annular detector is large enough to degrade the image quality. The clear conclusion is that for specimens at the zero-tilt geometry the ideal detector strategy is a single active detector area of maximum possible solid angle – ideally 180°.

Images taken at zero-tilt, while qualitatively quite similar to those at 70° tilt, are difficult to compare directly with the tilted, because the shortest easily practical detector-specimen distance in the tilted geometry (35mm) is considerably shorter than the longest distance possible at zero-tilt (27mm). However, in the zero-tilt geometry, best results were obtained from a small detector to specimen distance (5-10mm) and an additive (A+B) signal. It is clear from figs 32 & 36 that difference signals (i.e. EBSP "Kikuchi pattern" differences) are small in the zero-tilt geometry. It is clear from figs. 17 & 21 that the differences in overall backscatter signal (i.e. differences in η, the backscatter coefficient) are small in the 70° tilt geometry. That is to say, two strategies emerged for optimisation of orientation contrast images:

1) Small angle single detector -or- small multiple detectors some distance apart giving a difference signal from a specimen tilted to 70°. This corresponds to generating crystal-to-crystal contrast from the differing signal levels within the different electron backscatter patterns cast onto the detectors by different crystals and how they happen to fall on the active detector elements – i.e. the differing behaviour of backscattered electrons channelling/diffracting as they leave crystals with different lattice-to-detector orientations. This is sometimes called "channelling-out contrast".

2) A single large angle detector at the zero-tilt geometry, generating crystal-to-crystal contrast from the small changes in overall backscattering co-efficient (absorption) with beam/lattice orientation. I.E. differing electron behaviour on channelling in to crystals having differing lattice-to-beam orientations. Sometimes called "channelling-in contrast".

Approach 2, is close to Simkin's approach (see Chapter 2). This was chosen as the most practicable, because of the two hot-stages available, the stage with the highest temperature capability was very limited in its tilt capability. By contrast, the stage with the capability to be tilted to the 70° EBSD position had a more restricted temperature range ($\leq$ 700°C) and could not heat steel into its temperature range of interest, 725°C or more, the austenitic state.

3.4.3 HEAT/PHOTON EFFECTS ON THE ELECTRON DETECTORS

As discussed in the literature review, the only detector technologies readily commercially available to directly detect backscattered electrons are also photon sensitive (i.e. diodes, scintillator-photomultipliers). The "minority" technologies, the microchannel plate and its larger relative, the channeltron, are insensitive to infra-red and visible light but are sensitive to the UV that would be produced by "white-hot" specimens [Photonis, 2002]. This may or may not have prevented their successful use in this project, however, they also carry the disadvantages of high cost, high sensitivity to contamination (an almost inevitable consequence of hot stage use) and in the case of the channeltron, a physical size unlikely to be compatible with the available SEM. For all of these reasons, their potential was not explored in this project.

3.4.4 COATING/MASKING OF DIODE DETECTORS

Given the difference in electron penetration depth and photon penetration depth through certain light elements, it was considered likely that a photon-sensitive detector could be masked ("given sunglasses") with a film or layer opaque to photons but transparent to high-energy electrons.

The ideal coating or masking film would have the following properties:

- Opaque to photons
- Transparent to high-energy backscattered electrons
- Opaque to low-energy backscattered electrons and secondary electrons
- Vacuum compatible, stable on exposure to moderate heat and for storage
- Readily available as a thin coating or as a film

The first three properties would be available from a low (average) atomic number element (or compound).

Several candidate materials suggested themselves for a sputtered/PVD coating: beryllium, boron, carbon and aluminium. These are light elements, solid over a reasonable temperature range, chemically stable and not noted for transparency to photons.

Thin polymer films, probably with an additional coating or filler of one of the elements already discussed, were also considered.

Beryllium is attractive as the lowest Z solid element with any degree of chemical stability, but its slow surface oxidisation could cause problems, particularly in storage. Its metallic nature would be expected to give greater photon opacity than carbon, while its low Z and low density would give high electron transparency. Beryllium would be relatively

costly to acquire in the form of a sputtering target and would carry a significant toxicity risk if dusts or vapours were generated – highly probable with any PVD technique.

Boron has very attractive potential properties, but its actual properties would depend upon the degree of crystallinity that could be achieved in the coating.

Carbon is readily available as a coating and has the great advantage that it should be easily possible to remove it from detector diodes non-destructively in order to experiment with direct application and different coating depths. It has low Z and low density to give it high electron transparency, but, due to its lower conductivity/non-metallic nature, is more transparent to photons for a given electron signal loss compared to Boron and the metals. Unless stored under vacuum or similar conditions a carbon coat would be expected to degrade within a few days of application, requiring frequent removal and re-coating.

Aluminium offers long-term chemical stability, ready & cheap availability and ease of handling.

In anticipation of applying one or more of these coatings, a trial was conducted with a diode detector masked with a one-micron thick "Kapton®" (polyimide) polymer film, provided by DuPont. Imaging results were so disappointing [Fig 43] that further experimentation in this direction was suspended, pending the results of other approaches.

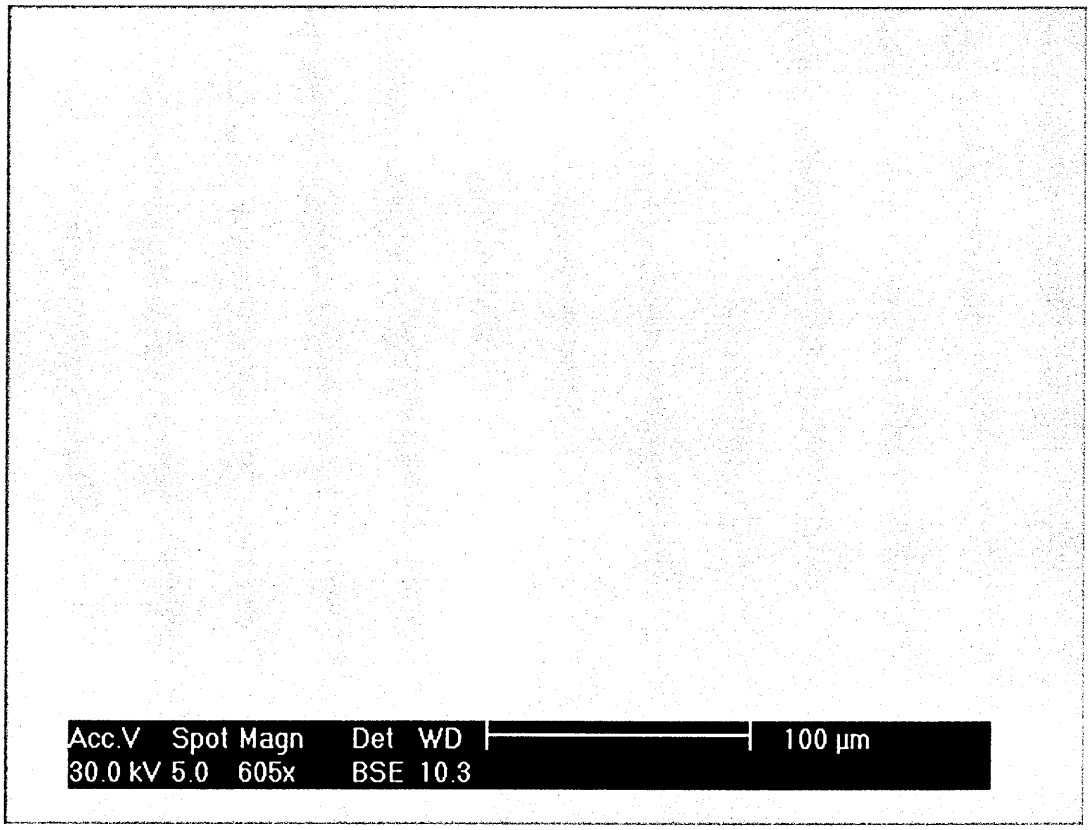

FIG. 43. 70° tilt, 35mm specimen-to-detector, detector screened with 1.0 µm Kapton polyimide film, difference signal from segments A-B.

Interestingly, after the problem had been solved, as described below, it was learned that the Liverpool geology group Seward et al. (2002) had independently conceived of the aluminised polymer film shield. They have achieved a useful extension to the temperature range of a semiconductor detector, from a limit of just under 450°C to just under 1000°C and some worthwhile results. However, the loss of electron signal in the film was such that required scan times were too long for the "real-time" ambition of this project and the probe energy was restricted to 15-20 KeV or above (Seward, 2003) – not ideal for channelling contrast.

3.5 DESIGN OF A DETECTOR INTRINSICALLY INSENSITIVE TO PHOTONS

An additional, in-depth literature search into backscattered/high-energy electron detection technologies revealed the converter plate (Reimer, 1998), developed by Moll et al. (1978) and Reimer & Volbert (1979). This was developed in the late 1970's and early 1980's as a cheap alternative to the "Robinson" scintillator-photo-multiplier detector and the then scarce semiconductor detectors. Although extremely cheap, it was very rapidly rendered almost entirely obsolete by the more expensive, but considerably more effective, semiconductor diode detectors – which became affordable and widely available in the early to mid 1980's.

A measure of the obscurity into which the converter plate has fallen in the intervening decades can be seen from the following: Reimer's own text book on SEM imaging physics devotes less than one of its 500+ pages to the converter plate. Another "standard" work on SEM, "Scanning Electron Microscopy and X-Ray Microanalysis" by Goldstein et al. gives less than half a page of nearly 600. In 2002 a Google search for "converter or convertor or conversion + plate + electron" gave only one "hit" related to electron microscopy – a passing mention in a set of notes from an undergraduate lecture course in scanning electron microscopy. Clearly the converter plate has had little impact on the world in the years since the rise of the internet.

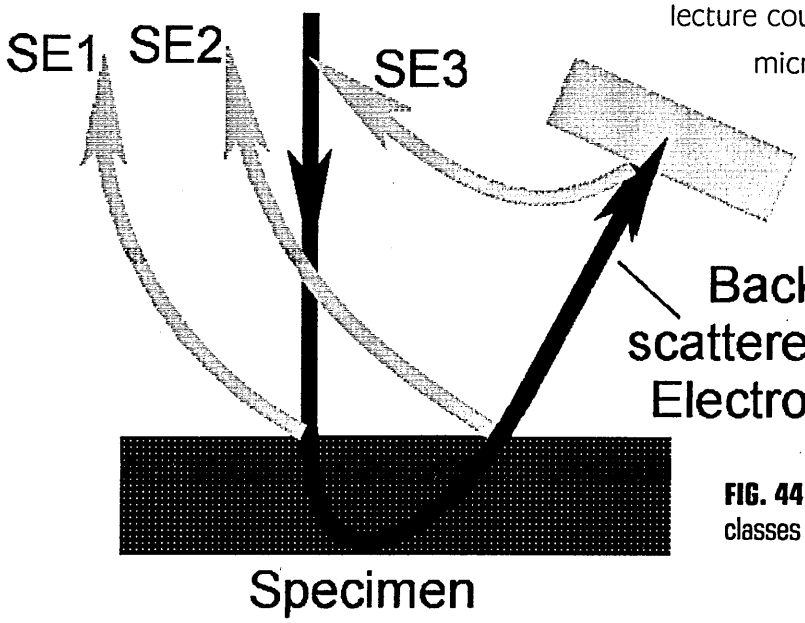

FIG. 44. The origins of the three classes of secondary electron

The converter plate generates secondary electrons Prom backscattered electrons by arranging for the backscattered electrons to hit a surface having a high secondary electron yield, usually in the form of a coated plate. These secondary electrons generated from backscattered electrons are referred to as “SE3” to distinguish them from the SE1 and 5E2 secondary electrons generated as beam electrons enter the specimen (SE1) or as backscattered electrons leave (SE2) (fig 44).

The Converter plate’s principle of operation - a high energy electron hitting a surface and releasing a secondary - is intrinsically invulnerable to the effects of photons and heat, and the plate and coating can be made of thermally robust materials. Thus, a secondary electron (SE) detection technology could be quite easily implemented that can indirectly detect the backscattered signal, via the induced SE3 signal, free of photon interference [fig 45], It allows us to “convert” the backscatter electrons that we need, but can’t detect into secondary electrons that we can detect, but which are carrying the backscatter contrast information. The nature of a converter plate allows it to be placed in line of sight of both specimen and SE detector, while specimen and SE detector are not in line of sight with each other (and would in fact have substantial shielding arrangements between them). Thus, the SE detector is protected from the majority of the photons. In addition to this, many modern variants of the Everhart-Thornley SE detector have considerably reduced photon sensitivity compared to both older Everhart-Thornley designs and established backscatter detectors.

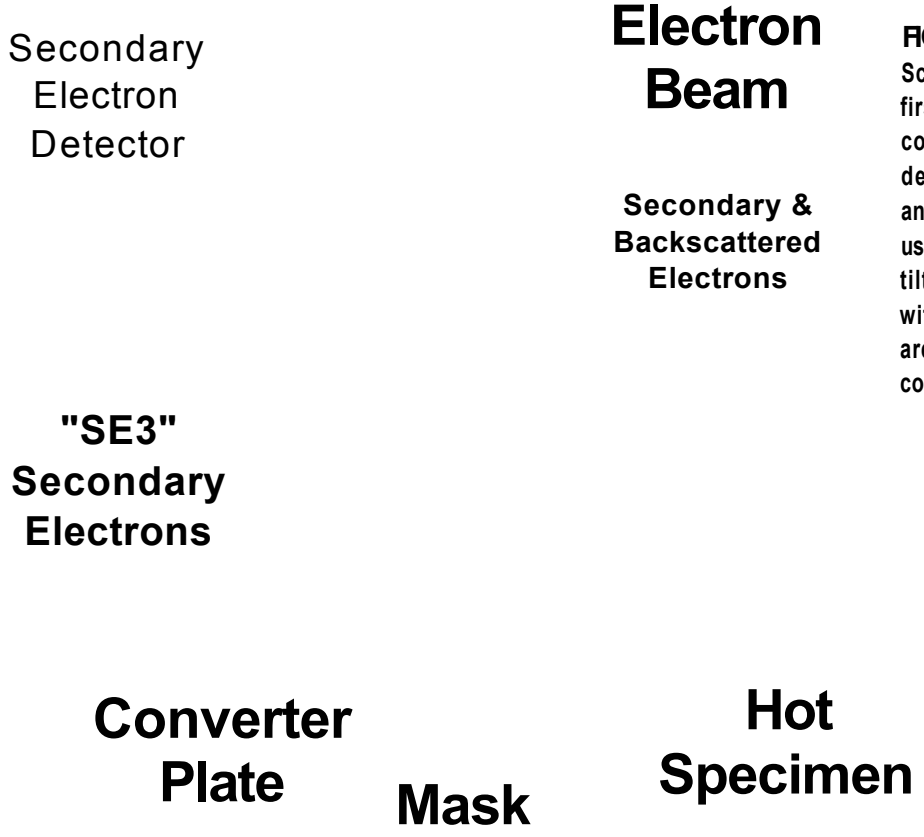

FIG 45. Schematic of first prototype converter plate detector then anticipated for use in the 70° tilt geometry, with the small area detector configuration.

Further advantages of the converter plate to this project were:

- It's very low cost (the bulk of the materials being obtained from the school of engineering scrap bin)
- Its ease of manufacture in the lab with basic hand tools
- The ability to readily make the plate in a variety of sizes and shapes to accommodate the evolving understanding of what the ideal detector and microscope geometry might be and how this could be accommodated to the XL30 SEM chamber and the available hot stages

3.5.1 THE SUCCESSFUL PROTOTYPE

The trials of the converter plate were running concurrently with the investigation into the influence of detector size and microscope geometry on channelling contrast. Thus, the first converter plate detectors were designed for the 70° tilt position, and these were indeed successful in imaging grains in a room temperature aluminium sample, to a quality level comparable to that given by the semi-conductor detector at the same geometry. However the image quality was still likely to cause problems with moving images, that is to say a long scan time was required in order to produce a decent image. The successful prototype (prototype five) was the first converter plate to be combined with Simkin's imaging approach, i.e. a detector for the zero-tilt geometry, covering the maximum possible solid angle at the specimen. The design concept was for a near hemi-spherical dome, with a small hole to admit the beam and a larger cut-out to permit secondary electrons to reach the SE detector. The cut out was designed such that the SE detector nearly had line-of-sight to the hot specimen, but not quite – thus protecting it from direct photon radiation.

The converter plate was made from aluminium sheet, cut, bent, filed and drilled by hand, then coated. The shape eventually achieved [fig 46] was less of a dome, and more akin to a miniature outdoor concert stage, such as the Hollywood Bowl [fig 47].

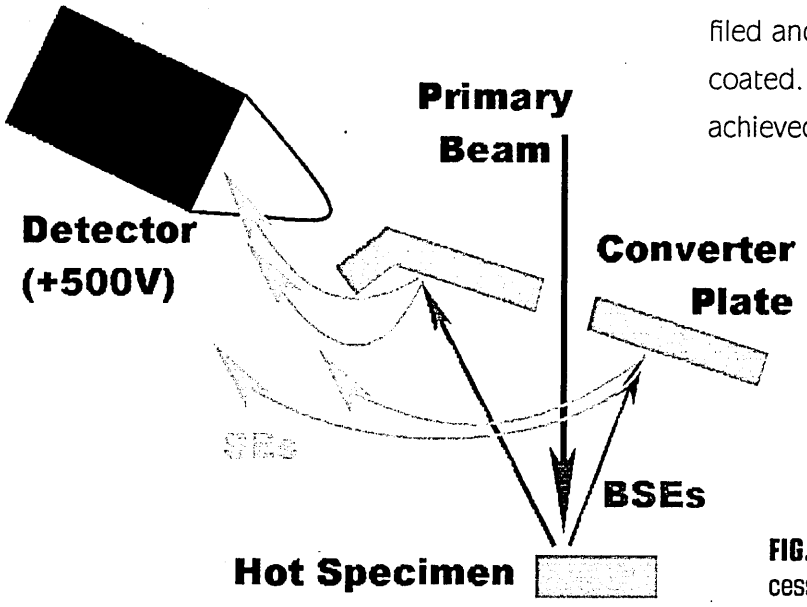

FIG. 46. Schematic of the successful mark 5 converter plate.

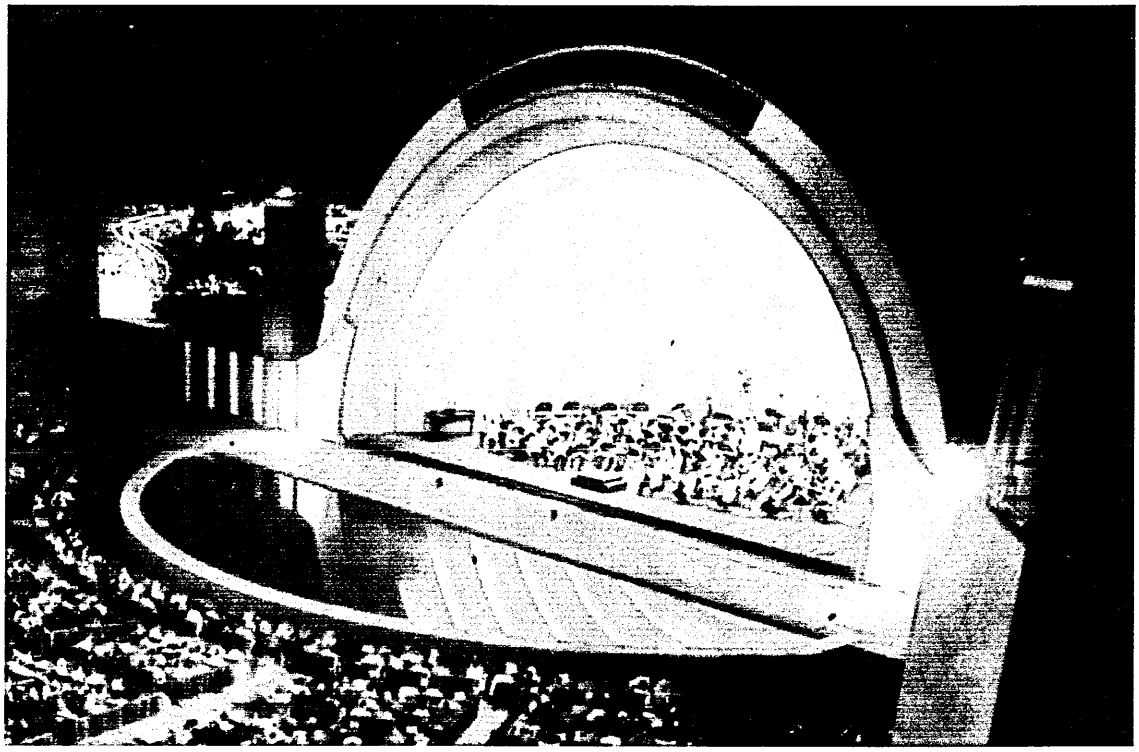

FIG. 47. The Hollywood Bowl. Imagine replacing the orchestra with the specimen, making a hole in the roof (about half of the way back) to admit an electron beam and heating the stage to 850°C.

These plates were tested in high-vacuum conventional SEM mode, using a single aluminium specimen at room temperature. Imaging was via the Everhart-Thornley detector, no attempt was made to use ESEM mode or heated specimens until a detector and geometry combination was found to give sufficiently promising images. Comparisons of different plate materials were undertaken at the 70° tilt geometry, with a moderately sized plate behind a vertical mask (fig 45). Comparisons of plate geometry (70° tilt versus large area 0° tilt) were undertaken with aluminium plates. The majority of size/geometry comparison tests were performed with semiconductor detectors, as described above.

Five possible coatings for the converter plate were investigated: magnesia (MgO), carbon, gold, diamond-like carbon and aluminium (uncoated). Magnesia and carbon were recommended by Reimer (1998). Gold was tried because of its high secondary electron yield, this proved inferior to the non-metals in imaging, probably due to the variation of its SE yield with incident electron energy. While heavy metals such as gold have a high SE yield, their "sensitivity" to low energy backscattered electrons is higher than their sensitivity to high energy backscattered electrons. Reimer states that the SE yield of lighter elements and non-metals is nearly independent of incident electron energy, and thus are more desirable for conventional BSE imaging. This work shows that not only is the SE/BSE conversion rate of metal plates more dependent on BSE electron energy, but that they are less well suited to producing grain contrast. The precise reason for this is unclear. Either the non-metals yield more SE from each high-energy

BSE than the metals do, or the metals yield a stronger "background noise" signal from the low energy BSEs – thus reducing the available contrast – or there is a combination of these two effects.

Aluminium (the uncoated plate) proved inferior to MgO, as expected, but yielded enough signal for "quick and dirty" initial comparisons of new plate designs and geometries. Carbon was found to be slightly inferior in imaging to MgO. Diamond-like carbon (DLC) – generously donated by Teer Coatings Ltd. – was found comparable to MgO, but MgO was more convenient in terms of cost and ease of rapid production of prototypes. Coating of MgO was achieved simply by placing a length of magnesium ribbon on a flame-proof surface in a fume cupboard, gripping the plate to be coated in small locking pliers or similar, then lighting the magnesium and holding the plate in the smoke, as close as possible to the burning magnesium. Gold and carbon coats were applied in vacuum coating machines intended for treatment of non-conductive SEM specimens. The MgO coating was physically fragile and required frequent renewal, due to handling damage and flaking in storage. In a "non-prototyping" environment, the DLC coating may well be more convenient.

The results were that the best coating was MgO and the best geometry was zero-tilt with a near-180° solid angle plate [figs 48-50]. Again the minimum specimen-to-plate distance was shown to be the best – i.e. maximum solid angle for the plate/detector.

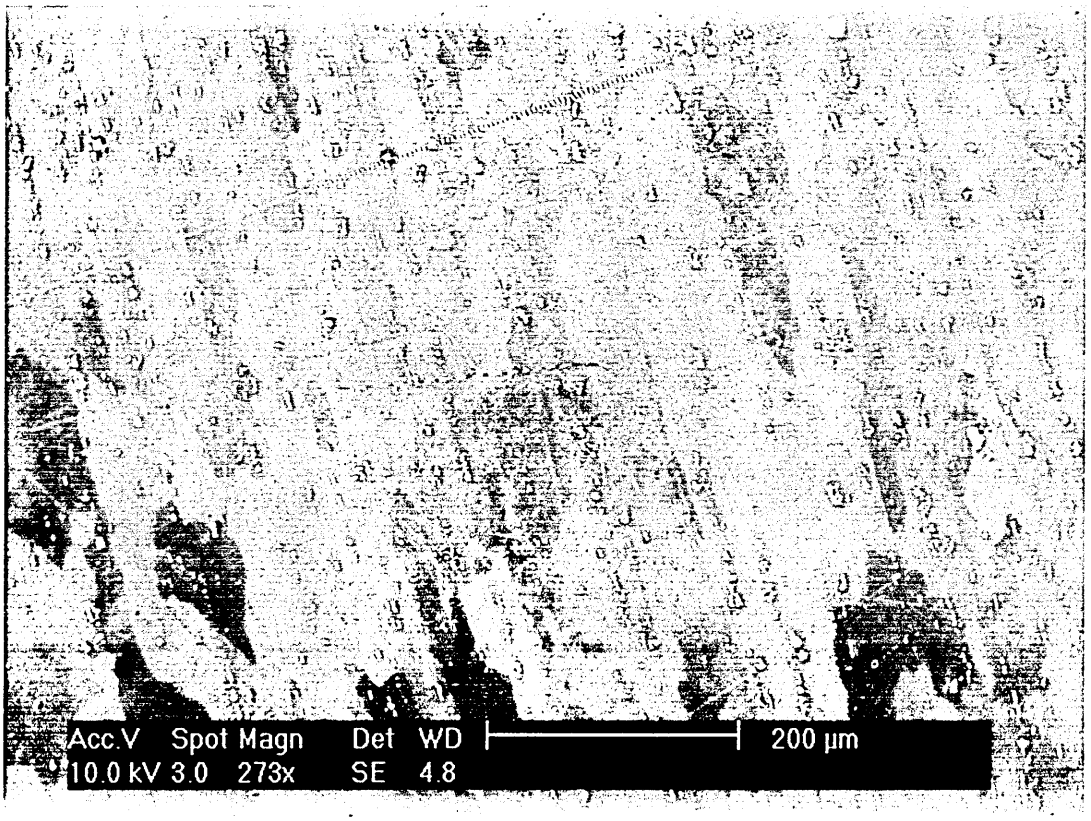

FIG. 48. Room-temperature aluminium, imaged at zero-tilt via mark 5 MgO coated converter plate – 5mm specimen-plate distance.

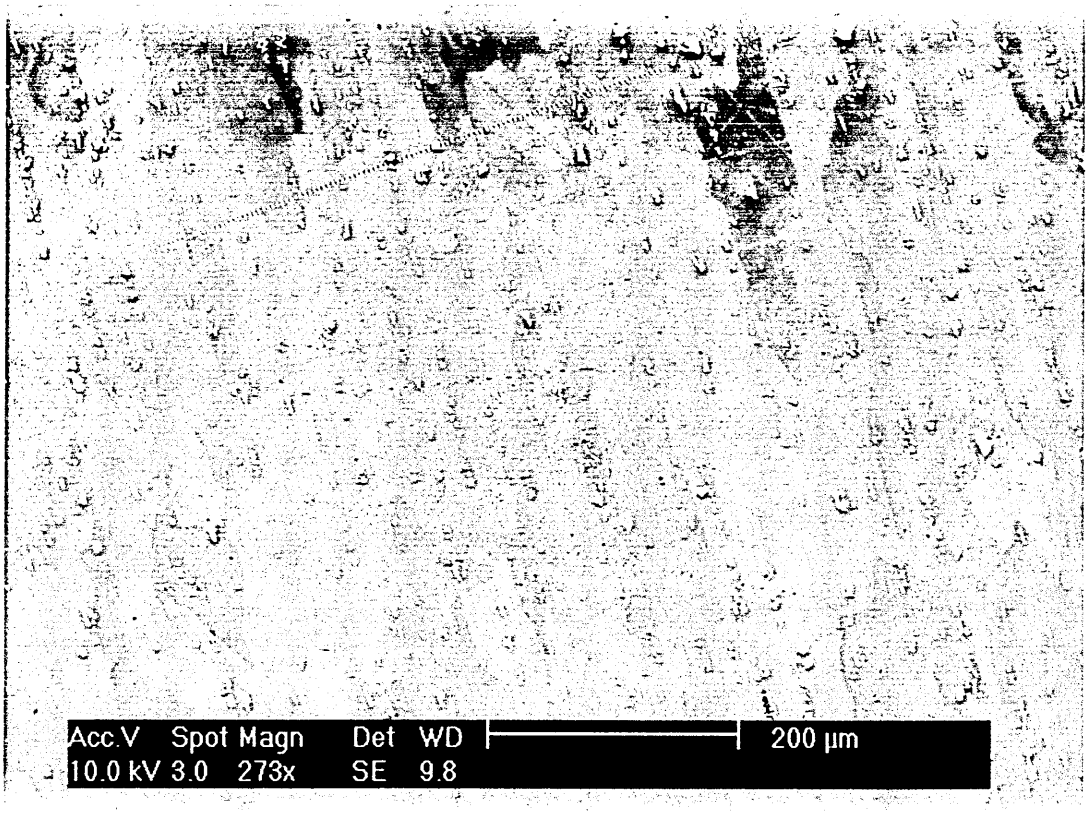

FIG. 49. Room-temperature aluminium, imaged at zero-tilt via mark 5 MgO coated converter plate – 10mm specimen-plate distance.

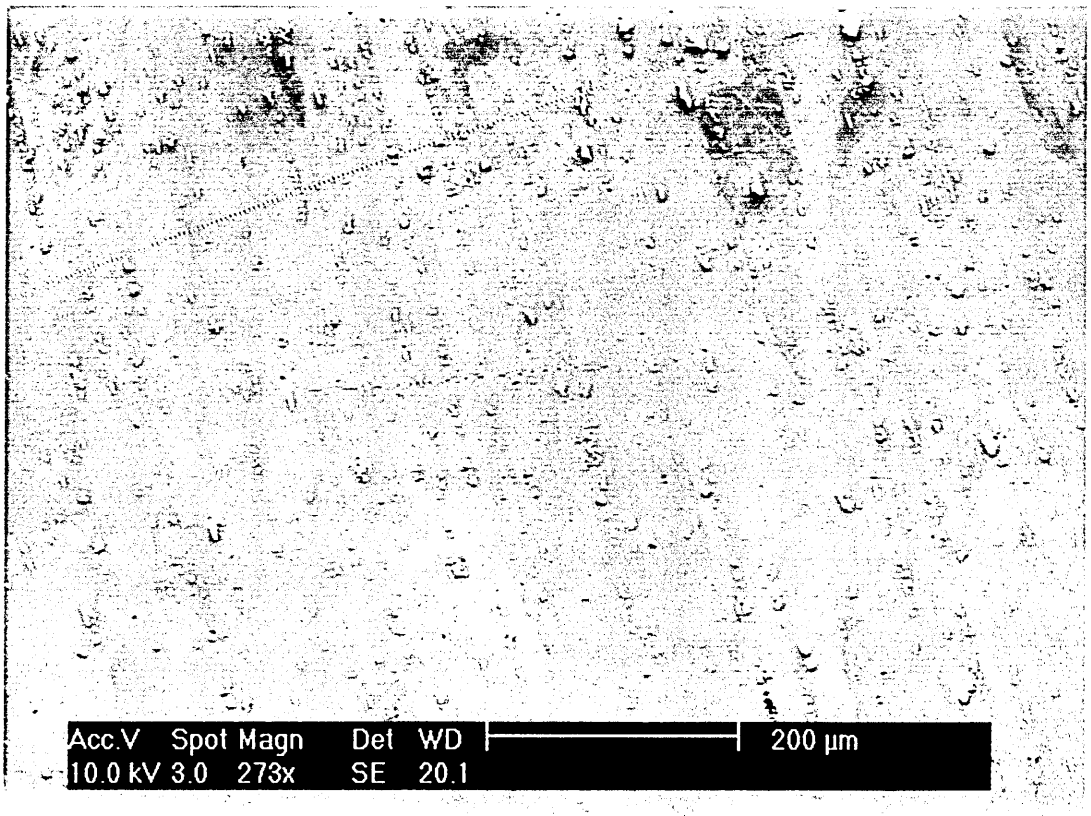

FIG. 50. Room-temperature aluminium, imaged at zero-tilt via mark 5 MgO coated converter plate – 20mm specimen-plate distance.

Of all the prototype converter plates tested, the "Hollywood Bowl" shaped 5th prototype, with an MgO coating, operated at the zero-tilt geometry, was the first detector regarded as sufficiently good in room temperature tests with an aluminium specimen to justify its use in a hotstage trial. The "mark 6" prototype was therefore produced, a smaller, simpler version of the mark 5, designed to sit on top of the hot stage, rather than attach to the polepiece as the mark 5 did. The mark 6 was therefore at a fixed specimen-plate distance of about 7mm, but the low-dome shape was made to maximise solid angle within the geometric constraints of the polepiece, the hotstage and allowing electrons to escape to reach the Everhart-Thornley SE detector (fig. 51).

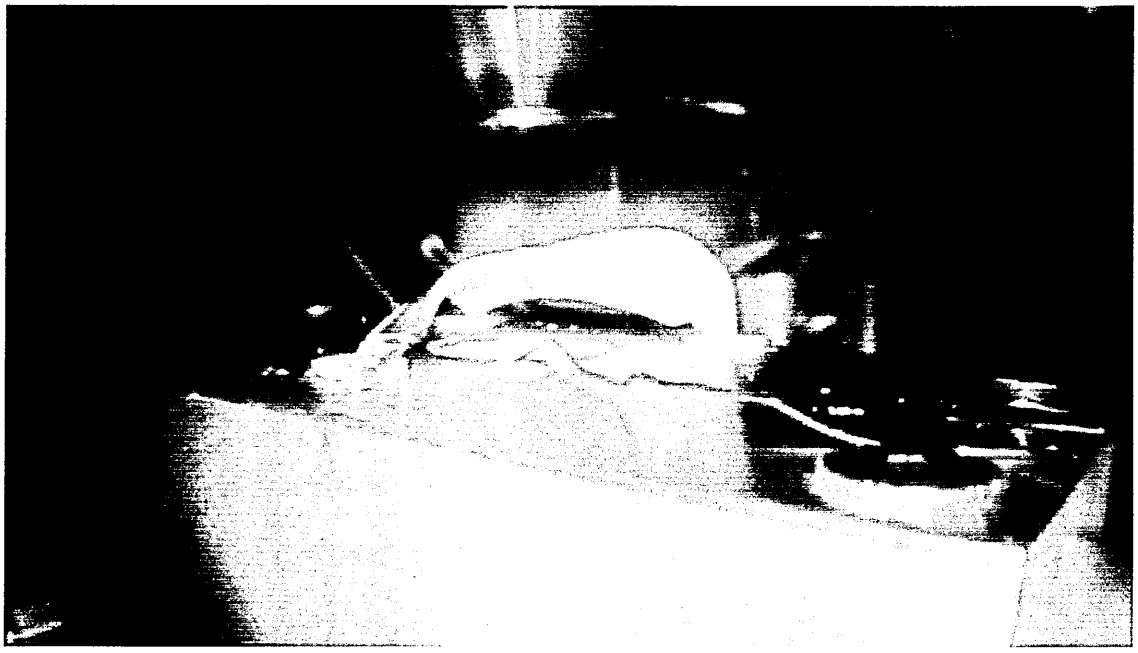

FIG. 51. The mark 6, MgO coated converter plate, in place on the hot stage just prior to the first successful heating run. The specimen is out of sight in the well in the hotstage. The wire is providing an earth for the specimen.

3.5.2 FIRST CONVERTER-PLATE HEATING TRIAL

The trial chosen was 1050 aluminium, in vacuum, using the mark 6 MgO coated plate and Everhart-Thornley SE detector. The reasons were fourfold. Firstly, this was the same material used as a specimen in the room-temperature proving trials. Secondly, aluminium, having a lower target temperature (350-550°C) was expected to be less problematic in general and therefore expected to give the best images. Thirdly, in vacuum (as opposed to ESEM mode) gave easiest comparison to the in vacuum room-temperature results. And finally, the geometry of a plate designed for conventional SEM mode was simpler than an ESEM mode design. Hotstage results with aluminium in vacuum were encouraging (figs 52, 53) and showed that a time sequence of closely spaced images was achievable. A frame rate of approximately 25 seconds per SEM frame was achieved with reasonable image quality and was successfully captured to digital video.

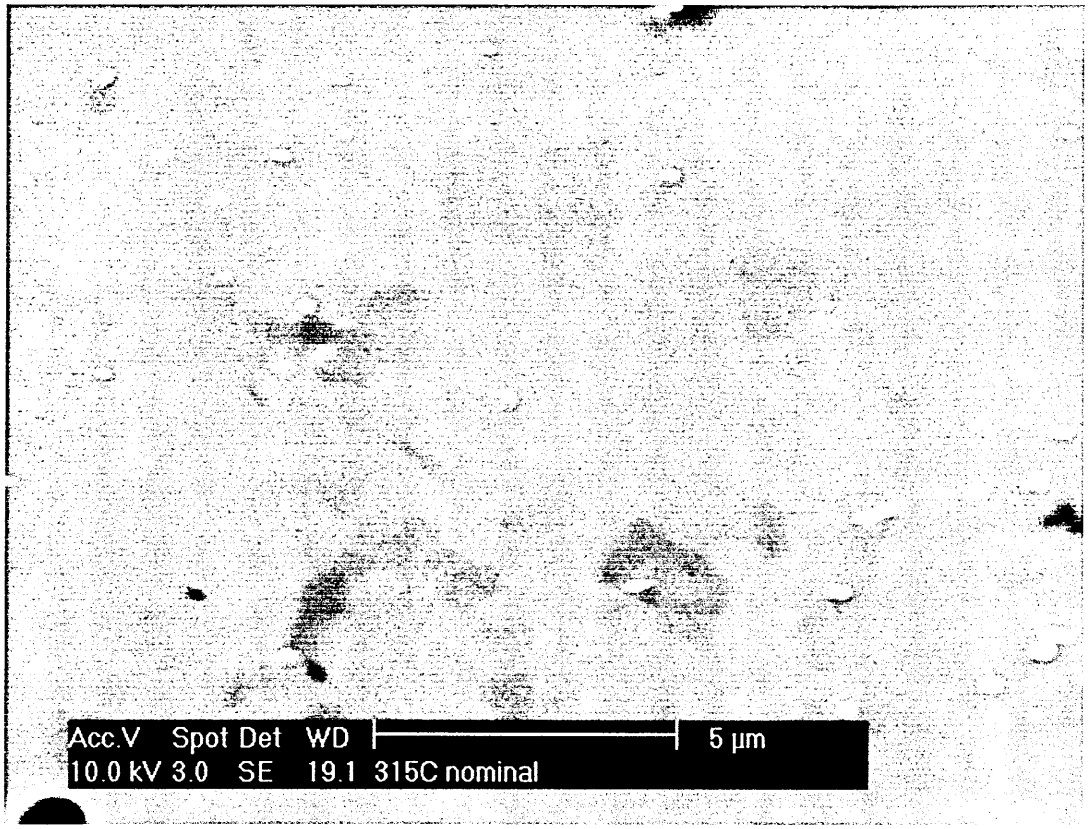

FIG. 52. 1050 aluminium wire (welding rod) at a nominal temperature of 315°C (probably 275-300°C in reality). The bright particles are suspected to be inoculants , used to nucleate grains on original casting.

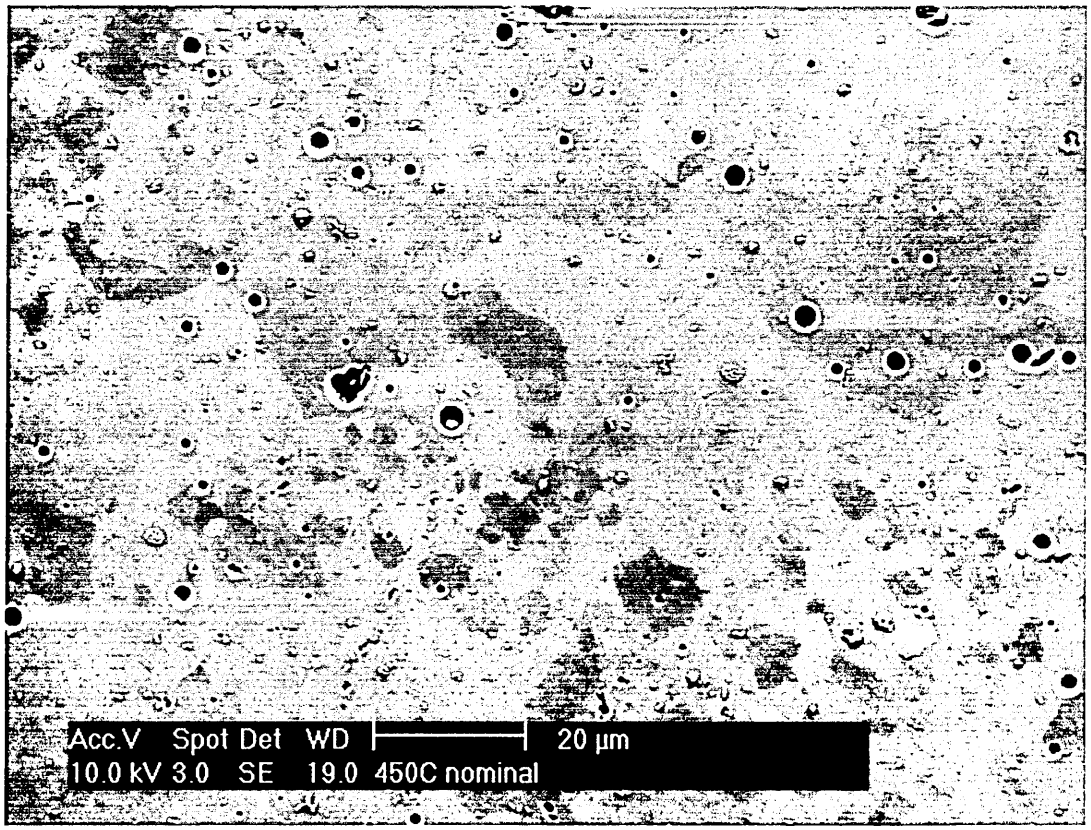

FIG. 53. 1050 aluminium wire (welding rod) at a nominal temperature of 450° (probably about 400°C in reality). Large areas of small grains have been consumed by large grains. Pitting has developed at higher temperatures, this seems to be associated with the inoculant particles-presumably they disrupt the alumina surface layer, allowing surface diffusion, clearly not all inoculant particles cause this effect.

The results were imperfect, as the operator was "learning the hard way" what magnification was appropriate to show the various phenomena occurring at any particular time. This experiment run was also the first experience gained with the "4-ball juggling act" of:

- Keeping the specimen in focus (focus drifted frequently, presumably due to thermal expansion).
- Maintaining good contrast and brightness settings – these occasionally underwent wild swings, probably due to the plate charging and discharging.
- Keeping the area of interest in the field of view – it tended to drift rapidly "south-east" if not constantly corrected, possibly due to expansion, possibly heater-current induced beam-shift.
- Making allowance for image disturbance due to heater current – the image was highly disturbed by any change in heater current.

Imperfect though the results were (see appendix 4, video 1 – aluminium), they clearly showed grain boundaries moving in a discontinuous ("jerky") manner, and no thermally etched boundaries until very close to the aluminium's melting point. The lack of thermal etching is due to the highly persistent, stable alumina layer that exists on the surface of any aluminium that has been exposed to air. This was not significantly affected by the heat or vacuum and prevented the surface diffusion mechanism that otherwise would have formed grain boundary grooves.

Following this qualified success with aluminium, the experiment was repeated with steel, although the higher temperatures required were expected to give significantly poorer results than aluminium. In the event, the results were unexpectedly excellent, with acceptable image results from a frame time of about 10 seconds per frame. The increase in temperature over aluminium was expected to degrade image quality, due to the effects of stray/multiply reflected light on the SE detector. However, the anticipated loss of quality did not materialise and was more than offset by the improvement gained from the stronger orientation contrast in this higher atomic number material. It is unclear whether this improvement flows from the overall higher backscattering co-efficient of iron versus that of aluminium, or from effects caused by differences in the relative penetration depth for an incoming electron on a channelling direction versus the probability of escape for an electron scattered at a particular depth. Both may well be playing a part. [fig 54]

FIG. 54. Grains growing in 0.61%C steel at about 850°C. Still extracted from video of second steel heating run.

Regrettably the digital video record of this first steel experiment was lost due to an ambiguous software interface. However, valuable lessons were learned in terms of how the specimen would react, what magnification to use, the practicalities of maintaining focus, retaining the area of interest in the field of view, operating the hotstage etc. As a result, when the experiment was repeated a few days later, a frame time of 4 seconds per frame was achieved with a good image quality. This experiment has provided the key results for this project. A subsequent experiment with steel and another with gold have reduced the frame time to 1 second per frame. A subsequent experiment with aluminium gave good results from about 10 seconds per frame.

3.6 TECHNIQUES AND REFINEMENTS ABANDONED DUE TO SUCCESS

In anticipation of poor results from steel, plans had already been made to further improve the intrinsically weak orientation contrast (and therefore improve the achievable frame rate) in the following ways:

- Biasing the specimen positively (to suppress emission of SE1 and SE2) – this was intended to remove the overlaid conventional SE signal, giving more latitude in the available contrast & brightness settings and further suppressing topographic contrast

- Interposing an earthed grid or low voltage positively charged electrode between the sample and SE detector, to capture SE1 & SE2, preventing them from reaching the detector
- Biasing the converter plate negatively, to enhance its SE3 yield.

However, with a very simple detector already capable of imaging all but the most highly dynamic of microstructural changes in the material of greatest interest, it was felt that the time had come to end the electron detector development phase. Detector development was not part of the original project brief and the time available to do metallurgy as opposed to instrument development was running short. The project therefore proceeded to imaging, and if possible analysing, microstructures evolving at temperature, in real-time. These results are presented in Chapters 4 and 5.

At this time another "plan B" approach was also abandoned – the use of EBSD. While it has already been shown that EBSD is too slow to capture dynamic microstructural events (and may always be so), it should be practical to set up a line-scan, a small area, or a "target list" of arbitrary points, in place of a full map. This would require considerably less time to scan. However no manufacturer has made provision for repeated scanning of an area, line or arbitrary point set Thus, in order to capture the necessary time-stream of data, an operator would be required to save results and re-set the equipment repeatedly, rapidly and with a consistent turn-around time and to continue this over a considerable period of time. It should be possible to achieve this automatically. However, given the complex proprietary computer programs that would have to be interfaced with, the author's relative inexperience in computer programming and the minimal support that appeared likely (based on initial approaches to the manufacturers), this did not appear practicable within the present project. While such a scheme would be of limited use as a sole investigation technique, it would be very valuable if combined with some kind of imaging.

3.7 FINAL EXPERIMENTAL TECHNIQUE

The technique finally adopted for the main experiments (used in all results given unless noted otherwise) was as follows.

FIRST: Specimen prepared as far as possible to a flat-polished, strain-free state.
For steel – conventional grind and polish to a one micron diamond finish, followed by 0.25 micron colloidal silica polish, if necessary followed by light etching in nital and re-polishing.
For aluminium – conventional grinding and polishing to a one micron diamond finish, followed by attack-polishing with 0.25 micron colloidal silica with an etchant addition

(modified Murakami's reagent 100 mL water, 10 g NaOH, 5 g $K_3Fe(CN)_6$).
No truly satisfactory technique was identified for gold or lead.

SECOND: Imaging at the zero-tilt microscope geometry, using a maximum-solid-angle converter plate (tending towards a hemisphere), with an MgO coating, in high-vacuum SEM mode (Everhardt-Thornley SE detector), using the Phillips-FEI water cooled hotstage (nominally 1000°C).

THIRD: Locating an "area of interest" on the specimen surface having:

- Good polishing quality
- A size (magnification) of a reasonable compromise between likely start and finish grain sizes
- A prominent non-metallic inclusion or other non-mobile microstructural feature, to allow repeated re-alignment of area of interest with field of view

FOURTH: Operation of the hotstage in "local-manual" mode (not software controlled) in order to directly control the current loading applied to the hotstage heater elements, not merely the target temperature. Experience showed that the Phillips-FEI hotstage control software was liable to apply an unnecessary and potentially damaging high current loading to the heater elements at the start of a room-temperature to high-temperature ramping program. This was therefore not used and manual ramping of heater current to achieve a heating rate of 0.05-0.1°C per second was used, to a final target current capable of driving the stage to target temperature (850°C at the specimen) and holding stable within a few degrees, or few tens of degrees, of that value. This also minimised image disturbance due to heater current changes.

FIFTH: Use of 480-line SEM scan modes in a selection of line times – 480 lines is close to the 520 lines output by the microscope's NTSC conventional "TV" video hardware, thus avoiding spending time generating high-resolution images that cannot be passed to or captured by the video hardware. As far as possible SEM scan rate to remain constant.

SIXTH: To capture video of almost the entire experiment run digitally to computer hard disc. In practice, the microscopist has a great many parameters to control, such as focus (which drifts), correction for sample drift, correction for heater current induced beam shift, hotstage control, and changes in brightness/contrast (probably due to charging/discharging of the converter plate). The microscopist is thus largely unable to follow events as they happen and may be quite unaware even of fairly major changes occurring in the specimen. The Microscopist is also not well able to appreci-

ate when changes begin to occur (experiment start), nor when they have entirely ceased (experiment end), hence the policy of over-recording.

SEVENTH: To review video later, using a variety of different playing speeds in addition to forward and reverse play. To trim off start & end footage showing no change even when reviewed at high playing speeds. To edit video to produce a finished clip running at 15-30 times original speed (finished video frame rate ideally an integer multiple of SEM scan rate) and review this to decide on final "presentation" play speed. For maximum picture quality, final play speed is achieved by "decimation" – the process of dropping N video frames in every X. Thus, a 1 in 2 decimation would drop one frame in every two and result in a double-speed playback. A 19 in 20 decimation would drop 19 frames in every 20 (or keep one in every twenty), resulting in a 20X speed playback. This was usually combined with "temporal" noise reduction – the use of algorithms designed to compare the grey level of a video pixel in any given frame with the values for the same pixel in adjacent frames both "upstream" and "downstream" in time – thus preserving spatial resolution while reducing noise.

For maximum video image quality it was found best to:

- Apply temporal noise reduction to the raw video, in order to cut video-rate noise – a large temporal window (averaging a large number of frames, e.g. five either side of the current frame) was found to be ideal, though a heavy load on the available computing resources.
- Decimate the temporally filtered video such that only one video frame remained from each SEM scan, and that this selected frame coincided with the scan line being lost in the top or bottom lines of the frame. This operation is relatively simple if a constant SEM scan rate is used; otherwise, it is tedious and quite challenging.
- Apply temporal noise reduction to the decimated video, in order to cut SEM-frame-rate noise – a small temporal window of 1-2 frames either side of the current frame was found to be best.
- Adjust the filtered-decimated-filtered video to presentation speed using the tools available as standard in most video editing software (in this case Adobe Premiere).

CHAPTER 4
RESULTS AND DISCUSSION 1: GRAIN GROWTH

4.1 INTRODUCTION

The principal results gained are in the form of digital video recordings of live, slow scan SEM images. These recordings have been minimally edited – excess footage has been trimmed from head and tail – and preserved as "raw" results. Selected copies have then been further processed to varying degrees, to produce "working" or "presentation" videos (which are included with this thesis in appendix 4). In most of these videos, temporal noise reduction has been applied, followed by acceleration to a playing speed that shows the events occurring at a rate more easily followed by the eye. Image enhancement by adjustment of video "Gamma" or by re-mapping grey levels was experimented with but found unhelpful in most cases (this technique is called "histogram functions" or "levels" in several popular image editing software packages). In the case of the "presentation" video of 0.6%C steel, frames showing re-focussing operations and/or the waveform monitor have been cut and replaced by duplicate copies of the last "good" frame from just ahead of the cut, to preserve the correct running time. In the finished presentation copy, this "cloning" or "freeze-framing" produces a frozen image lasting not more than 5 frames – 1/6th of a second – and is considerably less disruptive to the eye's following of the microstructural evolution processes than the frames that were replaced.

4.2 NAVIGATING THE RESULTS

To navigate the videos it is recommended to play them in Apple's "Quicktime" player (http://www.apple.com/quicktime – free download), or some other software that not only allows moving through the video by dragging the progress slider but which updates the image as the slider is dragged. The current major competitors to Quicktime (Real Player and Windows Media Player) are not capable of this. This capability is important as it allows the simulation of faster or slower playback speeds by dragging the slider at the desired rate and also allows reverse play by dragging the slider backwards. It is also useful to be able to repeatedly "shuttle" back and forth across some particular event, and this too can be accomplished by "rocking" the slider back and forth across the time range of interest.

To facilitate navigation, each video has a clearly stated acceleration factor, showing how much faster it plays compared to the original experiment recording. Times are quoted in two forms:

1) "Video Time" Minutes:Seconds (e.g. 2:04). This refers to the time position of a particular event, still image or sequence in one of the videos, and refers to the time standard of the accelerated video measured from the first frame of the video (even if that is a title screen). The "video time" stated should correspond to the time position displayed by the video player software. In most cases it has been rounded down to the nearest whole second, as seems to be the practice in most video player software. Most software will display the time position in a clip as Min:Sec or in a few cases Min:Sec.XX – where XX is either 1/10ths and 1/100ths of a second (figure from 00-99) or are numbers of video frames (0-29 as these are 30 frame per second videos).

2) "Experiment time" Seconds (e.g. 2400 sec). This refers to actual time in the experiment, from some identifiable "starting" event, such as first visible evidence of transformation/recrystallisation.

The two are inter-related by the acceleration factor of the video, with account taken of any title frames present in the presentation version.

4.3 RESULTS AND DISCUSSION PART 1 – GRAIN GROWTH AND RECRYSTALLISATION

4.3.1 RECRYSTALLISATION

This project was emphatically focussed on grain growth from its outset, and has produced no direct results on recrystallisation – depending upon what exactly one's definition of recrystallisation is. If the definition of recrystallisation is "that portion of the change from a cold-worked structure to an annealed structure that is dominated by dislocation processes", in other words, nucleation of new crystals/sub-grains and migration of sub-grain boundaries (which are simply very large arrays of edge dislocations), then this project has produced no results. However, several experimental runs came tantalisingly close to producing such results – the time window available to produce images from this part of the transformation is small and the highly-deformed parent structure used in these experiments is often very difficult to focus on. Thus, there is a large element of luck to capturing images of recrystallisation with this technique, this equipment and these specimens, and to date this luck has been absent. The microscope has always been either not sufficiently well focussed, in the process of being focussed, looking at an uninteresting "area of interest" or set at a good magnification to capture grain growth images (i.e. at too low a magnification to produce truly useful recrystallisation images) during the brief period of recrystallisation.

The project has produced results in aluminium showing that recrystallisation in that material is patchy [see fig 53 in Chapter 3]. Unfortunately, the "patch" being observed in detail at the commencement of that experiment was not one of those that recrystallised. However, this is not truly direct evidence from recrystallisation and this "patchy recrystallisation" phenomenon has been reported almost concurrently by other workers, e.g. Anselmino et al. (2004 B).

The project has produced results showing new crystal nucleation and growth during the ferrite → austenite phase transformation. This may or may not ultimately be shown to be analogous to recrystallisation from a highly deformed parent material, without a phase change. This process of forming new austenite crystals from a ferrite parent is sometimes referred to as "re-crystallisation" because new crystals are being formed, however as the new crystals have a different structure (face centred cubic as opposed to body centred cubic) the new crystals are a different phase. From the images, the process seems to be the formation of new crystals out of the parent material, which then grow into the parent material, i.e. a combined phase transformation and recrystallisation – in which the atoms change their packing mode and in doing so depart their parent crystal and cross a phase boundary to join or start a new crystal. This is as opposed to a "military" phase transformation in which the lattice of an existing crystal shears in concert to reach a new packing mode, with all atoms of the crystal shearing together and all (or most) remaining mutually associated as one crystal, with the same or equivalent relationships to their neighbours as before.

4.4 GRAIN GROWTH – ALUMINIUM

Refer to video 1 on the discs in appendix 4. Note – Events in this video can be somewhat confusing, as magnification is changed at certain points. The accelerated speed of the video makes these changes very abrupt, and it can be difficult for the eye to follow exactly what the change has been, especially if the viewer is not forewarned. Later videos either maintained a constant magnification or made slow changes in many small increments such that the eye could follow them in the accelerated version.

Aluminium has been one of the more challenging materials to work with in this project. This material was selected for hot stage examination first, in the expectation that the relatively low temperatures required would lead to easier imaging. This was not so, although lower temperature led to somewhat easier hot stage management.

The results produced from aluminium are less satisfactory than those produced from steel (discussed below) for several reasons. Many of these shortcomings could be at least partially rectified by application of experience gained subsequently. However, fol-

lowing the highly rewarding nature of the first steel results, effort was focussed more on steel at the expense of the less industrially significant non-ferrous metals that had initially been considered for inclusion in the project.

The specific shortcomings were as follows:

1. Poor Image Contrast

This necessitated relatively long SEM frame times (about 25 seconds). This poor image contrast arises from the lightness of aluminium's atoms – the reasons for this are suspected to be one or both of the following:

A) Aluminium has a relatively low overall backscattering coefficient and hence changes in that coefficient due to channelling effects are very subtle.

B) Aluminium has a relatively large penetration & escape depth for backscattered electrons. Thus, a small change in an electron's penetration to first scattering encounter (caused by channelling) would be a relatively small proportion of the maximum electron penetration/escape depth. It would therefore have a smaller effect on a scattered electron's ultimate escape probability than it would in a more electron-opaque material, with a shallower penetration/escape depth. In a more "electron-opaque" material, the distance travelled while channelling could be a much larger proportion of the normal penetration/escape depth.

Subsequent experience and technique/converter plate development would allow the 25 second SEM frame time for aluminium to be more than halved, to less than 10 seconds.

2. Inappropriate Magnification

Having no experience of live hot stage imaging of any material, let alone this specific material, an inappropriate initial magnification was selected. The mistake was not apparent until some way in to the experiment.

3. An Uninteresting "Area Of Interest"

The experiment on aluminium showed that this aluminium recrystallises in a very "patchy" manner, and that the area of interest – initially selected for its good polishing quality – was not one of the more immediately interesting areas. In future experiments this could be at least partially offset by:–

- Using low magnification to locate areas of high activity, then examining them in detail
- Performing much more cold work on the specimen to give a stronger driving force for general recrystallisation

- Taking exceptional care to maintain the specimen at room temperature (i.e. not above 40°C) to eliminate any possibility of recovery or partial recrystallisation occurring during sample preparation or storage. Specifically, slow-setting (≈24-hour) epoxy "cold" mounting material should be used, as opposed to conventional hot-mounting methods – even at the reduced temperature that was used. Rapid epoxy "cold" mounting media usually attain maximum temperatures comparable to hot mount, and should therefore also be avoided.

4.4.1 THE ALUMINIUM SPECIMEN

The aluminium specimen chosen was Al 1050 aluminium welding rod. This is the basic structural grade of unalloyed aluminium, its composition is shown in table 1.

Al	Fe	Si	Mn	Cu	Mg	V	Ti	Others
≥ 99.5	≤ 0.4	≤ 0.25	≤ 0.05	≤ 0.05	≤ 0.05	≤ 0.05	≤ 0.03	≤ 0.03 each

TABLE 1. Composition specification for 1050 aluminium, in mass %. After MATWEB (no date given)

Welding rod was chosen for the first experiment as it was a readily available form of this material, in a convenient diameter for use in the hot stage, and it had been cold-drawn to its finished size – giving a good driving force for recrystallisation. The material was cut transverse to the drawing direction, i.e. imaging was looking directly into the drawing direction, seeing the elongated structure end-on. Specimen selection was a compromise between metallurgical interest and anticipated convenience of proving the hot stage technique.

4.4.2 DISCUSSION OF ALUMINIUM VIDEO RESULTS

When this "working copy" video commences, at a nominal temperature of 260°C (probably 200-225°C) recrystallisation has already occurred and grain growth is under way. The crystallites seen initially (Fig. 55) are not recrystallised grains, but are pre-existing grains that have been able to grow. The welding rod has been produced by a wiredrawing process, which has induced a degree of cold work that is large by the standards of aluminium. However, as aluminium does not work-harden rapidly, it is unsuited to forming operations such as wiredrawing and the degree of cold work done, while high by the standards of aluminium, is modest by comparison to other metals in "as-drawn" condition, hence a relatively low driving force for recrystallisation.

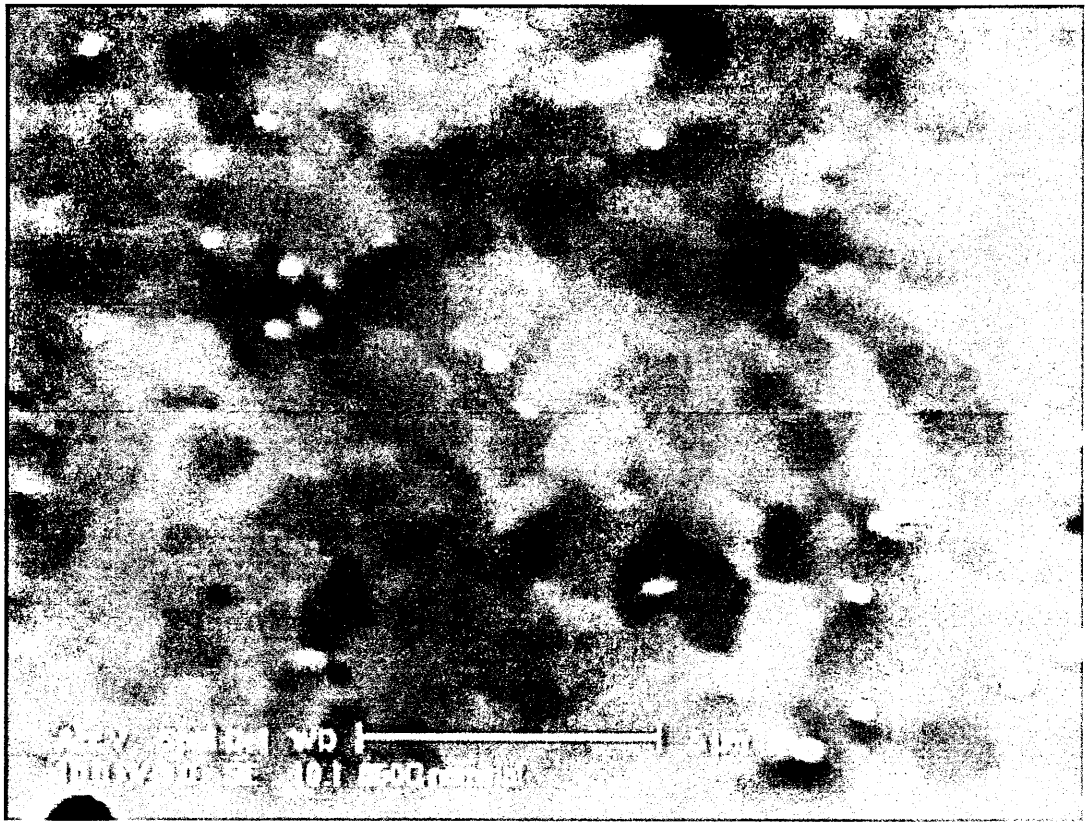

FIG. 55. 1050 Aluminium at 0:09 Scale bar is 5μm.

FIG.56. 1050 Aluminium at 1:21, scalebar is 20μm. Showing the large recrystallised grains surrounding the initial area of interest. The area shown in fig. 55 is the central $^1/_4$ of this view.

The video shows that recrystallisation of this alloy in this partially cold worked condition is a patchy phenomenon. At time 1:13, when magnification is lowered from an 18μm wide field of view to a 100μm wide field of view (Fig. 56), it can be seen that some grains surrounding the initial area of interest have grown to about 10 times the size of those within the initial area. These very large grains are assumed to be the recrystallised grains, formed from fresh nuclei, oriented so as to be able to grow. The pre-existing grains, while they have undergone some growth activity, retain the same neighbours that they were in near-equilibrium with on the previous occasion that the metal was above its recrystallisation temperature, hence the near-stalemate between them. It seems unlikely that a pre-existing grain could "break-out" in the manner that these very large grains have. This indicates that recrystallisation was patchy, with very few nuclei, widely dispersed. Grain growth from what few nuclei do exist is clearly the main mechanism of transforming this cold-worked microstructure into an annealed form.

The video shows discontinuous movement of grain boundaries at various stages. In some sections, this is best seen by dragging the progress slider to accelerate the video even more.

The video shows that thermally etched grooves do not form in aluminium until well after the grain boundaries have become mobile – this is due to the thin layer of alumina adhering tightly to the specimen surface. This layer cannot be avoided unless the specimen is prepared in the absence of oxygen and inserted into the microscope without contamination by oxygen.

At the end of the video, beyond 2:30 and nominally at 780°C (clearly about 650°C in reality) the grain boundaries suddenly appear more prominently, suggesting a topographic feature, such as a step or crack in the alumina coating. There is then a sudden, massive grain boundary grooving (fig.57), followed by clear grain boundary melting and the growth of two large cracks across the specimen (fig 58). These cracks are very likely to be cracks in the alumina, as they subsequently form short-lived "creases" on the now-molten surface and do not appear to disrupt the underlying grains.

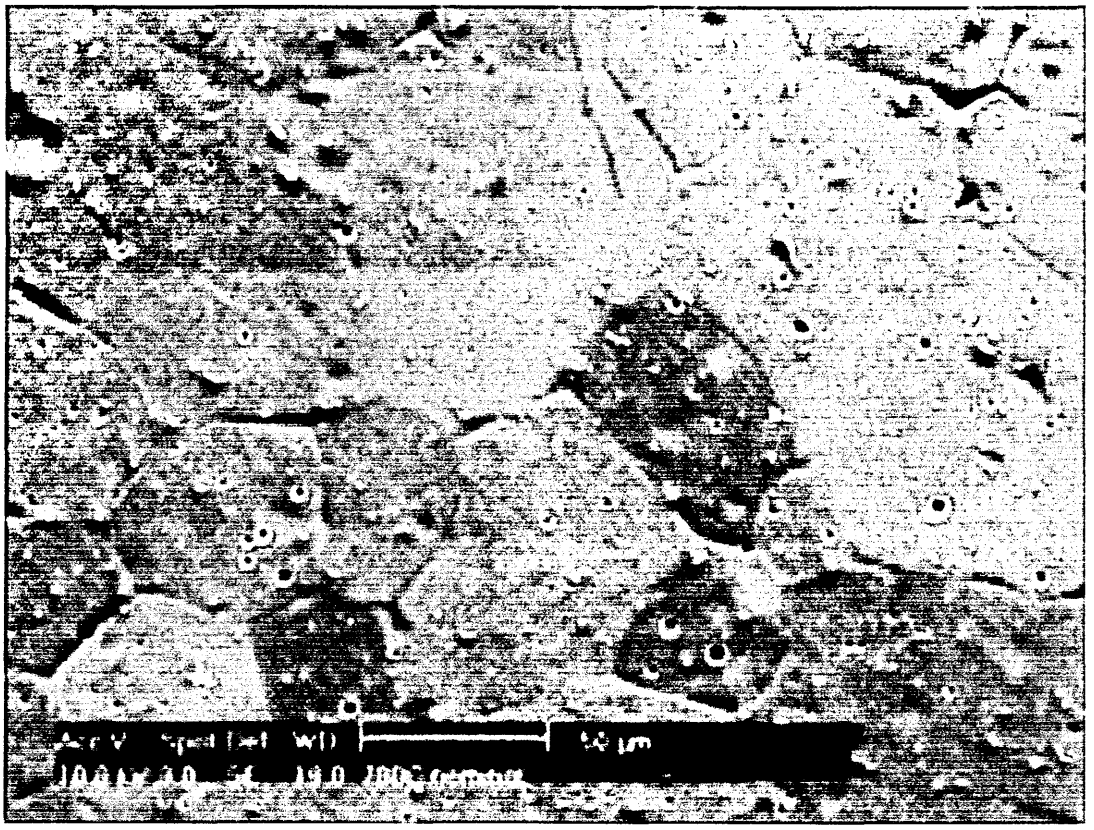

FIG. 57. 1050 Aluminium at 2:37 + 13 frames. Approximately 650°C, scale bar is 50μm.
Showing sinking/etching at grain boundaries and triple points, as melting commences.

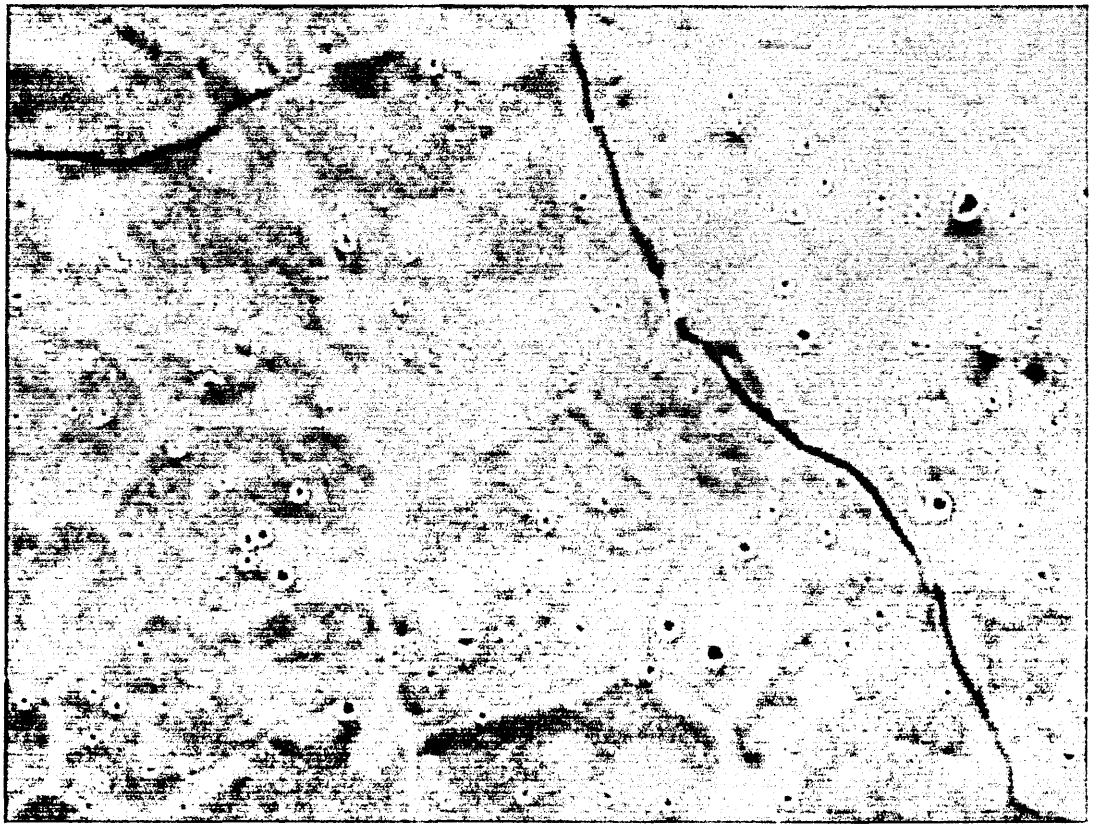

FIG. 58. 1050 Aluminium at 2:37 + 28 frames, i.e. 15 seconds real-time later than fig. 57.
Grain boundary liquation clearly visible, also cracks in alumina layer.

4.5 GRAIN GROWTH – GOLD AND SILVER/GOLD ALLOYS

After working with steel (see below) it was apparent that heavier atoms gave better imaging results, therefore gold was regarded as a good candidate material.

Gold was examined in two forms – "9 carat gold" (a 62.5 mass% silver - 37.5 mass% gold alloy) and "99-fine bullion" (99.99 mass% gold). Both were cold worked to an unknown but large degree, the 9 carat gold by rolling into strip form (performed by the original manufacturer), the bullion gold by repeated cold forging of a solidified bead[1] using a small hammer and anvil. The bullion gold reached a hardness of 70HV, significantly above the 60HV quoted by Goodfellow Materials for the "Hard" condition. The silver-gold strip specimen was polished longitudinal to the rolling direction, so that electron imaging was looking sideways on at the elongated structure. The bullion gold "lump" specimen was polished transverse to the direction of the last and most violent forging, but at zero degrees to many other hammer blows – it was not expected that this specimen would show strong directionality.

Preparation of gold in both forms was problematic. The silver-gold alloy was considerably harder and thus easier to prepare, but with no readily available etchant and a very small specimen size it was still a challenge. The silver-gold alloy was prepared to a good optical finish using conventional embedding, followed by very careful, very light grinding, conventional diamond polishing to a 1μm finish and final hand polishing using 0.25μm colloidal silica. The bullion gold was prepared similarly, but at best attained only a disappointing-but-passable finish under the optical microscope. High-power plasma etching using the GD-OES machine was considered but discounted, as the specimen was considered too small for the process.

When examined under the SEM, the finish of both specimens was observed to be initially similar to that observed under the optical microscope. However, with heating, these materials exhibited a high degree of surface diffusion effects, such that polishing marks and scratches that were largely invisible or at least unobtrusive when imaged at room temperature became clearly visible (fig. 59) and at worst highly obtrusive when the specimen was heated. The effect was considerably worse in the bullion purity material – so much so that it gave no useful results, as the topographic contrast swamped the orientation contrast before visible onset of recrystallisation.

[1] A small amount of bullion was re-melted on a carbon surface using a butane gas flame, producing a solid bead approximately 3-4mm in diameter. This was cold forged to form a flattened "doughnut", turned and stood on its edge, forged again to create flats on the sides of the doughnut, then turned a further 90 degrees and forged again to form a rough cube. The cube was then repeatedly cold forged successively in directions "X" "Y" and "Z", repeatedly flattening it and returning it to roughly cubic, until it became so misshapen as to be impossible to continue. It was then forged flat to a thickness of approximately 1mm, put in a metallographic mount, hardness tested and prepared for the SEM.

The 62.5%silver-37.5%gold material exhibited the same effect, but not to such a degree as to obscure the orientation contrast image. This gave some useful results showing discontinuous grain boundary movement and very ready grain boundary grooving in this material. In this material there can be no confidence that grain boundary motion is uninfluenced by boundary grooving, as it is unclear which manifests first.

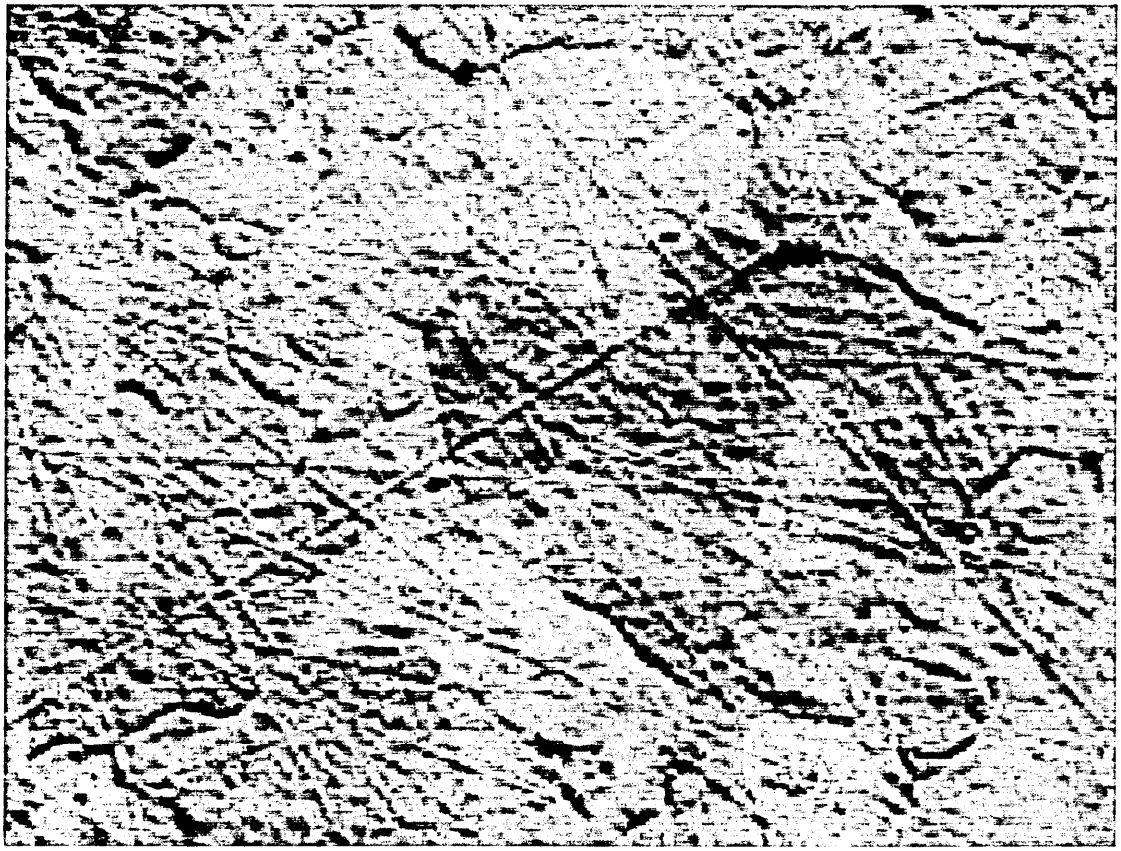

FIG. 59. Silver-gold alloy at about 500°C, field of view is 225μm wide. Showing grains, grain boundary grooving and prominent preparation scratches. The scratches had been practically invisible at room temperature, even at higher magnifications.

4.6 GRAIN GROWTH – STEEL

Refer to video file 2 on the discs in appendix 4

4.6.1 EXPERIMENT DESIGN FOR STEEL

The steel selected for initial experimentation was a "plain" carbon steel of nominally eutectoid composition, in the form spring wire, a very heavily cold-drawn grade of wire. This steel had a composition (by Glow Discharge Optical Emission Spectroscopy, GD-OES, analysis) of 0.61% carbon by mass with manganese (0.54%), and silicon (0.21%). The specification, BS 5216 (since superseded by EN 10270-1), equivalent to DIN17223, ASTM A227 etc., forbids any other deliberate additions and tolerances only sulphur and phosphorus among the "tramp elements". In this specimen, GD-OES detected 0.29% Cr, 0.10% Cu and all others <0.03% each.

The reasons for this choice of specimen were as follows:

- The material was readily available and inexpensive
- The material was a convenient size
- The experimenter was very familiar with the material, its heat-treatment responses and its preparation
- The high hardness of the material was expected to give ease of preparation (which it did)
- The material, being of nominally eutectoid composition and with no major alloying elements, is metallurgically relatively uncomplicated while still being of high industrial significance
- The material, being of nominally eutectoid composition, will transform from ferrite to 100% austenite with minimal intervening mixed structure, and at a temperature hoped to be within the capability of the Phillips/FEI "1000°C" hotstage
- The material had been cold worked to a very high degree in a continuous and highly uniform industrial process – something not readily achieved in a small experimental batch of material

It was also hoped that, with straining hot stages beyond the means of the project and incapable of high strain rates anyway, the material might provide an accessible model for industrial hot working of metals. It was anticipated that the highly distorted structure of the cold drawn wire would transform to a very fine-grained austenite, which would be initially pinned by the numerous very fine carbides, but would rapidly become "unlocked" by the dissolution of the carbides. Such a transformation might suddenly create a mobile/unstable fine-grained austenite. This is in fact what was observed. Such a structure may be reasonably representative of hot working just above the transformation temperature, in which transient large strains, such as hammer blows or roll passes, might reasonably be expected to create just such a fine-grained suddenly-mobile/unstable austenite structure, at a similar temperature.

The industrial processing of the material to reach the final wire-drawn form will have been as follows:

1) Hot rolling to a round wire-drawing rod of approximately 6-7mm diameter.
2) Austenitising, followed by controlled cooling in a lead bath or in heated air in order to produce the finest possible pearlite (processes known as "lead patent" "air patent" or "CCR" – air patent integrated with the rolling line).
3) Cold drawing through a series of powdered soap lubricated dies ("dry" drawing), to a total cold reduction of area of at least 80%.

The hardness of the material was checked and found to be 485-490 HV, consistent with an 80-90% reduction of area for this composition. The microstructure was checked by optical metallography of transverse and longitudinal sections, and found to be consistent with this composition, process route and reduction of area.

For the heating experiment, the material was cut transverse to the drawing direction, i.e. imaging was looking directly into the drawing direction, seeing the elongated structure end-on.

The specimen was placed in the Phillips/FEI SEM hotstage, under the sixth prototype converter plate, with a fresh magnesia coating, and imaged at room temperature. With the benefit of some previous experience, a field of view of approximately 150μm width by 115μm height was chosen as likely to show events to good advantage through most of the process. The microscope was then aligned and focussed on a prominent non-metallic inclusion in the otherwise largely featureless specimen.

The specimen was heated at approximately 0.1-0.2°C per second, under manual control. The non-metallic inclusion was used as a means of maintaining focus and correcting specimen position, both of which underwent quite gross changes due to thermal expansion and electro-magnetic interaction between the heater current and microscope beam.

4.6.2 DISCUSSION OF STEEL VIDEO RESULTS (GRAIN GROWTH)

4.6.2.1 STEEL GRAIN GROWTH VIDEO AND IMAGES

The highly distorted specimen structure was irresolvable at the selected magnification at room temperature and remained so throughout heating, until the transformation temperature was reached over an hour later. The preceding footage was edited out of the video record, and the video commences just before transformation temperature. As can be seen in the video, above the transformation temperature the structure suddenly becomes "unlocked" by rapid dissolution of the very fine carbide, and a plethora of fresh, micron-scale austenite crystals appear from a large number of widely and evenly spread nucleation points. These fine grains initially grow explosively into the matrix, very rapidly impinge on each other and then continue to grow in fierce competition with each other (Fig 60). Boundary movement is a mixture of smooth and discontinuous motion and occurs vigorously throughout the field of view.

After the initial flurry of grain growth activity, the grains settle into a regime of intermittent stability and growth, exhibiting some highly discontinuous behaviour. In this regime, at any one time, most of the grains in view will be stable, with isolated, localised areas of growth activity.

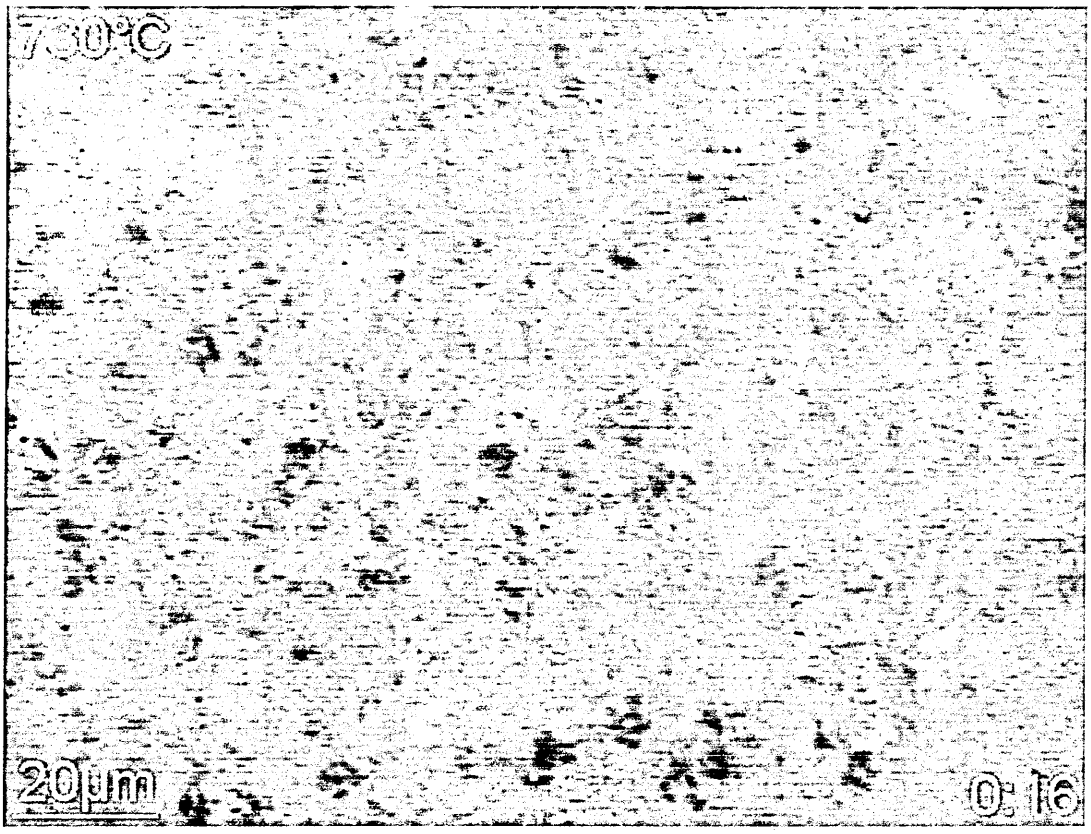

FIG. 60. Fresh austenite crystals, 120 seconds after first evidence of transformation. Initial explosive growth complete, growth by neighbour-annihilation underway.

Boundary motion often occurs by apparently discrete rapid events, such as the annihilation of grains (e.g. a previously fairly stable 10μm diameter grain, completely annihilated in 19 seconds of real-time, fig. 61) and the sudden "capture" of substantial areas of "territory" from neighbour grains, e.g. the sequence in fig. 62, which illustrates discontinuous boundary movement. In some instances it is clear that an advancing boundary may immediately retreat (fig 63).

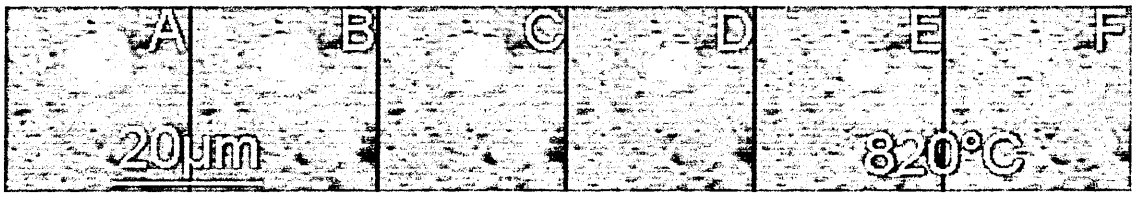

FIG. 61, A-F. The last 15 sec (real time) in the life of a grain. (1 frame = 1/30th second)
A: 0:49 + 6frames, B: +11frm, C: +14frm, D: +19frm, E: +24frm, F: +29frm

Fig. 64 shows a sequence in which crystallite X grows, contacting grain Z at 0:25, and bypassing it on one side at 0:27. At 0:29 crystallite + (apparently in some form of special relationship to X) forms, or appears from the sub-surface bulk, and grows, bypassing Z on the other side by 0:33. Grain Z is now an island, surrounded by X and +. This number of neighbours, a co-ordination number of 2, is much less than the theoretically stable co-ordination number of 6 – thus the grain would be expected to shrink rapidly. However, the newly islanded grain appears stable until about 0:45 when it starts to

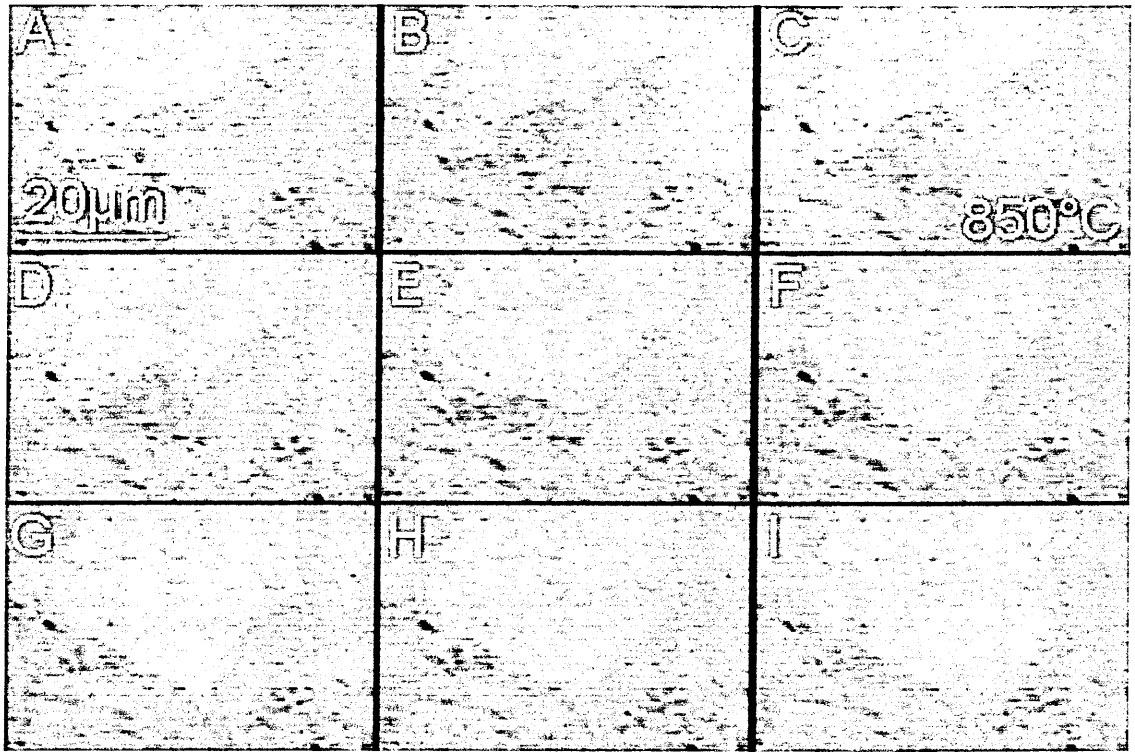

FIG. 62, A-I. 1:01-1:05 in 0.5sec (10 sec real) increments. Note that movement is larger between D-E-F-G than A-B-C. Even this relatively small time increment fails to show the full variability in boundary velocity.

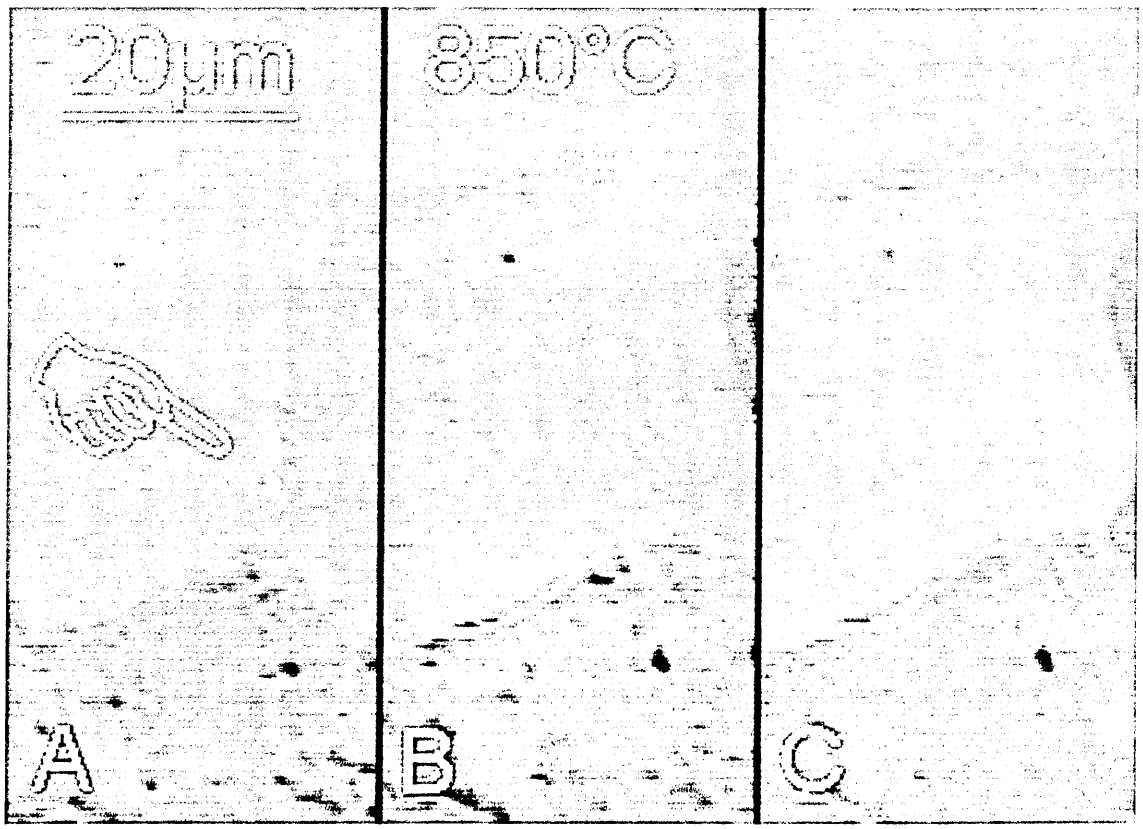

FIG. 63, A, B & C. Image sequence of grain boundary advancing & retreating. A at 1:16, B at 1:20, C at 1:28 (total 240 sec real time).

thin slowly towards a lenticular shape, of approximately the same length as the original grain. The lenticular remnant then vanishes rapidly, disappearing completely about 0:53

FIG. 64, A-F. **A 0:25, B 0:28, C 0:32, D 0:36, E 0:52, F 0:54 (sequence total: 580 sec real time). Temperatures: A : ~ 780°C, F : ~ 840°C.**

*k.*6.2.2 Steel Grain Growth - Grain Tracing

Grain boundaries can be identified by eye in the SEM images. Some efforts have been made with software to identify and characterise the grain boundaries and triple points, however the low contrast of the images in combination with the low resolution of NTSC video and noise introduced in the analogue transfer of video from SEM to computer have frustrated these efforts. Further refinements to the converter plate could very well improve contrast in future work.

Stills (fig. 65) are taken from the video stream at suitable intervals, digitally enhanced as needed and grain/twin boundaries are manually traced (fig. 66) using conventional graphics software and a digital tablet. “Missing” grain boundaries are relatively common at very early stages of the structure evolution, but rapidly become rare as development progresses. The low contrast makes some boundaries very difficult to identify in the still image, thus it is important to refer to both the still and moving images when tracing, as a low contrast boundary catches the eye much more readily when moving than it does in a still frame. Using this cross-referencing between still and moving images, identification of boundaries has proved quite reliable, though somewhat laborious.

FIG. 65. T=1300 sec (1:15), 850°C

FIG. 66. As Fig 65, with grain trace & grains marked with their graph symbols (see below).

Measurement of position in the image is done by reference to an invariant point on the specimen, in this case a non-metallic inclusion located near the centre of the field of view. The specimen has a strong tendency to drift in the image, due to expansion of the stage and disturbance of the beam due to the heating current, thus simple measurement with respect to the image frame is insufficient. Monitoring of the position of a single image feature (e.g. a triple point) is less laborious than performing a full grain trace, thus allowing more time points to be checked in such an analysis.

The traced grain boundary networks allow relatively easy measurement of the key parameters of some selected grains, e.g. the grain's area, longest dimension (L), dimension at 90° to L (W), and hence approximate aspect ratio. These measurements are complicated by the fact that some grains (especially the most active and interesting) grow beyond the field of view, or the specimen may drift to give that result.

Six grains and an anomalous crystallite, O, possibly a sub-grain, were selected. One grain does not survive to be visible in fig 65/6. The grains are identified by their graph symbols, □, △, ▽, ◇, +, X. The grains were measured at intervals of 100s real time (5sec video), with the following results:

Figs 67-70 show highly discontinuous growth behaviour, a clear link between size and survival and that survival seems to correlate with a highly productive initial growth spurt. It is interesting to note that +, the largest grain at 1800sec is also the last to appear, possibly nucleated when the growth of X comes to a halt against a pre-existing grain (which + rapidly consumes between 0:28 and 0:38) or possibly growing out from the sub-surface bulk. It appears that +, X (and O) have some special relationship. Their mutual boundaries show little tendency to move, i.e. some kind of "truce" exists between them, and their boundaries do not thermally etch. It is also interesting that of the monitored grains, ▽, the first to form, is also the first to vanish.

Another notable behaviour is boundaries and triple points locally reversing their motion (reflected in negative slopes in the L and W values, e.g grain + in Fig 70). This does not necessarily correspond to a loss of grain area (Figs 67, 68) in which for instance + shows only 2 very shallow negative slope segments.

As noted above, these figures yield qualitative information on grain behaviour, but little hard numerical data, other than successful grains tend towards an aspect ratio around 1:1.5. The inconsistent behaviour and sudden changes illustrated appear unpromising for simple mathematical analysis, though the situation may be better with a larger data set or a smaller time interval.

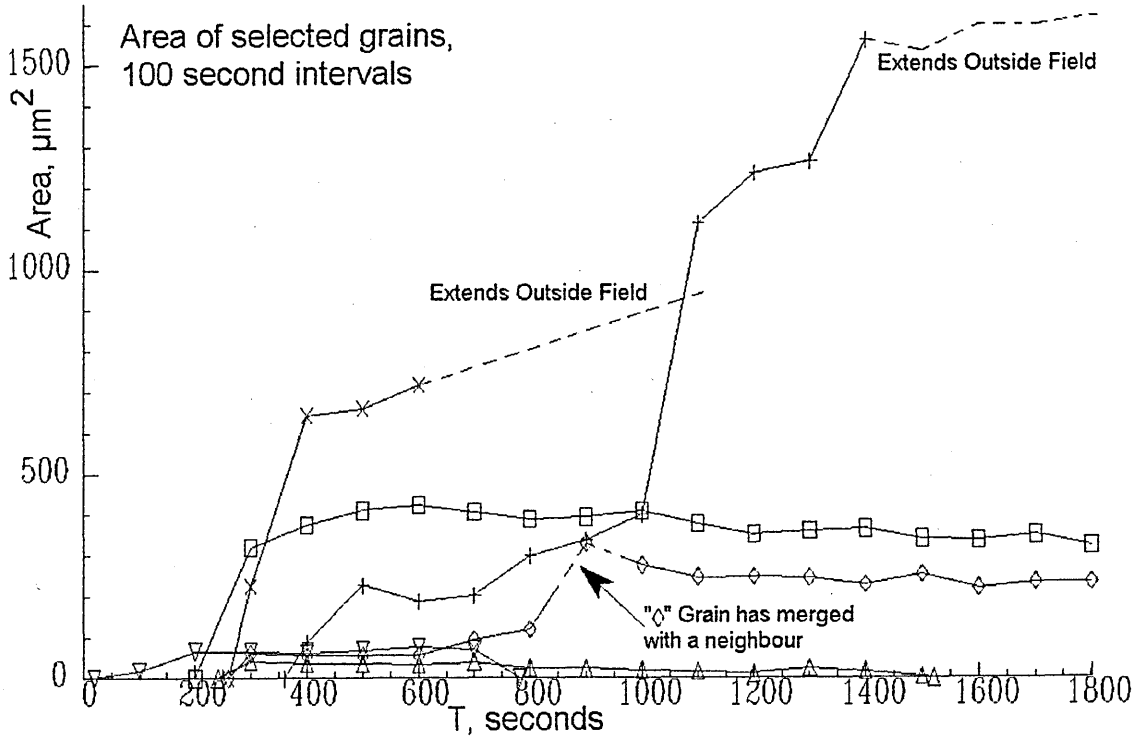

FIG. 67. Grain areas versus time since transformation to Austenite

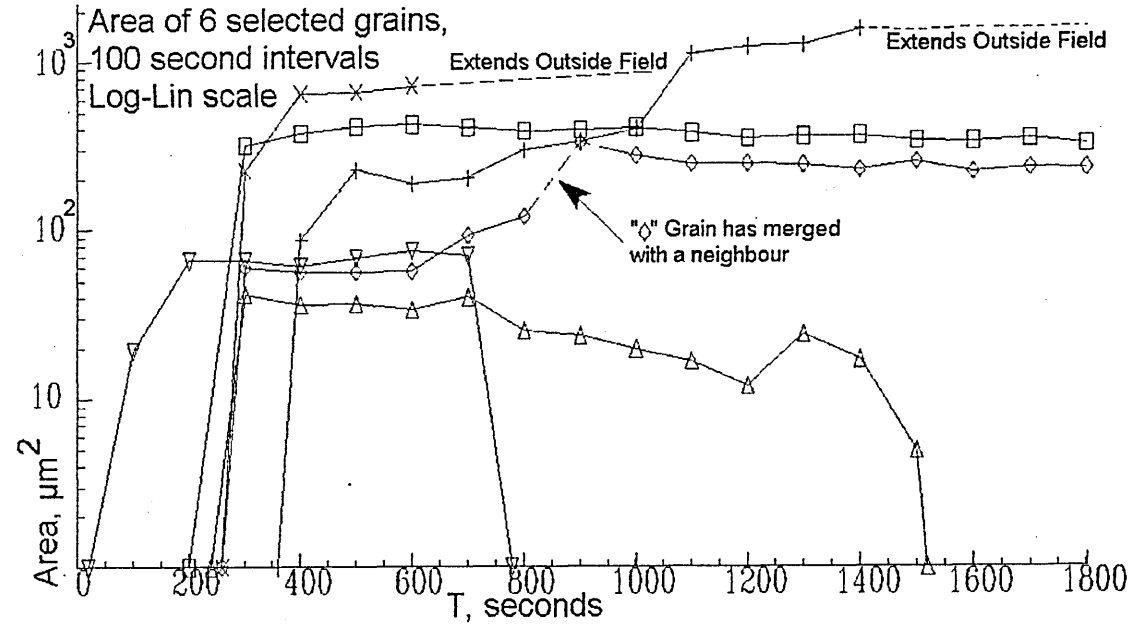

FIG. 68. As Fig67, Area shown as log scale to show detailed behaviour of smaller grains.

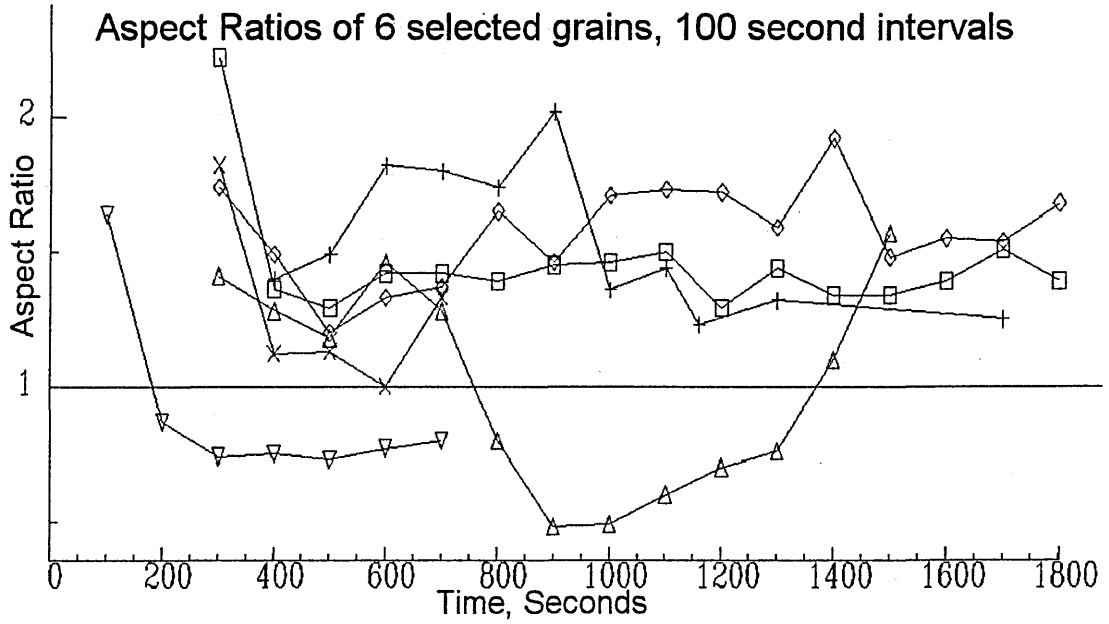

FIG. 69. Aspect ratios. Measured as (L) longest dimension : (W) largest dimension at ≈ 90° to L. The large dimension closest in direction to the original L remains denoted as L, thus the ratio can fall below 1.0 over time.

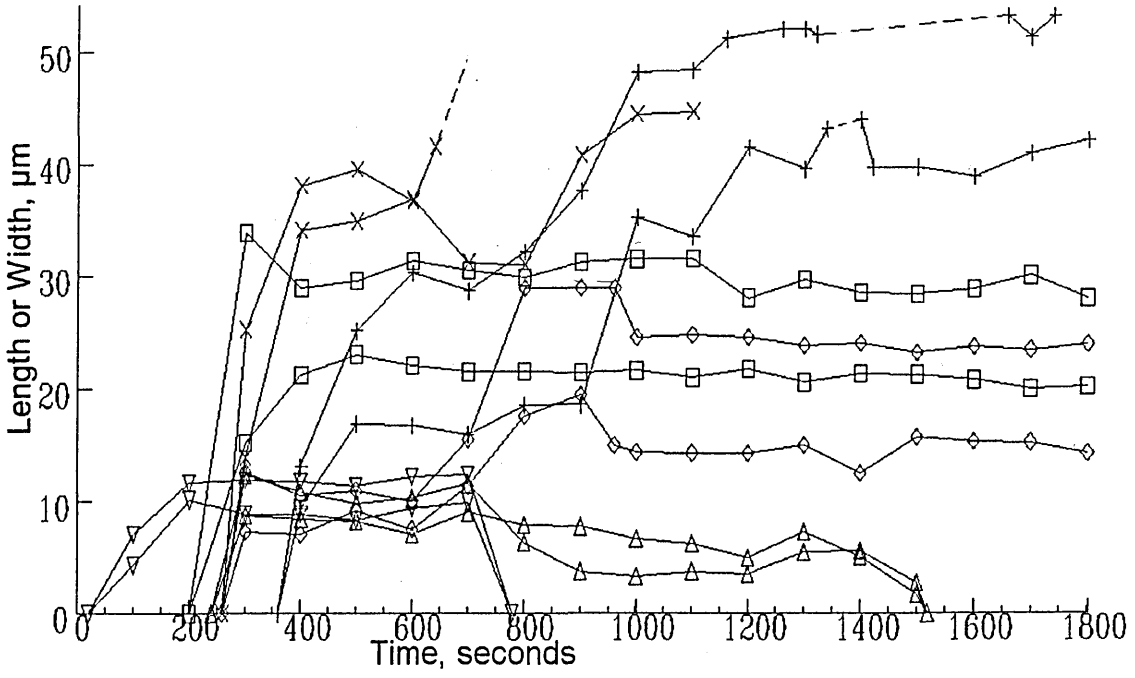

FIG. 70. Length & Width of 6 grains monitored over time.

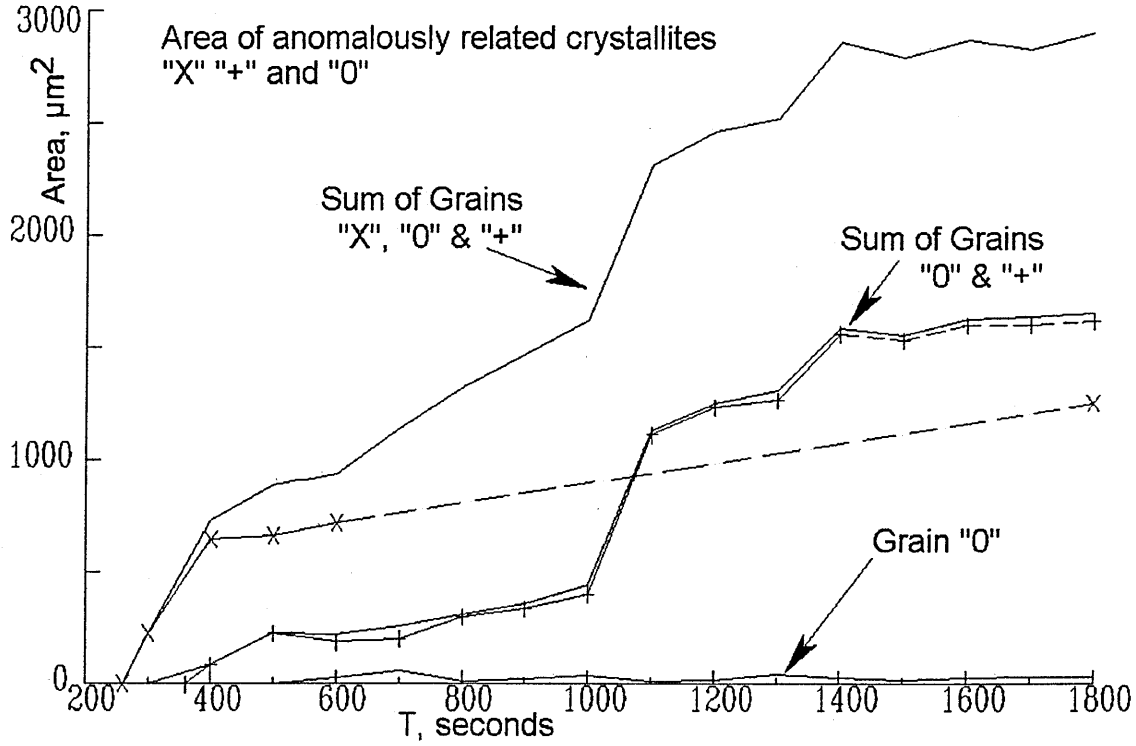

FIG. 71. Crystallites X,+ and 0 analysed separately and as one. The significance of large related grain areas (as opposed to needle shaped intrusions such as 0) and their treatment as separate grains (or not) is unclear.

4.6.2.3 STEEL GRAIN GROWTH – TRIPLE POINT TRACKING

The lower right triple point of grain X was tracked at 10sec intervals (0.5 sec video) as it crossed the field of view. When this point ceased to exist and neighbouring crystallite, +, appeared, tracking continued with the corresponding triple point on that grain. This generated a time stream of 2D co-ordinates relative to its starting point (arbitrarily (0,0)). The track of the point is given as Fig 72.

The triple point positions shown in fig 72, again clearly illustrate discontinuous motion, particularly the high speed of initial movement, with 3 dense clumps of positions indicating the triple point dwelling in near-stability at one place for some considerable time. However, it is interesting to note that the triple point, although it appears stationary to the eye in the video, is in fact rarely stationary. This behaviour is reflected in the "speed" timestream, fig 73. The "speed" is more properly the displacement of the point at 10 second intervals, roughly rendered into 1 dimensional motion from 2 dimensional motion, by reference to its overall $x \approx y$ trend. The calculation was a simple Pythagoras $\Delta s = \sqrt{(\Delta x^2 + \Delta y^2)}$. This scalar result was then assigned a sign, as follows. If Δx & Δy are positive, assign Δs positive. If Δx & Δy are negative, assign Δs negative. If $|\Delta x| > |\Delta y|$ assign Δs the sign of Δx. If $|\Delta y| > |\Delta x|$ assign Δs the sign of Δy. If $|\Delta x| = |\Delta y|$, assign Δs the sign of Δy. As the triple point makes very few major moves that are at or near 90° to the x=y direction, the approximation seems to work fairly well.

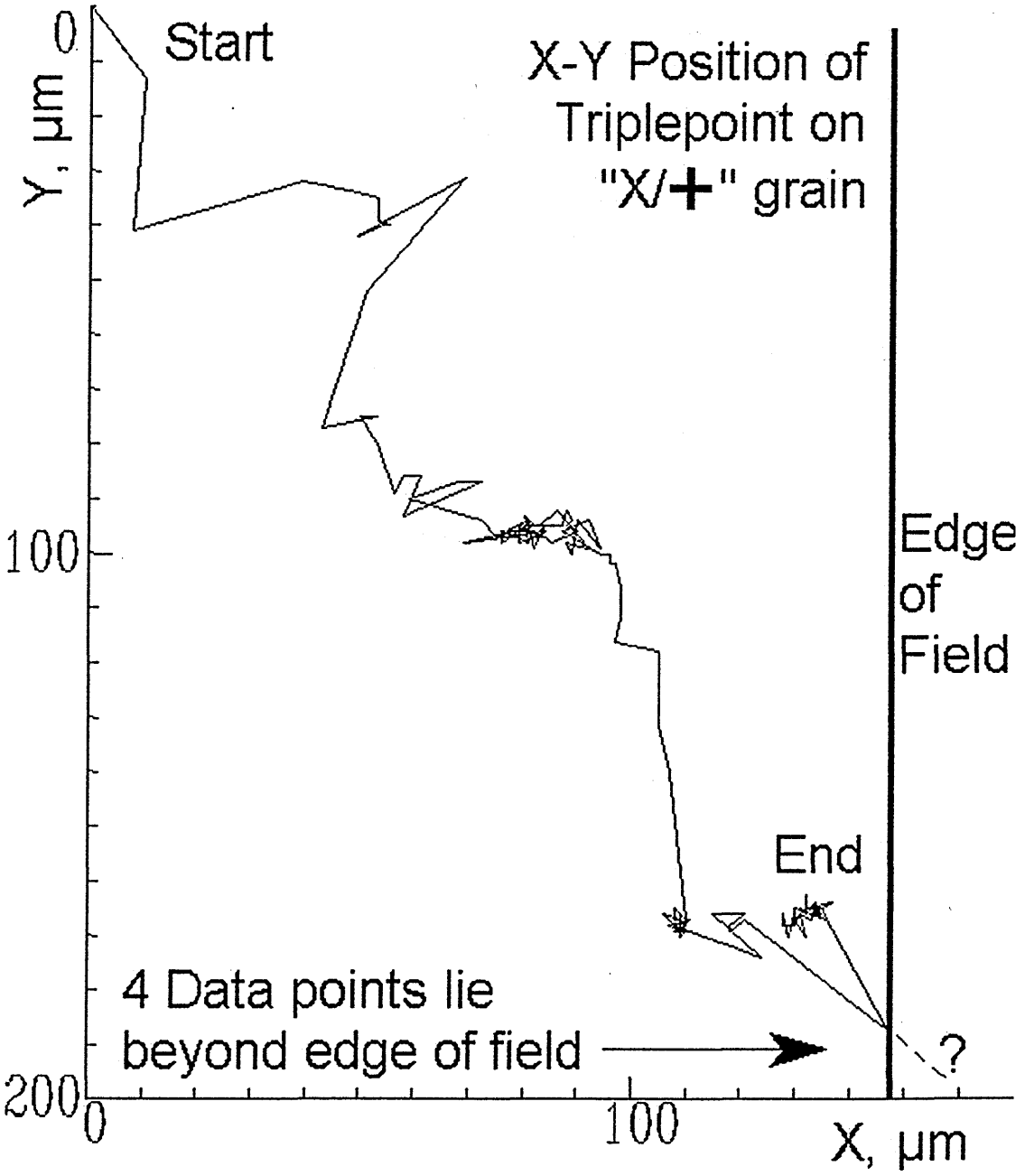

FIG. 72. Track of triple point position at 10 second intervals

The statistics shown on Fig 73 demonstrate that, as expected from Fig 72, the "speed" distribution does not fit a "normal" statistical distribution. Four percent of its data points lie more than ±3 standard deviations away from the mean, an order of magnitude higher than would be expected if the distribution were Gaussian-normal.

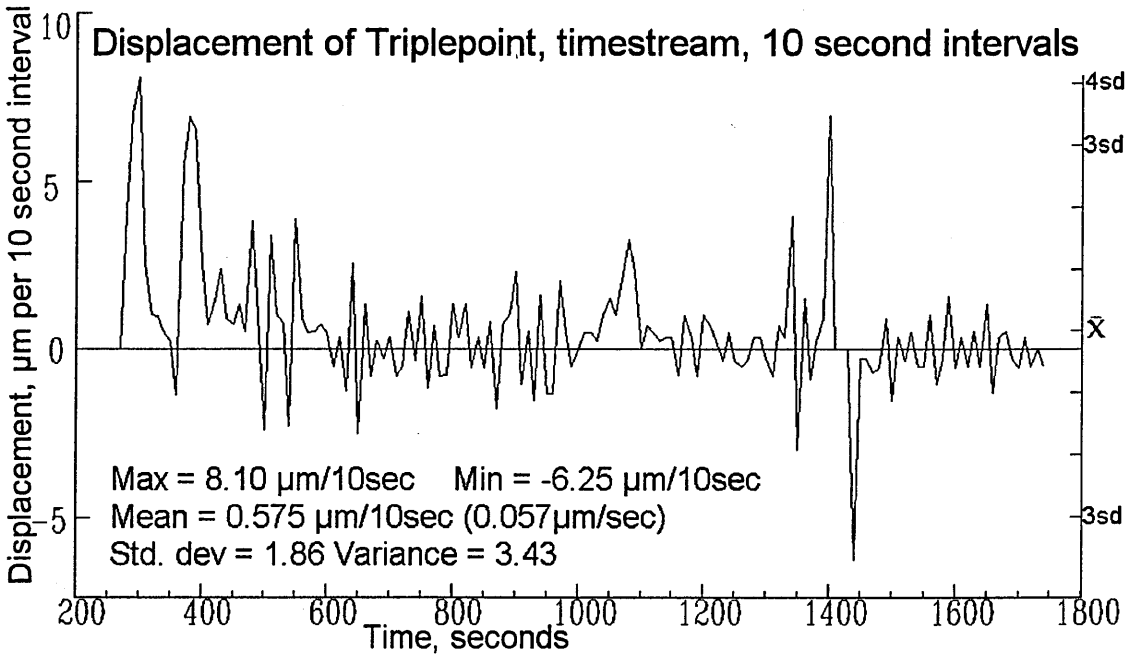

FIG. 73. Triple point speed as a timestream, with basic statistics.

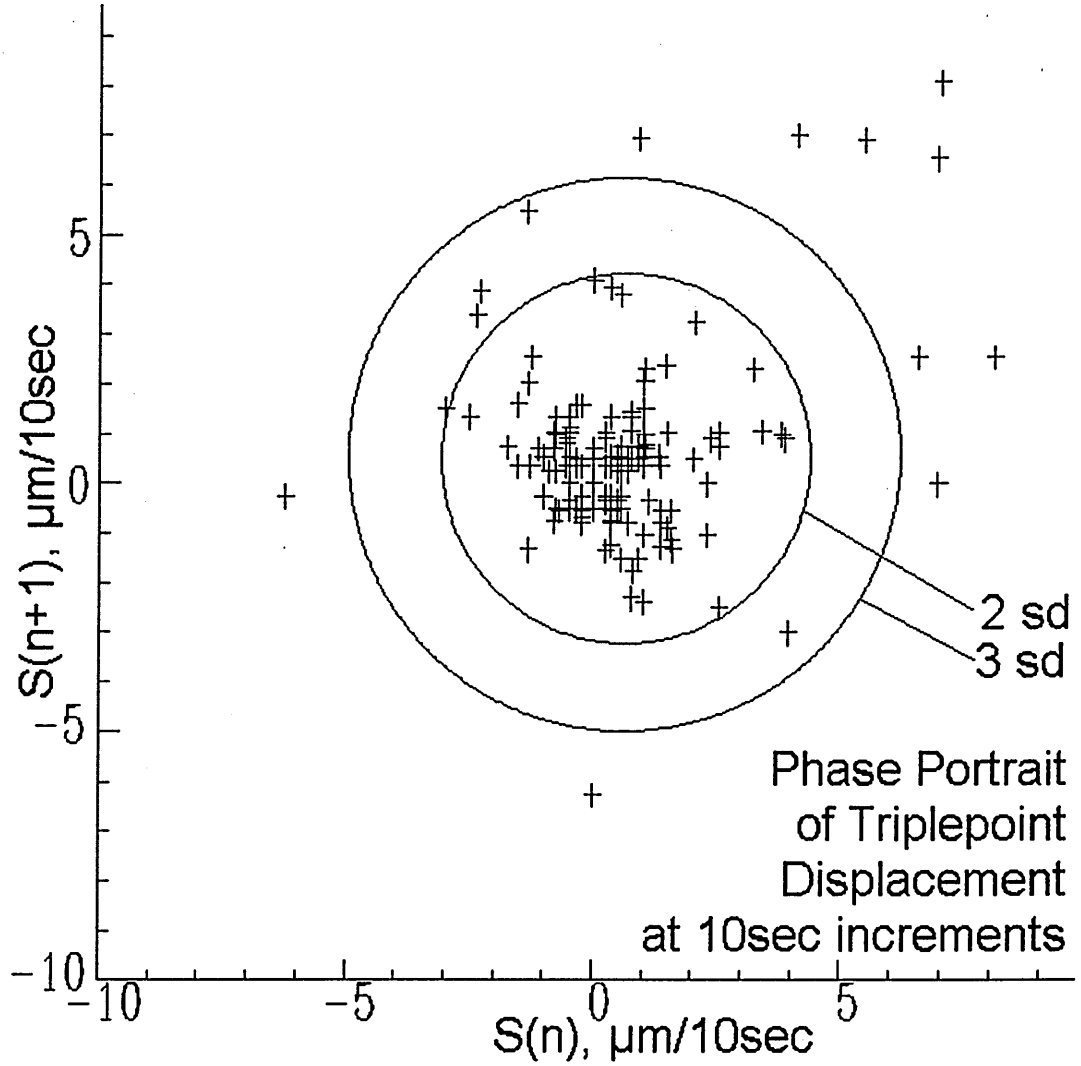

FIG. 74. Simple phase portrait of speed time stream, showing 2X & 3X standard deviation

Fig 74 is a simple phase portrait (after Packard et al. (1980) and Takens (1981)), giving a different view of the timestream data shown in Fig 73. This was constructed very simply by plotting $(s_1,s_2)(s_2,s_3)....(s[_n],s[_{n+1}])$. This type of timestream analysis is capable of showing the presence (or absence) of periodic and quasi-periodic effects by their effect on the size and shape of the "cloud" of data points on the plot. A large quantity of data is often required, usually more than in this "speed" timestream if the effects are subtle. This plot shows a compact and roughly circular centre to the data cloud, which clearly corresponds to a normal or near-normal distribution of speeds when the triple point is stationary or slow moving. This distribution clearly has a standard deviation considerably less than the calculated s.d. for the whole set (shown by the circles). Overlaying this compact normal distribution is a more complex and diffuse distribution of data points, corresponding to the large and rapid excursions of the triple point. With a much larger data set, this diffuse distribution might yield some useful insights into the kinetic behaviour of triple points.

The cloud does not appear to have any strong shape (though it would be highly unusual to detect such an effect with so few "rapid motion" data points). This suggests that the distribution is more likely stochastic (due to random/normal distribution factors) than deterministic (due to some truly predictable or short-range predictable chaotic process).

If the value plotted on a phase portrait is truly random, points will be distributed "sprayed" evenly throughout the graph space corresponding to the values physically possible for the system. If the value is varying in a Gaussian-normal distribution, the data cloud will look like a target that has been fired at by a marksman, points denser around the mean (or bullseye), becoming more diffuse with distance in all directions. If the value varies in a genuinely predictable manner, the data will form a definite shape – for example sine-wave data will form a circle or ellipse, like a "Lissajous figure" produced on an oscilloscope. If the value varies in some chaotic or quasi-periodic manner, with short-term predictability, then a diffuse shape is produced – perhaps something like a marksman who has had to contend with a very strong and gusty wind.

This phase portrait shows that triple point kinetics is not one single behaviour – the behaviour of triple points appears to be different depending upon whether they are in fast motion or slow motion.

The phase portrait and time stream do give some guidance for future experiment design. Clearly a larger data set is required, implying a longer experimental run, or hotter (more active grain growth) and with finer time resolution to generate more data points. The sharp spikes in the timestream suggest that a smaller time increment in point tracking would probably be beneficial.

The central portion of the data cloud in the phase portrait is showing signs of dividing into a grid of points and of bunching at certain values ($\sqrt{2}$, $\sqrt{5}$, $\sqrt{10}$, $\sqrt{13}$ etc. corresponding to $\Delta x,\Delta y$ values of [1,1] [1,2] [1,3] [2,3] etc.). This indicates that the spatial measurement resolution at this magnification (0.25μm per pixel) is just adequate.

The trade offs to be made are obvious and invidious. Short of major electronic modifications to the SEM or purchasing a new instrument, image resolution is limited by the 720 x 484 pixels NTSC video standard, thus spatial resolution can be increased only by higher magnification. Higher magnification will give a shorter experimental run before the features of interest move out of the field of view, probably reducing the amount of data gathered and dictating ultimately a trade of spatial resolution against time resolution/data volume.

4.6.3 IMPLICATIONS FOR GRAIN GROWTH MODELLING

The video results from all of the metals show that grain growth generally is not a continuous process. After the brief initial flurry of explosive and competitive grain growth activities, a quasi-stable situation is reached. In this regime, most grains are not significantly growing/shrinking and most boundaries are not significantly moving at any given time. The growth activity that is occurring happens in relatively isolated "patches" and the grains that are growing are only advancing on one front at any time.

These qualitative observations are borne out by the grain tracing and grain area results from the steel experiment. Any model would have to take account of the observation that a grain can be in one of two states, quasi-stable or actively growing/shrinking.

Further evidence comes from the triple point tracking results. Again, these show the triple point in two regimes of behaviour, corresponding to the overlaid distributions observed on the phase portrait. The first of these regimes is the "slow-motion" behaviour, in which the triple point is displaced only a small increment from its previous position, with no strong directional bias and seems to be almost "in orbit" through a locus of preferred positions, as the grains and boundaries pushing and pulling on the triple point "jockey for position". This corresponds to the compact core of the data cloud on the phase portrait, fig. 74. The second regime is the "fast motion" regime, in which the triple point moves rapidly, with a strong directional trend as one of the grains gains an advantage over a neighbour and undergoes a growth spurt. This corresponds to the more diffuse and less-circular distribution overlaid on the compact "core" distribution seen in fig 74.

Thus, it is clear that any growth model considering the grain as the basic unit is inadequate if the grain's only possible actions are "grow" "shrink" and "do nothing". The grain must be able to do all of these things not as a whole, but at each of its boundaries with a neighbour.

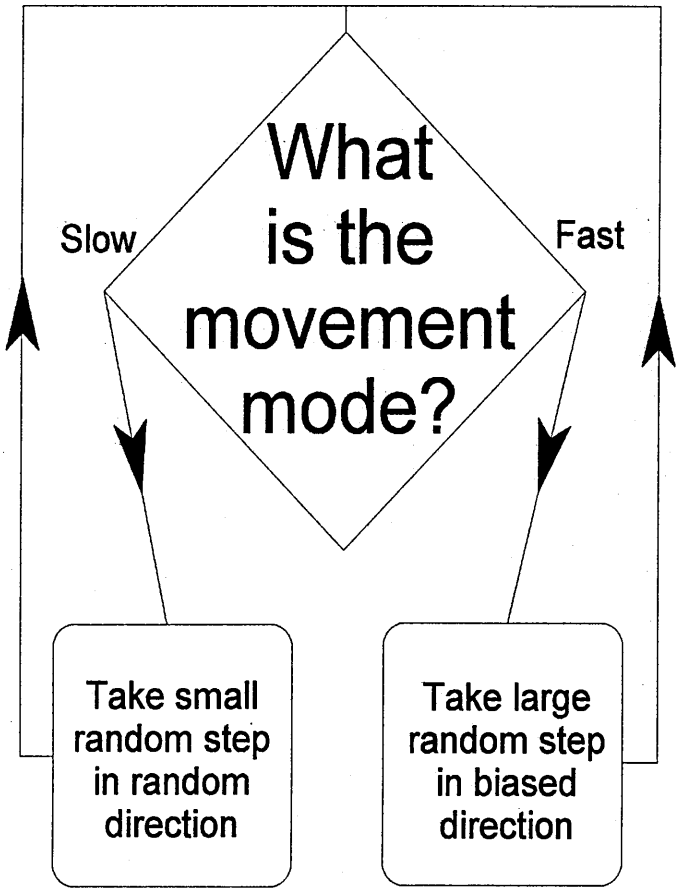

The triple point in fig. 72 follows a dramatic "drunkard's walk", and the mathematical "2D random walk" may provide a reasonable modelling tool to simulate its behaviour. The algorithm would have to take account of the two behaviour regimes by being a random walk with two step sizes, one of which has a moderately consistent direction. A candidate algorithm may look something like Chart 1.

CHART 1.
Potential framework for triple point motion modelling of grain growth

The test for "Fast" or "Slow" movement could be very basic or very sophisticated, with testing of how far the triple point has moved in the last few steps, whether a neighbour grain has been annihilated, current "balance of power" between the neighbour grains etc. The test may differ depending on which mode is then prevailing. The small random step action will probably contain a bias tending to retain the point within the "family of preferred positions" so that the model point does not randomly drift to a degree that would be energetically or microstructurally unfeasible.

4.6.4 GRAIN BOUNDARY GROOVING

Thermally etched grain boundary grooves (fig 75) are visible in the later stages of the steel experiment, i.e. at higher temperatures and when the structure has become less dynamic, with many boundaries static for considerable lengths of time (grooves are visible in figs 75, 63 & 65, not visible in figs. 60, 61, 62 & 64). The morphology and video history of the crystallites and boundaries gives some guidance on which are separate grains and which have a twin relationship or some other special relationship. Twin

boundaries do not appear to undergo thermal etching, but it is clear that most non-etching boundaries are not twins.

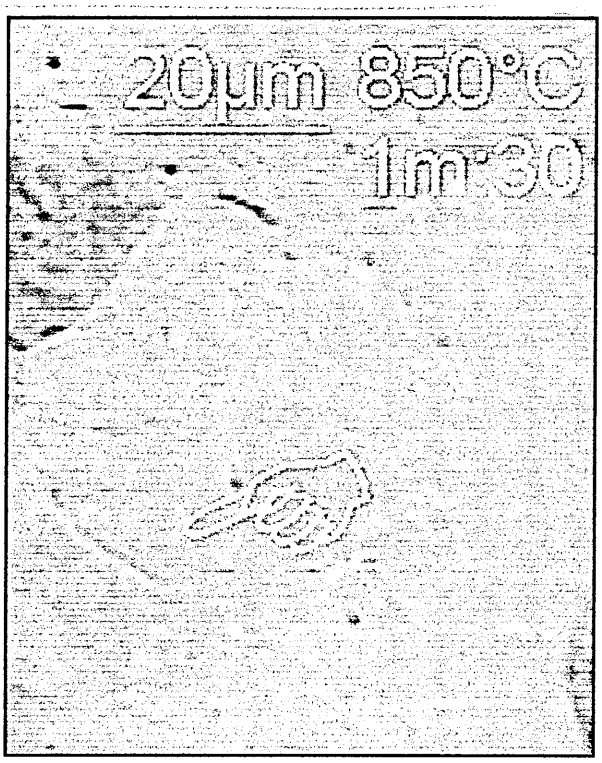

For example, the video history shows that the Fig. 75 crystallite is in fact a separate grain, not a twin to any of its neighbours, despite its straight sides, but only one of its 3 boundaries has become grooved. It is also interesting that that the austenite-pearlite transformation front is later able to cross its boundaries unimpeded (2:00-2:01).

FIG. 75. Showing thermal etching at many, but not all grain boundaries. Particularly highlighted is a grain on which one boundary has etched but the others have not.

The driving force for thermal grooving is the energetic undesirability of a 90° sharp corner to a grain. The mechanism of the groove's formation is surface diffusion, a time-and-temperature dependent phenomenon (fig 5 in chapter 2). Surface diffusion occurs at the surface-breaking grain boundary for two reasons 1) this is where the geometric driving force acts 2) the atoms are free (or freer) to move by diffusion, due to the disrupted lattice at and around the boundary. This means they are less firmly bonded to their neighbours, or have less neighbours to be bonded to, than atoms in the crystal bulk.

If a boundary does not show thermal grooving while others do, this implies that either the driving force is locally reduced, the diffusion mechanism is locally inhibited, or the atoms at the boundary are less free to move/more tightly bonded (higher activation energy required for diffusion).

It is almost inconceivable that the driving force could be reduced, as it is a geometry-mandated driving force and geometry should be more-or-less common to all surface breaking grain boundaries, particularly late on in the grain growth process.

Local alteration of the diffusion mechanism is conceivable, for instance by the presence of an impurity or segregate at the grain boundary. However 1) in this aggressively processed steel, a high level of homogeneity would be expected on the micron to mil-

limetre scale 2) most impurities increase the rate of grain boundary migration (probably by promoting cross-boundary diffusion) and thus might logically be expected to increase, not decrease surface diffusion.

Occam's razor thus leaves the third possibility – that the atoms at the non-etching boundary are more tightly bonded than at most other boundaries in the network. This implies that the structure of the non-etching boundary is different from the majority of the boundary population, which will be random high-angle boundaries (see 2.2.2 in chapter 2). Section 2.2.2 also details the two other types of boundary, i.e. low-angle boundaries and Special high-angle boundaries (high-Σ/CSL boundaries). Both of these boundary types could fulfil the criterion of more tightly bonded atoms or a less-disrupted lattice at the boundary and would constitute a minority of the boundary population in this sample.

As described in chapter 2, low-angle boundaries are formed of large "wall" arrays of dislocations. These are believed to be formed when strained crystals having a high dislocation density start to re-crystallise (Humphreys and Hatherley (1995)). The dislocations migrate, come together in arrays, and form "sub-grain" boundary arrays of dislocation walls between differently-tilted parts of the same parent crystal lattice. Looking at the video history of the non-etching boundaries present at the end of the steel video sequence, shows that all of them have formed when two previously entirely separate crystallites have grown to meet. Thus, this building of dislocation walls would not have been possible and the only mechanism that could account for a dislocation wall type of boundary would be an effective merger between the lattices of two minimally misoriented grains at the boundary plane, followed by boundary dissolution into an array of dislocations and dislocation walls. A logical consequence of this would be the possibility of grain mergers – a phenomenon that has not yet been apparent, although grain ◊ does appear to either merge with a neighbour, or undergo a very rapid takeover by its neighbour. Such a lattice merger might be expected to be problematic, given the segregates likely to have been contributed by the two (presumably random) boundaries and presumably now either trapped in the new boundary or forced to diffuse rapidly away elsewhere as the two lattices "zip up". Small atom segregates could reside or diffuse interstitially in near-boundary dislocation strain fields, but larger atoms (most frequently found as grain boundary segregates) would have to diffuse away into otherwise "perfect" neighbouring crystal or be forced into solid solution, an outcome that would presumably require considerable energy to drive it. It seems unlikely that large-atom segregates would be able to easily diffuse away along the boundary itself, if the entire boundary had ceased to exist as a distinct entity, having "zipped up" to form a large-dislocation-array boundary from the two prior random boundaries. Theory and some prior work (Rollett and Kalu (2005), Humphreys and Hatherley (1995)) also

show that such a low-angle boundary would be expected to have very high mobility (not necessarily large actual motion), yet the non-etching boundaries show little tendency to move. Thus, while quite conceivable and not wildly at variance with any of the observations, the explanation of non-etching grain boundaries as being low-angle boundaries seems to rely on a great many assumptions and imponderables.

The remaining possibility is therefore high-sigma special boundaries. It is quite possible that these would be more resistant to the removal of constituent atoms by diffusion, as a good proportion of atoms are in co-incident site positions for both lattices, and thus presumably more-or-less bonded to the neighbour grain in addition to their parent. These may further serve to help pin their non-coincident neighbours, thus impeding the atoms' ability or readiness to diffuse. It has also been established that high-sigma boundaries have less free volume at the interface. One logical consequence of this is that the atoms on the final layer of each crystal will be in more intimate contact with and thus more influenced by/bonded to the atoms of the other crystal, enhancing the coincident site effect.

Another logical consequence of less free volume at the boundary is less segregate. However, with a distinct grain boundary remaining, the excess entrapped segregate from the two colliding boundaries would be expected to have a considerably greater opportunity to diffuse rapidly away along the boundary plane. This could be important to the larger-atom segregates that are much less able to travel interstitially along dislocations or through the crystal itself. As noted above, boundaries having less segregate might be expected to show less surface diffusion, and high-sigma boundaries would fit this expectation too.

As with the low-angle boundaries discussed above, the unexplained feature of the non-etching boundaries (assuming they are high sigma boundaries) is why do they show little tendency to move, given that most high sigma boundaries are established as having relatively high mobility? One possibility is that these are sigma boundaries of the particular sigma values that do not show significantly increased mobility (Molodov, 2001)). Another possibility is that while high-sigma boundaries have higher mobility, this does not necessarily mean that they will be more mobile. Movement of the boundary comes from boundary mobility and the driving force. Driving force comes primarily from the imbalance between crystal volume free energy and the energy of the boundary surface (and associated dislocation structures etc.). If the boundary is high-sigma and has a "better fit" than other boundaries, this implies that it has a lower energy. And thus the energy "payoff" for the grain network in eliminating or reducing the area of such a boundary is lower – thus the energy available for boundary movement driving force is lower.

There is also the observation that high-sigma boundary population (as a proportion) tends to rise after vigorous thermo-mechanical treatments. This is assumed to be because the high-sigma boundaries are more mobile and thus "their" grains will be more successful at growth and in devouring their random-boundaried neighbours.

The validity of this assumption will now be tested in a thought experiment to consider what behaviour might constitute a survival trait for a grain boundary.

Consider an "average" grain boundary, over a time period sufficient for the number of boundaries present in the network to be cut by a quarter, i.e. about half of the grain boundaries present will move, encounter another boundary and combine to form one boundary from the original two:

In the time required for the boundary population to drop as described, a grain boundary that moves will almost inevitably collide with another boundary ($P_c \approx 1$ – the observations show that once moving, a boundary rarely stops for very long). When boundaries collide/coalesce there is a finite probability that the result will be a high-sigma boundary. The high-sigma boundaries are only a small proportion of the possible misorientations, thus this probability is low if the crystals are randomly oriented. Two grains encountering each other for the first time, particularly later in the grain growth process, are highly unlikely to have been close neighbours when first nucleated, thus it is assumed that their lattices will be randomly oriented with respect to each other (unless there is some long range order – i.e. texture – in nucleus orientation). Thus in a meeting of boundaries (of any character) of randomly oriented crystals, the probability of forming a high sigma boundary, P_Σ, is significantly less than 0.5

Thus if a high-sigma boundary moves, the probability of it forming a new high-sigma boundary (i.e. probability that a high sigma boundary survives in the microstructure) is:
$P_c \times P_\Sigma \approx 1 \times P_\Sigma \approx P_\Sigma$
If a high sigma boundary does not move, the probability of it either surviving or forming a new high-sigma boundary is the probability of it not undergoing collision from another moving boundary (≈ 0.5 if boundary population is cut by a quarter), plus the probability of it undergoing collision and forming a new high sigma boundary,
$P_c \times P_\Sigma = 0.5\ P_\Sigma$
P_c is 0.5, as this boundary is not moving, but 50% of the boundary population will move.

This treatment is very simplistic, but clearly $0.5+0.5\ P_\Sigma$ is larger than P_Σ, as P_Σ must be less than 1. This suggests the possibility that although high sigma boundaries generally have high mobility (move further/faster for a given driving force), their survival and predominance in heavily processed microstructures may be due to a tendency

to "sit tight and survive". Meanwhile their random cousins move around and mutually annihilate each other, occasionally annihilating a stationary high sigma boundary, occasionally producing a new high sigma boundary.

If the material is highly textured, the P_{Σ} figure may be dramatically different from the random grains case, but can never exceed 1.

The effect of grooves on grain boundary kinetics is unclear. The appearance of grooves coincides with a more static structure and (subjectively) more discontinuous movement in the relatively few boundaries that remain mobile, however at this later stage an overall less dynamic structure would be expected. It is worth noting that discontinuous movement behaviour is also apparent earlier in the experiment, before boundary grooves are first visible, thus it would appear that discontinuous movement is independent of grain boundary grooving. It is possible that grain boundary grooving exists before it becomes visible at this magnification. However, visible grooves first appear between 0:40 and 0:55 (around 780°C-820°C) and they appear on both very recently mobile boundaries and those which have been static for a short time. This suggests that the factor limiting the appearance or non-appearance of the grooves is not the rest-time of the boundary, but the temperature of the specimen. This implies that the surface diffusion process that forms these grooves was not activated until the specimen reached this temperature and that the earlier part of the grain growth process occurred under non-grooving conditions.

Rabkin et al. (2000) show discontinuous grain boundary motion, with boundary grooving, in a high-purity (zone refined) NiAl intermetallic polycrystal, suggesting that discontinuous motion is not dependant on impurity. This present study shows discontinuous motion in an impure polycrystal, both with and without grooving, suggesting that discontinuous motion is not dependent on grooving. Schmidt et al. (2004) show discontinuous boundary motion inside a bulk of impure polycrystal, further demonstrating that discontinuous motion is not dependent on surface effects. Meanwhile, Gottstein et al.(2001 and Mattisen et al. (2001) show continuous motion in high purity bi- and tri- crystals. While not entirely conclusive, these results, taken together, strongly suggest that discontinuity of boundary motion, while almost certainly influenced by impurities and grooving, is a property of polycrystalline networks and not solely a consequence of impurities or grooving.

It should be borne in mind that the assessment of continuous/discontinuous dynamics is a subjective "eyeball" assessment and is hence based on absolute velocity of grain boundaries. That is to say, the kinetics of the later structure, assessed as "subjectively more discontinuous" has that assessment because the moving boundaries show a

wider range of *absolute* velocities. The earlier structures also show discontinuous boundary motion, but a smaller range of velocities. A boundary that suddenly moves 10μm in the later, mostly static structure, is very eye-catching, but is relatively unlikely to annihilate its neighbour grain. A boundary suddenly moving 2μm in the earlier, highly dynamic structure, is much less eye-catching, but may be consuming proportionately as much or more of its neighbour grain. A more rigorous assessment of boundary motion and its variability, both in absolute terms and relative to instantaneous grain size, is a highly desirable but labour intensive piece of future work.

CHAPTER 5
RESULTS AND DISCUSSION 2: PHASE TRANSFORMATIONS IN STEEL

5.1 TRANSFORMATION ON COOLING AUSTENITE TO PEARLITE)

Refer to Video 2 - Steel in appendix 4

Transformation on cooling appears to divide into three distinct behaviours, transient austenite decomposition phenomena, the precipitation of isolated carbides at surfaces and the main austenite/pearlite transformation fronts sweeping through the specimen.

5.2 AUSTENITE DECOMPOSITION

Almost simultaneous with the formation of the first surface carbide (see below), the appearance of the neighbouring crystallite changes to a patchy, subtly mottled appearance of slightly darker irregularly shaped cellular areas on a background of about the same grey level as the parent crystal [fig. 76]. These cellular features have a size in the range 1-5μm. Given that the imaging contrast is sensitive to both atomic number and crystal orientation, it is possible that this image contrast is due to either:

1) segregation of carbon (directly affecting atomic number contrast – darker areas being carbon enriched) or
2) lattice distortion due to concentrations of dislocations and/or concentration of solute.

In fig. 76C a surface carbide is precipitated from one of these slightly darker areas, suggesting either a localised enrichment of carbon or a localised reduction in ability to hold carbon in solution. The same subtly mottled appearance becomes visible, though less obvious, on several more austenite grains a short while later, while some other grains do not show the effect at all (e.g. the last area to transform, top left corner of field around 2:00 - 2:04, Fig 8D).

The fact that some grains do not seem to show this effect, and that those that do tend to appear relatively light in the image (i.e. oriented to give high electron backscattering), suggests that localised lattice distortion is somewhat more likely to be the cause of the image contrast. If the contrast were solely due to localised changes in average atomic number then it would be expected that this effect would appear more or less equally in all crystallites, regardless of their orientation to the incoming beam. In addition, the difference in average atomic number between Fe 0.61%C (the bulk composi-

FIG. 76, A, B & C. Showing (A-B) mottled texture appearing on crystallite simultaneous with first carbide precipitation and (B-C) carbide precipitating at the position of a dark area and away from boundaries. A: 1:49 B: 1:54 C: 2:01

tion) and Fe 0.75%C (eutectoid composition, which is what any segregation is assumed to be attempting to create) is about 0.1 Z, which is in the order of the limit of detectability, even with the exaggerated Z sensitivity of the channelling contrast set-up.

It is in the nature of channelling contrast that electron backscattering (and hence lightness of any pixel in the image) is not directly proportional to the angle between the incoming beam and the target lattice. There are certain orientation conditions in which a very small change in beam-lattice angle will generate an eyeball-detectable change in contrast and other orientation conditions in which the same change will not give any detectable change. The fact that the subtle mottling effect is visible on only some grains suggests that these grains happen to be favourably oriented to show the effect, while others are not.

Taken together, these facts suggest that, simultaneous with the first, isolated, precipitation of carbide and before the activation of the main transformation fronts, there is a generation of dislocations within the austenite. Presumably, this is provoked by atoms attempting to reach a body-centred cubic packing arrangement and thus deviating from their ideal FCC lattice positions, generating strain fields and dislocations. It is possible that there is some transient intermediate crystal packing arrangement present, such as the meta-stable body centred tetragonal structure encountered in Martensite. However, if this were so, then it would likely be much more clearly visible than this subtle effect and would probably have sharp, well defined boundaries.

Assuming that this effect is, as seems most likely, due to dislocations, it would appear that they then form some meta-stable cellular-type dislocation structure, presumably by dislocation migration and entanglement/array formation. The localised precipitation of carbide is independent of the pearlite transformation reaction and is in some instances observed to be associated with this cellular-type structure. This suggests that the cellular structure has caused a locally saturated or super-saturated carbon solid solution as its atom packing and dislocation density change, locally reducing carbon solubility.

This cellular sub-structure in the decomposing austenite may possibly account for, or influence transformation packet/lath packet size in Martensite and Bainite.

5.3 CARBIDE PRECIPITATION

The first definite and lasting new microstructural feature to appear on cooling is an isolated dark area, which forms quite rapidly and then grows slowly [fig. 77 A, B & C]. Many more of these features appear during the transformation [fig. 77 D], but they seem independent of, and uninfluenced by, the main "transformation front" growth of pearlite (described below). A few of these features do appear to nucleate on the free surface of grains, away from boundaries, particularly just before the arrival of a transformation front, but most appear at, or adjacent to, boundaries. A few seem to form or accelerate their growth as the transformation front approaches and passes through their position, probably due to the locally increased carbon level that is expected in the untransformed material ahead of the transformation front. However, most form before the approach of the transformation front and grow steadily until the front passes. In all cases, growth halts as the front passes and no new features appear in the transformed material. Distribution of these features is not uniform, there is some clustering, and the area towards the top left of the field (the last to transform) is largely free of these features.

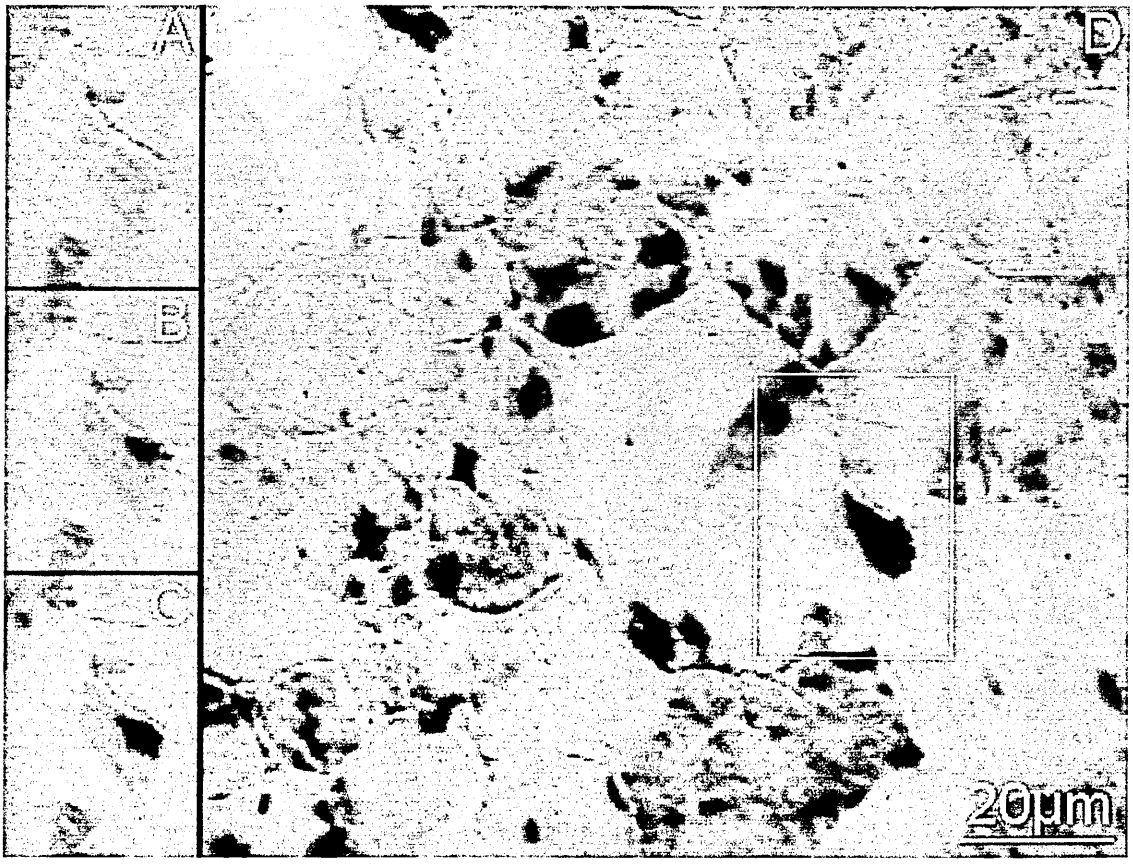

FIG. 77A, B, C, D. Transformation from austenite to pearlite, showing precipitation of surface carbide. A: 1:44, B: 1:53, C: 1:55, D: 2:00 ≈ 650°C.

On close observation after completion of the transformation it is possible to see more of the morphology of these features [fig. 78]. The dark appearance of these features implies a low average atomic number (as the orientation contrast detector set up has an exaggerated sensitivity to atomic number contrast). This implies high carbon content. Their morphology and carbon content, in combination with the observation that these features are the last to disappear on reheating, indicates that they are solid dendrites/ films of surface carbide, probably similar to those described and mapped in 3D at grain boundaries by Kral and Spanos (1999). The conditions and constraint at a free surface are similar to those at a grain boundary. Thus, it seems reasonable to suppose that if carbide precipitation is occurring at the free surface it will be occurring simultaneously at the grain boundary surfaces in the bulk via a similar mechanism, and that this precipitation is the first lasting manifestation of the transformation to pearlite.

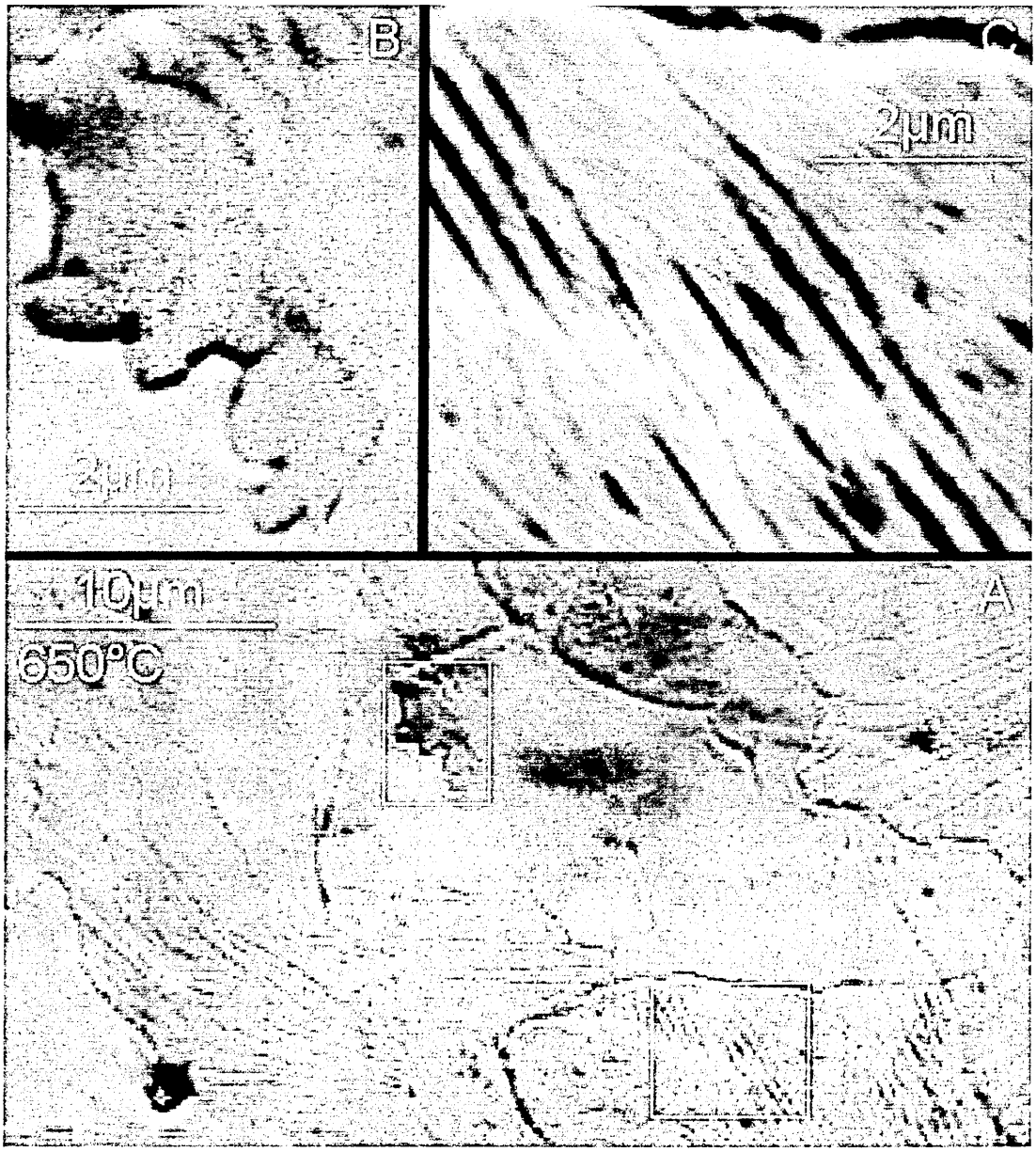

FIG. 78 A, B, C. After a cooling transformation, detail of a surface carbide (B) and parallel line features (C), suspected to be pearlite laths (discussed below)..

Despite the effects of the alloy and impurity elements present, this specimen's composition (0.61%C) is slightly hypoeutectoid, so the appearance of sizable carbides as a first transformation event is an unexpected result. The heat of the specimen and the geometry of the converter plate prevent confirmation of composition by EDX microanalysis.

5.4 PEARLITE TRANSFORMATION FRONTS

The main transformation on cooling (the transformation fronts) appears to nucleate from triple points and possibly also from grain boundaries. Nucleation from twin boundaries cannot be discounted. The number of nucleation points in this 110 x 150 µm area is small. There appear to be three or four transformation fronts nucleated within the field of view, with other fronts later sweeping in from outside the field and up from within the bulk of the specimen. This number of nucleation points means that the number of pearlite nuclei per austenite grain is quite low, three or four in a field of view covering about 50 grains, i.e. one nucleus per 10-15 grains.

This number of nuclei is an unexpected figure – the generally accepted model of pearlite formation is that the transformation nucleates on the boundaries of the austenite grain and that, if cooling is rapid enough, there will be more than one nucleation point per grain. The theory is that pearlite then grows into the grain from these nuclei, until the new pearlite grains meet and stop – thus, there are >1 pearlite grains per prior austenite grain, hence pearlite grain size is smaller than the prior austenite grain size.

However, a comparison of the figures 79 and 80 and the transformation sequence in video 2, suggest that this may not be so. Fig. 79 shows the austenite structure, just at the onset of transformation. There are about 50 grains in view. Viewing the video between 1:50 and 2:06 it can be seen that this area is swept by about 8 transformation fronts, including those coming in from outside. This implies that there would be eight grains present at completion of transformation, and this clearly is not so.

Pearlite grains cannot easily be discriminated in the SEM image (fig 82), a phenomenon that is discussed below. However, figs 80 & 81, optical micrographs of the cooled specimen, (N.B. probably not the same specimen area as shown in the SEM images) show a pearlite grain size comparable to or somewhat smaller than the austenite grain size. This implies that each transformation front may produce several pearlite grains, probably due to perturbations of the front by encounters with microstructural features such as austenite grain boundaries, austenite twin boundaries (can be seen around 1:56), inclusions, pro-eutectoid carbide dendrites (see 5.3) or other transformation fronts.

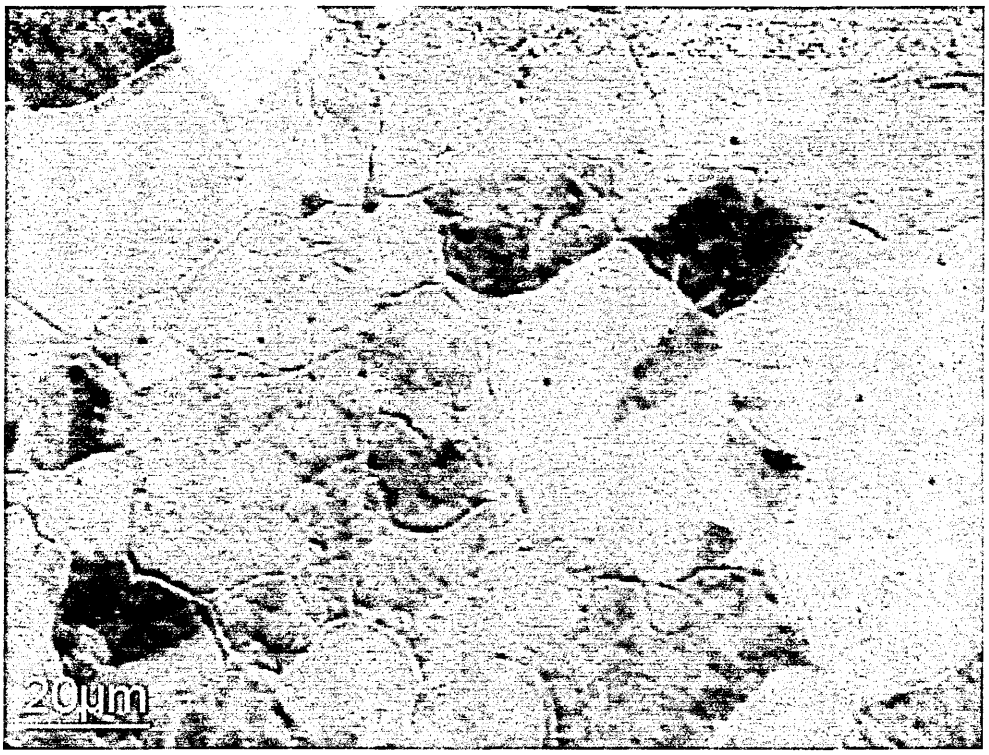

FIG. 79. SEM image of austenite structure at onset of transformation

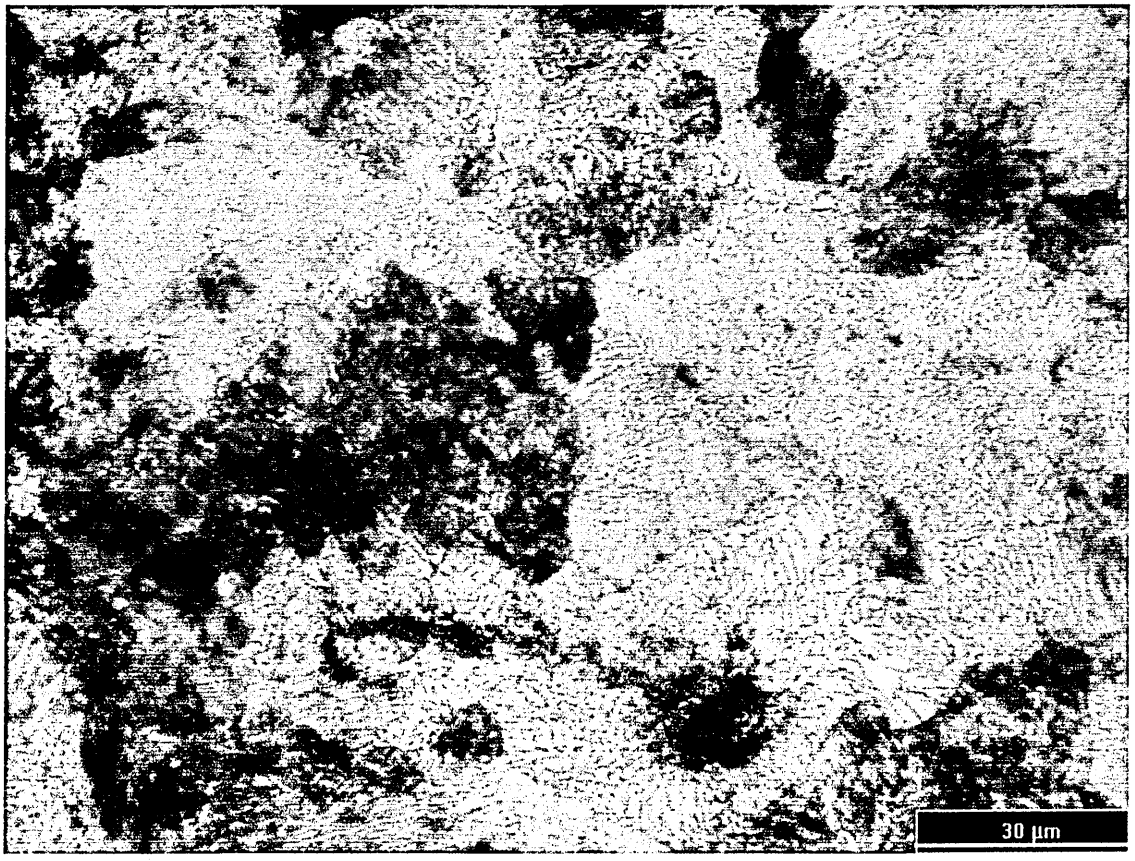

FIG. 80. Optical micrograph of cooled specimen (nital etch). N.B. view is a few microns below the surface and not the same area as shown in Fig 79.

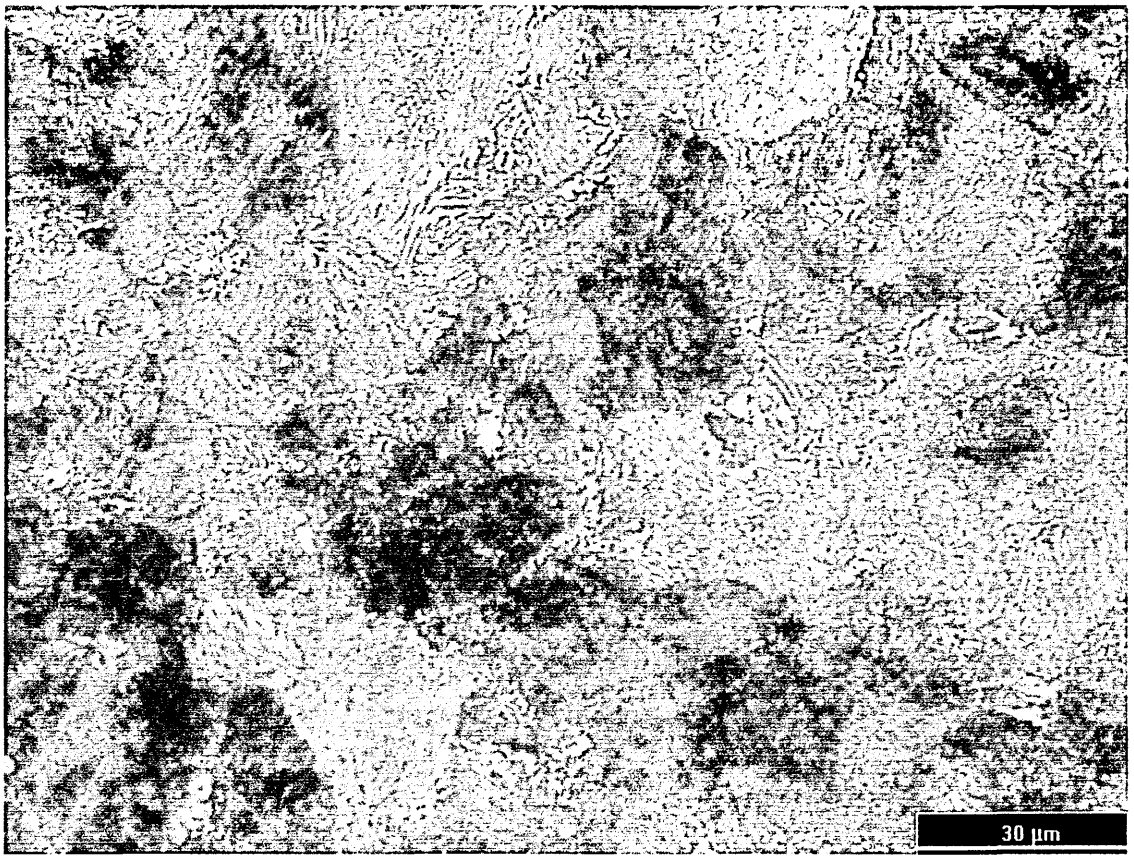

FIG. 81. Optical micrograph as Fig. 80, after grinding back approximately 200μm. N.B. Not the same area of the specimen as shown in Figs 79, 80 or 82.

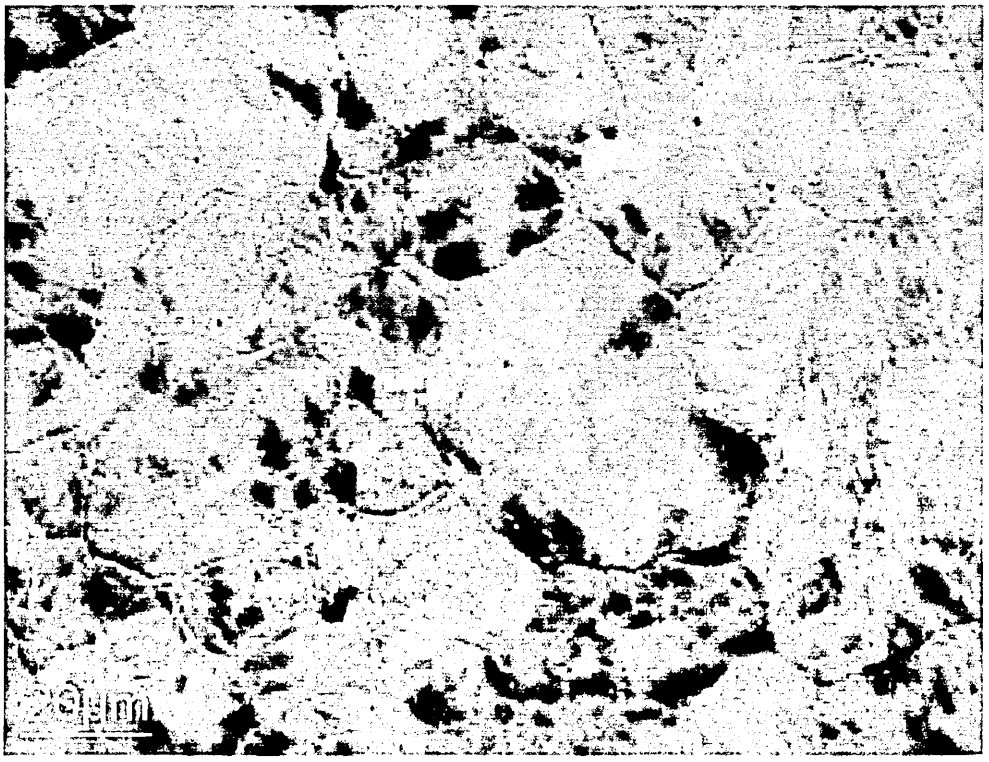

FIG. 82. SEM image of freshly transformed specimen, same area as Fig 79.

The similarity of the cooled-specimen microstructures shown in figs 80 and 81 strongly indicates that the processes observed from the exposed surface are very similar, if not identical to the processes occurring deeper within the specimen. Note, for convenience, figures 79-82 are presented at the same magnification.

The reasons for the highly complex, mottled appearance seen in fig 82 are unclear, but are discussed in 5.5, below.

Once nucleated, transformation fronts seem to progress from both sides of the boundary/all sides of the triple point, though often with some delay. The most obvious/active transformation front in this sequence appears to originate from a grain boundary triple point (figs 83 & 84).

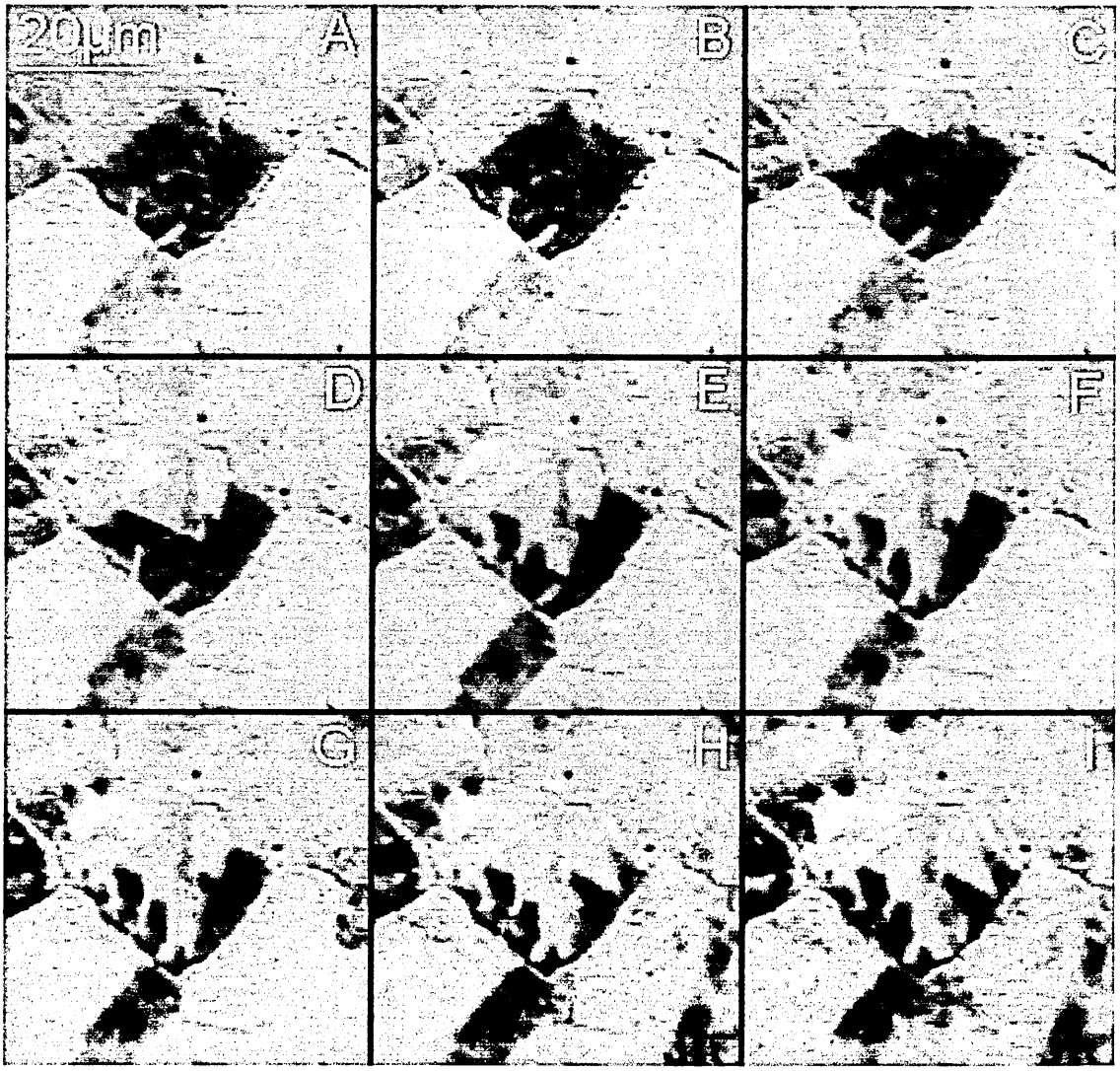

FIG. 83. First transformation front to appear, seen at intervals of 0:01 (20 sec real) from 1:53 (A) to 2:01 (I). $T \approx 650°C$, $\delta T \approx 0.15°C/Sec$. H is a detail from Fig 77D.

The isolated surface carbides described in 5.3 do not appear to trigger or otherwise influence the transformation front growth of pearlite originating from the grain boundaries, despite the fact that they nucleate and grow both before and during transformation front activity. Transformation fronts do not appear to have any strong tendency to originate from sites where surface carbides have precipitated, nor do they show a tendency to be pinned, slowed, accelerated or deflected by the surface carbides. This however is not particularly surprising, it is clear from later re-heating that these surface carbides are lying on the surface and that grain boundaries can pass easily beneath them.

The transient cellular sub-structure described in 5.2 and the presence of twins does influence the motion of transformation fronts and the transformed structure. The transformation front advancing downwards in Fig 83/84D is roughly straight, but in E and F is broken up into “fingers” presumably “reaching” around the cells of the sub-structure and in one case apparently reaching towards a twin.

FIG. 84. As fig 83, but with pearlite tinted blue and austenite tinted red for greater clarity. Position of phase boundary has been determined from visually tracking its movement in the video record, in which it is more visible than it is in a still.

When a transformation front crosses an austenite grain, the front will usually continue into the adjacent grain, usually after being briefly checked. However, in at least two instances where the front is seen sweeping along a boundary (i.e. the direction of the front is approximately parallel to the boundary) then there is no immediate change in the neighbouring grain/twin on the other side of the boundary (figs 83/84E, F, G & H). The motion of the fronts is as if they had a physical momentum in the direction of their movement, a momentum that transfers relatively easily across boundaries that they hit near "head-on" and not across those hit at a shallow angle. The transformation fronts do not appear to be significantly impeded or greatly deflected by the grain or twin boundaries that they encounter, nor by the surface carbides.

This said, it appears highly likely that although the motion of the transformation fronts is largely unaffected by these microstructural features, the nature of the pearlite being deposited behind the transformation front is profoundly influenced. It is clear from the micrographs above, and from decades of previous work, that the pearlite grains are smaller than the parent Austenite grains and much smaller than the area swept by an active transformation front. Thus each transformation front must deposit many pearlite grains, not just one, nor even one pearlite grain for each parent austenite grain or twin crossed. Clearly, pearlite grains of different orientations are being deposited simultaneously and side-by-side behind each moving transformation front. It is easy to conceive of how this could be when the front is travelling along an existing austenite grain boundary, as sketched in fig 85. This mechanism could easily account for why pearlite grains are smaller than the areas swept by transformation fronts. However, this mechanism is insufficient to account for the observation that pearlite grains are generally smaller than the parent austenite grains, when the number of nuclei for the transformation fronts is so low that a front will cross more than one complete grain before encountering another transformation front.

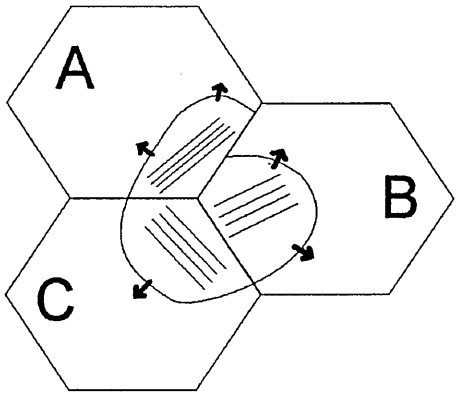

FIG. 85. Possible mode of pearlite deposition behind transformation front

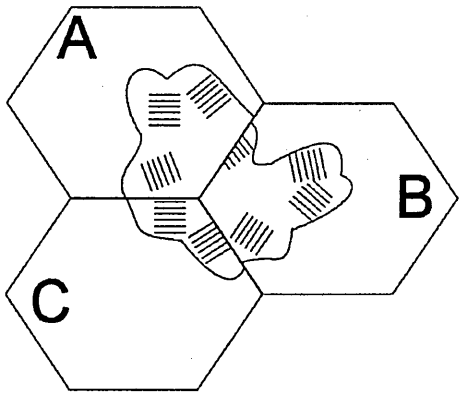

FIG. 86. Multiple orientations of pearlite grain deposited by each transformation front. Contrast with fig 85 and compare with figs 83 and 84.

Conventionally, the small size of pearlite grains is accounted for by a large number of pearlite nuclei, but this work clearly shows that the number of nuclei is small. Therefore to account for the small pearlite grain size some mechanism similar to that sketched in fig 86 is necessary.

Such behaviour requires that there be two classes of pearlite nuclei – Transformation Front Nuclei and Pearlite Grain Nuclei. Transformation Front Nuclei are clearly few in number and the delay in their appearance determines the onset time and temperature for the transformation. Once the fronts are on the move, they will encounter, or generate, Grain Nuclei – from which the moving front will deposit a new orientation of pearlite. The nature of these pearlite grain nuclei is unclear, but there are a number of obvious candidates. Pre-existing austenite boundaries are discussed above and several instances can be seen in the video where boundaries produce a different grey-level, implying a different orientation, in the pearlite on either side of them.

Microstructural features such as non-metallic inclusions, isolated undissolved carbides (e.g. vanadium carbide) or other precipitates, both pre-existing or recently precipitated, are all good and obvious candidates for the nucleation of a new pearlite orientation.

The observation of transient austenite decomposition phenomena (section 5.2 and fig 76) provides another candidate. The cellular structure causes micron-to-10-micron-scale inhomogeneity in the un-transformed material and persists until the arrival of the transformation fronts. If this were due to a dislocation cell structure then it would be reasonable to expect this to have a significant effect on the diffusion of carbon. This could cause segregation of carbon, causing inhomogenous composition in the material ahead of the transformation front. Even without any prior segregation of carbon, the local differences in the diffusivity and or solubility of the carbon being pushed ahead of the front would cause micron-scale localised super-saturation and under-saturation zones that could lead to something akin to turbulence in the motion of the transformation front. Such turbulence, once some critical level is reached, could force a deposition of carbon "out-of-synch" with the current grain, thus starting a new grain without any obvious arrest or disturbance in the overall motion of the transformation front.

5.5 AFTER TRANSFORMATION

The reasons for the black & white mottled appearance of the transformed structure are unclear, but are suspected to be a combination of changes in contrast due to crystal structure and distortion effects and atomic number contrast arising from localised carbon enrichment/depletion in the surface volume corresponding to the electron beam's effective penetration depth for backscattered electrons. The trans-

formed structure as imaged by the large angle converter plate detector is highly complex, making ferrite grain boundaries difficult if not impossible to see.

It is possible to estimate the effective backscattered electron penetration depth in this material, and at the 10 KeV beam energy used, it corresponds to approximately the thickness of one carbide lath plus one ferrite layer in the cooled specimen shown in fig80. Thus, at a position where the specimen consisted of a surface/near-surface carbide lath/film plus a ferrite layer, with the local ferrite/carbide stack oriented approximately perpendicular to the beam, the backscattered electron interaction volume would have an average Z approximately 2-3 atomic units lower than an interaction volume consisting solely of ferrite. By contrast, the lateral resolution is less than the thickness of a ferrite layer, thus the apparent average Z can change with beam-pearlite lath orientation as the interaction volume may include more or less carbide. Under the conditions of the channelling contrast setup, this might be expected to make a visible contribution to image contrast, in addition to the orientation contrast.

Detailed examination of the specimen surface after transformation reveals closely spaced near-parallel lines in some areas; these are likely to be carbide laths breaking the surface at near 90° angles [fig 78C]. Conventional etching of the specimen after the experiment confirms a moderately coarse pearlite structure, with lath spacings consistent with the parallel lines observed on the freshly transformed specimen. The fact that these surface breaking laths are seen at relatively few positions suggests that the carbide laths rarely extend all the way to the surface. Possible reasons for this would include effects due to the orientation of the laths relative to the surface. The case for orientation effects is supported by the observation that all the surface-breaking carbide laths appear to meet the surface at a high angle, around 90°. There is no evidence of carbide laths breaking the surface at shallow angles. Another possible reason for the lack of surface-breaking carbide laths would be a carbon denuded layer at the surface. This could arise simply by slight decarburisation from heating the metal or from carbon segregating away from the surface. If the latter were true, it would imply that most carbide laths would terminate just short of the grain boundary, giving a pure ferrite film at surfaces and grain boundaries.

5.6 TRANSFORMATION TO AUSTENITE

Refer to Video 3 – Steel-full experiment, in appendix 4.

5.6.1 RE-HEATING AFTER COOLING TO MEDIUM-COARSE PEARLITE

The surface carbides are the last feature of the pearlitic microstructure to vanish on re-heating. These features are highly persistent, lasting long after the bulk material has transformed and undergone initial crystallisation of new austenite grains and competi-

tive grain growth. First visible change in microstructure is again assigned T=0. Explosive grain growth starts at 495s, competitive grain growth at 525s, the surface carbides are first seen to have reduced in size at 690s, the last of the carbides disappears at 1320s (video 3 3:50-5:10). The moving boundaries of the new grains are apparently uninfluenced by the presence of these surface carbides. If grain boundary carbides were to behave similarly, it would be reasonable to expect them to dissolve more rapidly than the surface carbides, being surrounded by austenite, as opposed to being in contact on only one surface.

The relatively long delay between T=0 and the onset of explosive growth is noteworthy and indicative of both the relatively longer time required to dissolve the larger carbide particles and the energy bound up in the distorted structure that existed before the first heating. In the transformation from the cold drawn state there is no visible change in microstructure distinguishable from the onset of explosive grain growth, which gives way to competitive growth at about 120s, a factor of 4 more rapidly than on re-heating.

This has significant implications for critical specialist heat-treatments, e.g. of high performance spring materials.

Assuming first visible transformation to correspond to the metal first attaining the Austenitising temperature, and the commencement of competitive growth to correspond to complete dissolution of the carbides (except the surface carbides), this implies a major difference in carbide dissolution time – i.e. Austenitising "soak" time" – for a relatively minor change in structure. The pearlite produced after final cooling was only moderately coarse and would be expected to give very good results as a feed material for heat treatment operations, so such a large difference from the cold-drawn material is unexpected.

The heat-treater's traditional rule of thumb is "one hour soak per inch of section" (or half that in "special cases"). This soak time is generally measured from when the furnace reaches its target temperature or when the furnace load is observed to be glowing with the same colour as the furnace walls (the load appears to vanish into the background). The soak time allows for both the heating through of the metal – a considerable time lag in a large section – and for sufficient time to dissolve all of the carbide. Complete dissolution of carbide is critical for most heat treatments (i.e. those aiming to produce Martensite) as Martensite properties are highly dependent on its carbon content and only the carbon dissolved in the Austenite can become part of the Martensite. The allowance is therefore generous as "a little" grain growth or "a little" decarburisation is much preferable to incomplete dissolution of carbide. However, it is clear from this factor of 4 difference in dissolution time between very fine, drawn

pearlite and moderately coarse raw pearlite that this one-size-fits-all approach is non-ideal for high-strength, high-fatigue resistance high-performance parts (e.g. springs).

For instance, in the initial heating, full dissolution of carbide is estimated at 120s, at which time grain size is estimated at around 5μm. By 495s – when the dissolution of the coarser pearlite would be complete – the initial finer structure has undergone grain growth to about 20μm grains, with several much bigger than that. If such a material were treated with a soak time appropriate to a spheroidised structure, Austenite grain growth would be considerably larger again.

It is in fact the case that most industrially treated parts are processed on a one-size-fits-all, rule of thumb or trial and error basis, however in most cases it is of little importance because the finished parts will have the properties that the designer expects. If the strength is slightly reduced due to the grain growth, it is easily compensated for by a slightly reduced tempering temperature.

However, this approach does not allow high-performance parts to be fully optimised. Even in parts intended for heat-treatment to Martensite (conventional hardening or Mar-tempering), although properties can be adjusted by tempering parameters, a large prior austenite grain size will influence strength and will limit the ductility. Ductility is important because it is traded for strength in the tempering operation and insufficient ductility brings the risk of brittle fracture in all its forms, plus high sensitivity to hydrogen embrittlement and stress-corrosion.

Austempering (a lower Bainite finished structure) is even more dependent upon prior Austenite (Kazeminezhad and Taheri, 2004) and is increasingly used. In Austempering, parts are Austenitised then dropped into a molten salt bath, such as to maintain them at a temperature too high for the formation of Martensite. This allows the slow nucleation and growth of acicular (lower) Bainite, a process that can take hours. The salt bath temperature can be lowered to produce a finer, stronger Bainite structure, but subject to two limits. Firstly, the temperature at which Martensite starts to form provides an absolute lower limit; otherwise an undesirable mixed structure will be produced. Secondly, the length of time required in the salt bath rises very rapidly with decreasing temperatures, going from tens of minutes to hours for a drop of tens of degrees Celsius. This rapidly increases cost. The only other means of influencing the properties of the Bainite of any particular steel is to create finer Bainite grains by having a finer grained starting Austenite. Thus, for critical applications, optimisation of the Austenitising process is fundamental, and all but impossible without good knowledge of the carbide dissolution behaviour of the material in question and its alternatives.

CHAPTER 6
CONCLUSIONS

The converter plate has proved itself successful in orientation contrast electron imaging of hot specimens – despite the constraints imposed by the design of the available microscope, the hotstage and the lack of refinements such as plate biasing and/or SE1&2 suppression. The suitability of the converter plate to high temperature work and orientation contrast SEM work was not previously known, but it's future potential, for recrystallisation, grain growth and phase transformation work is clear, particularly if refinements were implemented.

The electron detection mode of the converter plate, while never originally intended for this purpose, is intrinsically immune to the effects of photon radiation or heat. Thus, the electron detector is now effectively removed as the limiting factor in high-temperature SEM.

Results from steel and aluminium show that grain boundaries in industrial polycrystalline metals migrate discontinuously, regardless of the presence or absence of thermally etched grain boundary grooves. In steel, thermal grooving is first observed some time after grain boundaries become mobile – indicating that activation temperatures for surface diffusion and boundary motion are slightly different. In aluminium, boundary groove formation is prevented by the presence of a tightly adherent aluminium oxide layer overlaying the entire specimen surface. Again, this leads to significant boundary motion – showing discontinuous character – before the first appearance of boundary grooves.

Some workers in this field show discontinuous motion in a high purity polycrystal with boundary grooving or discontinuous motion within a bulk polycrystal. By contrast, other workers show continuous motion in bi- and tri- crystals. Taken with the evidence added by this project, there is a strong indication that discontinuous boundary motion is a fundamental property of metal polycrystals, independent of grain boundary grooving, surface effects or impurities. This work has added significant evidence in this area of investigation.

The motion of triple points in a polycrystal is observed in detail for the first time and found to be complex and near-constant. A triple point is tracked through the microstructure and shown to migrate discontinuously, to make frequent and large changes of direction as well as speed. It is often found to be "orbiting" through some complex locus of preferred locations, even when apparently stationary in the image. Such real-time tracking of a triple point has not previously been done.

Austenite decomposition and pearlite formation are observed "live" for the first time. The first manifestation of austenite decomposition in this 0.6%C steel, cooling at 0.15°C per second is an as yet unexplained "mottled" appearance in the backscattered electron image, indicating a meta-stable austenite state involving the migration and micron-scale localised concentration/depletion of either carbon and/or dislocations.

The second manifestation of austenite decomposition is the precipitation of isolated solid dendritic films of carbide at surfaces (and by implication, at grain boundaries also). This occurs independently of pearlite formation, and so may be expected to occur in other austenite → ferrite + carbide transformations, provided that there is sufficient time for precipitation of the carbide dendrite at any given point on a surface before the main transformation reaches it. The presence of carbide films/dendrites at grain boundaries and surfaces has been previously reported, but the means by which they are deposited and its position in/interplay with the sequence of phase transformation was not known.

The austenite to pearlite transformation is, as classically taught, a "wave-like" phenomenon, sweeping through the austenite microstructure and leaving fully transformed pearlite behind it. These transformation fronts are shown to be able to cross from one austenite grain to another with relative ease – not a feature of the classical model.

The pearlite transformation fronts originate from triple points and probably from grain boundaries. The fronts tend to propagate from these nucleation points in all directions, though not necessarily simultaneously. The classical model shows nucleation on a grain boundary and growth on only one side of that boundary.

The difficulty of nucleating the pearlite transformation is shown to be relatively high – the number of pearlite nuclei generated at 0.15°C per second cooling is observed to be much less than one nucleus per austenite grain, more nearly one nucleus per ten austenite grains in this material at this cooling rate. Despite this, finished pearlite grain size is comparable to or smaller than austenite grain size prior to transformation. This differs sharply from the classical theory, which has more than one nucleus per austenite grain, producing one pearlite grain per nucleus.

Dissolution of carbide and onset of grain growth on transformation to austenite is shown to be very rapid in cold-worked fine-pearlite material. Approximately 120 seconds elapses from first visible evidence of transformation to a 100% austenitic structure with no evidence of undissolved carbide and with vigorous grain growth already well underway. This has significant implications for optimisation of heat-treatment for high performance components, particularly for treatments in which finished properties are highly dependent on initial austenite grain size, e.g. Austempering.

CHAPTER 7
FUTURE WORK

In the short term, the bulk behaviour of the material should be more thoroughly investigated, by serial sectioning, sectioning at 90° through the cooled specimen etc. A more rigorous assessment of grain size, such as digital image analysis of an optical micrograph or EBSD mapping would allow statistical tests to determine the significance of any differences between surface and bulk. The work should also be repeated with a suitable alloy steel, (e.g. 30% nickel steel) to allow imaging of Austenite grain growth in an austenite structure that will persist at room temperature, allowing bulk-vs.-surface comparisons for the Austenite phase.

In the longer term, the work should be repeated with a number of different materials, e.g:

1. Suitable "air hardening" steel to image the Martensite transformation in situ at the available cooling rate.
2. Suitable alloy steel to image Bainite transformation in situ at the available cooling rate.
3. Suitable alloy steel to image "ideal" pearlite formation in situ at the available cooling rate.
4. Duplex stainless steel, to image the formation of the duplex microstructure from the original simple Austenite.
5. Copper
6. Further work on aluminium
7. More conclusive work on gold and other high-purity model materials.

The technique should be integrated with an in-situ straining device in order to directly investigate dynamic recrystallisation and hot-working processes.

A dedicated microscope should be designed and built, capable of undertaking hot stage work as a more routine operation. This should be optimised for the converter plate, with the risks of damage to the microscope, and high-maintenance levels due to hot stage operations, minimised by appropriate microscope design.

The technique should be integrated with EBSD such as to gain orientation information from crystallites of interest alongside imaging of their motion.

CHAPTER 8
BIBLIOGRAPHY

Abdou, S. Solorzano, G. El-Boragy, M. Gust, W. Predel, B. (1996) "In-Situ Study of Discontinuous Precipitation in Al-15 at% Zn" *Scripta Materialia*, **34**(9), p1431-1436

Anselmino, E, Miroux, A, van der Zwaag, S, Seward GGE, Seaton, NCA, Prior DJ. (2004) "In-situ Observations of Recrystallisation in AA3103 using FEG-SEM and EBSD" in *Proceedings of the 9th International Conference on Aluminium Alloys, Brisbane 2004* eds. Nie, JF, Morton, AJ, Muddle, BC. Institute of Materials Engineering Australasia Ltd, 2004 p811-817

Anselmino, E. Miroux, A. Van der Zwaag, S. Prior, D. Seward, G. Seaton, N. (2004 B) "In-Situ Observations of Recrystallisation in AA3103". Unscheduled oral presentation at *2nd Joint international conference on recrystallization and grain growth, ReX and GG2, Annecy (FR), 30 Aug - 2 Sep 2004*. Not included in conference proceedings. Electronic copy of presentation received (2005) as private communication.

Anselmino, E. (2005) Private communication

Aust, K.T. Rutter, J.W. (1959), "Secondary Recrystallization In Copper" *Transactions of TMS-AIME* 215, p119-127.

Blamire, MG, Humphreys, CJ, Moore, DF, Greer, AL, Newcomb, SB. (2001) "The Development and Application of Focused Ion Beam Fabrication and Scanning Ion Microscopy" [online] last accessed 21 July 2005 at http://www.msm.cam.ac.uk/dmg/reports/L21044/Report.html

Chongmo, Li and Hillert, M. (1982) Diffusion induced grain boundary migration in Cu---Zn *Acta Metallurgica* **30**(6), p1133-1145

Czubayko, U. Molodov, DA. Gottstein, G. Shvindlerman, LS. (1995) "An X-ray device for continuous tracking of moving interfaces in crystalline solids", *Measurement Science and Technology*, **6**(7), p947-952

Danilatos, G.D. (1983) "A gaseous detector device for an environmental SEM". *Micron (Microscopica Acta)* **14**(4) p307-319

Estrin, Y. (2001) "Vacancy Effects in Grain Growth" in *Recrystallisation and Grain growth : Proceedings of the First Joint International Conference* (Vol.1) eds. Gottstein, G. Molodov, DA. Springer-Verlag p135-144

Fibics Incorporated (2001) "Grain Orientation Contrast" [online] at http://www.fibics.com/MS_FIBGrainOrientation.html last accessed 21 July 2005

Fielden IM, Cawley J, Rodenburg JM (2003), "Backscattered SEM Imaging of High Temperature Samples for Grain Growth Studies in Metals" in *Electron Microscopy and Analysis 2003: Proceedings of the Institute of Physics Electron Microscopy and Analysis Group Conference, 3-5 September 2003*, eds. McVitie, S. McComb, D. IOP Publishing, 2004 p181-184 [this paper is appendix 1]

Fielden IM (2004), "Results From In-Situ, Real-Time SEM Observations of Grain Growth in Polycrystalline Metals" in *2nd Joint international conference on recrystallization and grain growth, ReX and GG2, Annecy (FR), 30 Aug - 2 Sep 2004*. eds Bacroix et. al. *Mater. Sci. Forum* (2004) **467-470 (Part 2)**, p875-880 [this paper is appendix 3]

Fielden IM, Rodenburg JM (2004), "A Technique for Real-Time, In-Situ SEM Observation of Grain Growth at Elevated Temperatures" in *2nd Joint international conference on recrystallization and grain growth, ReX and GG2, Annecy (FR), 30 Aug - 2 Sep 2004*. eds Bacroix et. al. *Mater. Sci. Forum* (2004) **467-470 (Part 2)**, p1385-1388 [this paper is appendix 2]

Goodfellow Materials ltd. (not dated) "Gold Au" [online] last accessed 28 July 2005 at http://www.goodfellow.com/csp/active/gfMaterialInfo.csp?MATID=AU00&form=All

Gottstein, G. Molodov, DA. Winning, M. (2001) "Grain Boundary Dynamics: A Novel Tool for Microstructure Control" *Interface Science*, **9**(3/4) p297-306

Gottstein (2001 B) Private communication/laboratory tour.

Hall, EO. (1951) "The Deformation and Ageing of Mild Steel: III Discussion of results" *Proceedings of the Physical Society, Series B*, Vol. 64, pp. p747-753

Hough, PVC. (1959) "Machine Analysis of Bubble Chamber Pictures" in *Proceedings of the International Conference on High Energy Accelerators and Instrumentation*, CERN 1959, ed Kowarski, L. p554-556

Humphreys, F.J. & Hatherley, M. (1995) "Recrystallization And Related Annealing Phenomena" Pergamon, ISBN 0080418848

Humphreys, FJ. Ferry, M. Brough, I. Johnson, CP. (1996) "Combined In Situ SEM Annealing and EBSD of Deformed Materials" *Textures and Microstructures* 26-27, p281-301

Humphreys, FJ. (2001) Private communication

Juul-Jensen, D (2001) Private communication.

Juul-Jensen, D, Lund, MD, Larsen, AW, Bowen, JR. (2004), "Recrystallization kinetics in the bulk and at the surface" in *2nd Joint international conference on recrystallization and grain growth, ReX and GG2, Annecy (FR), 30 Aug - 2 Sep 2004*. eds Bacroix et. al. Mater. Sci. Forum (2004) **467-470 (Part 1)**, p147-152

Kazeminezhad, M, Taheri, AK, (2004) "Prediction of Ferrite Grain Size and Tensile Properties of a Low Carbon Steel" *Materials Science and Technology* **20**(1) p106-110

Kral, MV, Spanos, G. (1999) "Three-dimensional analysis of proeutectoid cementite precipitates" *Acta Materialia* **47**(2) p 711-724

Kronberg, ML, Wilson, FH. (1949) "Secondary Recrystallization in Copper" *Metals Transactions* **185** p501-514

Lauridsen, EM. Schmidt, S. Marguiles, L. Poulsen, HF. Juul Jensen, D. (2001) "Growth Kinetics of Individual Cube Grains as Studied by the 3D X-Ray Diffraction Microscope" in *Recrystallisation and Grain growth : Proceedings of the First Joint International Conference (Vol. 1)* eds. Gottstein, G. Molodov, DA. Springer-Verlag, p589-594

Lauridsen (2003) Private communication.

Lücke, K (2001) "Main Steps In The Development Of The Statistical Theory Of Grain Growth" in *Recrystallisation and Grain growth : Proceedings of the First Joint International Conference (Vol. 1)* eds. Gottstein, G. Molodov, DA. Springer-Verlag p3-7

Marguiles L, Winther G, Poulsen HF. (2001) "In Situ Measurement of Grain Rotation During Deformation of polycrystals" *Science*, **291**(5512) p2392-2394

Mattisen, D, Molodov, DA, Gottstein, G, Shvindlerman, LS, (2001) "In-Situ Measurement Technique of Grain Boundary and Triple Junction Mobility" in *Recrystallisation and Grain growth : Proceedings of the First Joint International Conference (Vol. 1)* eds. Gottstein, G. Molodov, DA. Springer-Verlag p421-427

Mattisen, D. (2001) Private communication

MATWEB (no date given) "Aluminum 1050-O" [online] last accessed 27 July 05 at http://www.matweb.com/search/SpecificMaterial.asp?bassnum=MA1050O&n=1

Miodownik, MA. (2002) "A review of microstructural computer models used to simulate grain growth and recrystallisation in aluminium alloys" *Journal of Light Metals* **2**(3) p125–135

Moll, SH, Healey, F, Sullivan, B, Johnson, W (1978) "A High Efficiency, Nondirectional Backscattered Electron Detection Mode for SEM" in *Scanning Electron Microscopy*, 1978, 1 ed. O. *Johari*, SEM inc. p303-310

Molodov, DA, Czubayko, U. Gottstein, G. Shvindlerman, L.S. (1998) "On the Effect of Purity and Orientation on Grain Boundary Motion" *Acta Materialia*, **46**(2) p553-564

Molodov, DA (2001) "Grain Boundary Character - A Key Factor For Grain Boundary Control" in *Recrystallisation and Grain growth : Proceedings of the First Joint International Conference (Vol.1)* eds. Gottstein, G. Molodov, DA. Springer-Verlag p21-38

Moncrieff, DA. Robinson, VNE, Harris, LB. (1978) "Charge Neutralisation of Insulating Surfaces in the SEM by Gas Ionisation" *Journal of Physics D: Applied Physics*. **11**(17) p2315-2325

Moncrieff, DA, Barker, PR, Robinson, VNE. (1979) "Electron Scattering by Gas in the Scanning Electron Microscope" *Journal of Physics D: Applied Physics*. **12**(4) p481-488

Morrison WB. (1984) "This Week's Citation Classic – Morrison WB. The Effect Of Grain-Size On The Stress-Strain Relationship In Low-Carbon Steel" *Current Contents/Engineering Technology & Applied Sciences* (4) Jan 23 1984: p14

Mullins,W. W. (1957) "Theory of Thermal Grooving" *Journal of Applied Physics* 28, p 333

Mullins, W. W. (1958) "The Effect of Thermal Grooving on Grain Boundary Motion" *Acta Metallurgica*. **6**(6), p414-427

Oxford Instruments (1995) *Link Opal Operator's Guide* (Rev 3.0 issue 1)

Packard, NH, Crutchfield, JP, Farmer, JD, Shaw, RS. (1980) "Geometry from a time series" *Physical Review Letters* **45**(9) p712-716

Petch, NJ. (1953) "The Cleavage Strength of Polycrystals" *Journal of the Iron and Steel Institute*, May 1953 p25-28

Petch, NJ. (1982) "This Week's Citation Classic – Petch N.J, The Cleavage Strength of Polycrystals", *Current Contents/Engineering Technology & Applied Sciences* (19) May 10 1982: p24

PHOTONIS SA, (2002) "Nouvelle Page 1" [online] last accessed 14 July 2002 at http://www.photonis.com/awards/nasa.htm

Poulsen, HF, Fu, X, Knudsen, E. Lauridsen, EM, Margulies, L, Schmidt, S. (2004) "3DXRD - Mapping grains and their dynamics in 3 dimensions" in *2nd Joint international conference on recrystallization and grain growth, ReX and GG2, Annecy (FR), 30 Aug - 2 Sep 2004*. eds Bacroix et. al. *Mater. Sci. Forum* (2004) **467-470 (part 2)**, p1363-1372

Rabkin, E, Semenov, V, Izyumova, T. (2000) "Jerky Motion of Grain Boundaries in NiAl: an Atomic Force Microscopy Study" *Scripta Materialia*, **42**(4), 359-365

Rabkin, E, Klinger, L. (2001) "Effects of Surface Anisotropy on Grain Boundary Grooving" Oral presentation at IIB 2001 (Haifa) and abstract in programme booklet "*10th International Conference on Intergranular and Interphase Boundaries*" ed. Shneck, R. Technion-Israel Institute of Technology

Randle, V. (1993) "The Measurement of Grain Boundary Geometry", IOP Publishing

Randle V, (1996) "The Role of the Coincident Site Lattice in Grain Boundary Engineering", Institute of Materials

Reimer, L. (1998) "Scanning Electron Microscopy: Physics of Image Formation and Microanalysis", 2nd ed. Springer-Verlag

Reimer, L, Volbert, B, (1979) "Detector Systems for Backscattered Electrons by Conversion to Secondary Electrons" *Scanning* **2**(4) p238-248

Robinson, VNE. (1975) "The Elimination of Charging Artefacts in the Scanning Electron Microscope" *Journal of Physics E: Scientific Instruments* **8**(8) 638-640

Rollett, AD, Kalu, PN. (2005) "Misorientations and grain Boundaries" [online] last accessed 28 July 2005 at http://neon.mems.cmu.edu/rollett/27750/Misorientation_HowTo_17Feb05.ppt

Rost MJ, Quist DA, Frenken JMW. (2003) "Grains, growth and Grooving" *Physical Review Letters* **91**(2), article 026101

Schmidt, S, Nielsen, SF, Gundlach, C, Margulies, L, Huang, X, Juul-Jensen, D. (2004), "Watching the growth of bulk grains during recrystallization of deformed metals" *Science* (2004) **305**, 229-232

Seward, G. (2003) Private communication

Seward, GGE, Prior DJ, Wheeler, J, Celotto, S, Halliday, DJM, Paden, RS, Tye, MR, (2002) "High-Temperature Electron Backscatter Diffraction and Scanning Electron Microscopy Imaging Techniques: In-situ Investigations of Dynamic Processes". *Scanning* **24**(5) p232

Shvindlerman, LS. Gottstein, G, Molodov, DA. Sursaeva, VG. (2001) "Triple Junction Motion in Metals" in *Recrystallisation and Grain growth : Proceedings of the First Joint International Conference (Vol.1)* eds. Gottstein, G. Molodov, D.A. Springer-Verlag p177-192

Simkin, BA. (2001) "Ben Simkin's Electron Channeling Contrast Imaging (ECCI) How-To". [online] formerly at: http://www.egr.msu.edu/~simkin/ECCI.html Slightly modified, and re-titled as *"Electron Channeling Contrast Imaging (ECCI) Information"* and moved to http://www.chems.msu.edu/curr.stud/mse.sops/ECCI.htm dated 2003, last accessed 3 July 2005

Taguchi, G. (1987(1976)) "System of Experimental Design". Kraus International Publications, New York, 1987. A translation of *Jikken keikakuho*, Maurzen Co. Tokyo, 1976.

Takens, F. (1981) "Detecting strange attractors in turbulence" In *Dynamical systems and Turbulence* eds. Rand, DA, and. Young, LS. Springer-Verlag Berlin p366-381

Van Swygenhoven H. (2002) "Grain Boundaries and dislocations" *Science*, 296(5565), p66-67

Winning, M (2001) "Grain Boundary Mechanics" in *Recrystallisation and Grain growth : Proceedings of the First Joint International Conference (Vol.1)* eds. Gottstein, G. Molodov, D.A. Springer-Verlag p193-204

Zener, C (1948) quoted in Smith, CS. (1948) *Transactions of AIME* 175, p47

ACKNOWLEDGEMENTS

I would like to express my gratitude to my Directors of Studies, in chronological order: Dr Jess Cawley, Prof. John Rodenburg and Dr Alan Smith. I would particularly like to thank Prof. Rodenburg, who joined my supervisory team well after the project had started, but who had already given me advice and useful discussions above and beyond the call of duty, long before he actually joined the team.

I would like to express my gratitude to Dr Karen Vernon-Parry, who provided invaluable advice and encouragement during a critical stage of writing-up, when some of my "official" supervisory team were unavoidably unable to do so.

I would like to thank my wife for supporting me in my determination to finish, for being good-natured in the face of my need to keep some anti-social hours and for putting up with me spending our money on going to conferences in semi-exotic places, especially when she could not join me.

I would like to thank Len Reynolds, my former colleague at The Spring Research Association and a previous winner of the materials National Measurement Award, for encouraging my early interest in metallurgy, teaching me a great deal of it and for introducing me to phase portraits and related techniques of data analysis.

I would like to thank Prof. Ian Stuart of Warwick University for giving me some of his time for a very useful and stimulating discussion on analysis of my results and potential approaches to modelling the results.

I would like to thank Dr Peter Morris and Corus plc for advice, giving a solid industrial foundation to the work and providing specimens.

I would like to thank Dr Vanessa Fox at Teer Coatings Limited for applying DLC coating to a prototype converter plate.

I would like to thank KE Developments Limited for the loan of forward-scatter electron detectors.

I would like to thank Dr. Daniel Bultreys of Phillips/FEI for useful discussions on the ESEM, hot stages and FIB instrument capabilities.

I would like to thank The Gordon Research Conferences organisation and the Electron Microscopy and Analysis Group of the Institute of Physics, who part-funded my attendance at some very worthwhile and enjoyable conferences.

I would like to thank the organising committee of "ReX-GG2" for accepting my paper for oral presentation, giving me a great time slot for it, and topping off an excellent conference by giving me a prize.

I would like to thank the many people I have met and had discussions and/or drinks with at the conferences I have attended. I would particularly like to mention (in no particular order) Dr Stefan Zaefferer, Dr Elizabeth Holm, Prof. Tadao Watanabe, Prof. Eugen Rabkin, Prof. Anthony Rollett, Prof. Günter Gottstein, Dr Dorte Juul-Jensen, Dr David Saylor, Dr Stephen Celotto, Gareth Seward and the mad geologists of Liverpool.

I would like to thank The Sheffield Universities Materials Forum, who successfully bid to EPSRC for the project and gave some matching funding of their own.

I would like to thank the numerous members of the MRI and MERI who gave encouragement, expressed interest, bought me the occasional pint and happily lent me various small pieces of equipment.

The contributions of these substances should not be overlooked:

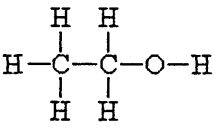

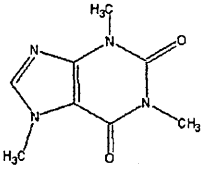

Last, but by no means least, I would like to thank EPSRC, without whose funding the whole thing would have been impossible.

No Thanks To: Our neighbour's energetic young cat, who has taken to visiting and "helping" me to concentrate on writing this, by loudly demanding that she should play the "chase the laser-pointer dot around the house" game every 15 minutes.

CANDIDATE'S STATEMENT

The aims of this project were

1) to gain experimental data regarding the grain growth of metals of a face-centred cubic crystal structure

2) to develop a characterisation technique to obtain this data

More details are given in chapters one and two.

A number of published and unpublished sources have been consulted; these are mentioned in the text at the appropriate point and cited in full in chapter eight, the bibliography. Assistance received is generally mentioned in the acknowledgements. Where appropriate, assistance received may alternatively or additionally be cited as "private communication" in the text and Bibliography.

This work is original and has not been submitted for any other award.

Some of this work has been published, these publications have been appended as appendices 1-3 and are referenced in the text and bibliography. Some aspects of the work, particularly the earliest stages, have also been presented at conferences in poster format or as short seminars within Sheffield Hallam University. These have not been published in book or journal form, and have not been included in this thesis.

APPENDICES

Backscattered SEM Imaging of High Temperature Samples for Grain Growth Studies in Metals

I M Fielden, J Cawley*, J M Rodenburg**

Materials Research Institute, Sheffield Hallam University, Howard Street, Sheffield S1 1WB U.K. **Mappin Building, Mappin St. Sheffield S1 3DJ *Solutio (Sheffield) Ltd, 22 Carterknowle Road, Sheffield S7 2DX, U.K.

Abstract. A novel technique is presented for SEM backscattered electron imaging of hot specimens, in-situ, in real time. The technique has been applied to recrystallisation, grain growth and phase transformation studies in metals, principally steel. Temperatures attained were in the order of 850°C and were limited by the capability of the specimen heater, not the detector. Representative results are presented as stills and video.

1. Introduction

1.1 The Materials problem

Grain size and (where they occur) phase transformations are key determinants of microstructural evolution and hence materials properties. Large gains in strength and toughness are available by engineering a smaller finished grain size. There are many methods for characterising static or room temperature microstructures. However, in almost all real-world thermo-mechanical processing (e.g. hot rolling of steel) it would be highly advantageous to have some knowledge of the kinetics of these phenomena. Many methods exist for modelling the dynamics of recrystallisation, growth and/or phase transformation, but these have proved very hard to confirm experimentally: kinetics are generally inferred from "post-mortem" studies.

1.2 The Electron Microscopy Problem

The most attractive ways of generating grain-to-grain contrast are crystal orientation sensitive techniques relying on backscattered electrons. Established backscatter detectors are intrinsically sensitive to the IR and light photons emitted by a hot specimen. Imaging with diode detectors rapidly becomes problematic with increasing temperature, and is impossible beyond temperatures of about 450°C. Scintillator/photomultiplier detectors are similarly affected. Topographic techniques (e.g. SE imaging) show grain boundaries via secondary phenomena (e.g. thermally etched boundary grooves). These features do not form rapidly (or even at all) under all conditions. Thus high temperature SE imaging via the ESEM is unhelpful.

2. Technique Development

Initial trials used room temperature specimens and conventional diode detectors. These covered several configurations:- zero-tilt and high-tilt (EBSD-like "forward scatter") geometries, large and small detector areas, single/summed/difference signals from two detector elements and differing distances between two detector elements. Results showed that an electron channelling contrast (ECCI) geometry [1], of a single detector subtending a large solid angle at a specimen of zero tilt, was superior.

Diode detectors overlaid with thin polymer films were trialled at room temperature. The intention was, if successful, to thinly coat the polymer with a light metal to exclude/reflect photons. Results were variable, but at best, somewhat disappointing.

The micro-channel plate detector was considered and discarded, due to cost and risk of damage from the contaminants anticipated from a heated specimen.

2.1 Modified Converter Plate Detector

The converter plate appears to be little used in current SEM practice. It appears in the literature, notably the more comprehensive textbooks [2], but the authors have found only one reference to it on the Internet and no indication that the technique is in regular use, or was ever applied to hot specimens or orientation contrast.

The converter plate emits secondary electrons (designated SE3) when struck by energetic backscattered electrons. This allows images to be generated from BSE information via an SE detector. The conversion gives little or no amplification, and SE1+SE2 signal from the specimen must be suppressed if a "pure" BSE image is desired, hence its lack of popularity. However, the converter plate is inherently immune to photon radiation, can be made of thermally robust materials and is easily made in any desired size and shape. It is equally applicable to SEM and ESEM, with an SE detector shielded from the specimen or one immune to photon effects.

Converter plates were trialled at room temperature, with encouraging results. The plate designed for the zero-tilt ECCI geometry was not only an effective detector but could also function as a heat shield. An early prototype plate was coated with diamond-like carbon (DLC), but there was no obvious advantage over the established MgO coating, which allowed coating in-house & rapid prototyping of plates.

A Phillips/FEI XL30 ESEM-FEG was fitted with a Phillips/FEI hot stage (nominal capacity 1000°C) and an optimised converter plate. A low-deformation polished specimen of cold deformed 1050 aluminium (commercially pure) was heated and images captured as digital video. The instrument was operated in "hi-vac" conventional SEM mode, but with differential pumping activated and a "hot-stage" ESD/PLA assembly in place to protect the column.

Grains were clearly seen and in accelerated video playback the growth process could be followed. However, acceptable image quality dictated a scan time of 20-30s per frame, so highly dynamic events could not be followed. 660°C was attained.

The experiment was repeated with a heavily cold deformed, nominally-eutectoid carbon steel wire, cut in transverse section. Image quality was greatly improved, due to the higher backscattering coefficient of the steel. Maximum specimen temperature was ≈860°C, limited by the specimen heater. Improved image quality allowed a faster scan speed, ≈5s per frame. A subsequent experiment gave acceptable images with a one second per frame scan time, meeting the "in-situ, in-real-time" goal and allowing highly dynamic events to be followed. Image quality was not degraded by increasing temperature. Gold has since been investigated as a model FCC material.

3 Results

To appreciate the kinetics, it is best to watch a video sequence. These have been made available in highly compressed form as supporting media files, and will be placed on, or linked from, http://extra.shu.ac.uk/fielden-emag2003 and http://www.srama.demon.co.uk/iain/publications/emag2003. No address can be indefinitely guaranteed not to change. In case of difficulty, try this paper's title as a search term or contact the author for information or a CD containing uncompressed video.

Space dictates that only the first steel results are considered here. Full size figures show the same specimen area, others a selection from it. The full field is « 150pm wide, all scale marks are 20pm, specimen temperatures approximately calibrated (estimated ±15°C), as the thermocouple monitors the heater, not the specimen.

3.1 Transformation to Austenite

The initial highly-deformed pearlite structure is irresolvable at this magnification. Above the transformation temperature the structure becomes "unlocked", presumably by dissolution of carbide, in the newly transformed Austenite, and a plethora of fresh y crystals rapidly appear, (figl).

3.2 Grain Growth

After an initial flurry of grain growth activity (figs 1-3), grain growth occurs in a localised manner, often with only one boundary in the field moving (fig 4).

Fig 1. Austenite grains at 765°C

Fig 2. As Fig 1, +70 seconds, 785°C

Fig 3. As Fig 1, +140 seconds, 795°C

Fig 4. The only growing grain in the field. 860°C, 60 second interval

Movement is a mixture of smooth gliding with some stop/start behaviour and speed/direction changes. In one instance it is clear that a growing grain's boundary has reversed direction and retreated immediately after having annihilated a neighbour. While the average velocity of boundaries is slow enough to be easily followed, some boundaries (e.g. those in the act of annihilating a neighbour grain) move very rapidly indeed (fig 5).

Fig 5. The last 19 seconds in the life of a previously stable grain, 845°C

Later in the growth process, thermally etched boundary grooves appear (fig 6, 7, upper part of fig 4). The grain boundaries do not show any strong tendency to become pinned by these (this becomes particularly evident when the specimen is re-heated).

3.3 Transformation to Pearlite

Transformation on cooling appears to nucleate mostly from grain boundaries and possibly twin boundaries. The first evidence of transformation visible in the microstructure are small, relatively slow growing islands that appear dark in the ECCI/BSE-Z image (fig 6). These features do not go on to play a part in the main "wavefront" growth of pearlite originating from grain boundaries. The most obvious/ active growth front in this sequence appears to originate from a triple point (fig 6c, 7).

Fig 6abc. (above) at 695°C. Showing high Temperature microstructure and first signs of transformation (at +18s & 96.5s)

Fig 7. At +97s. Showing context of fig 6 & rapid motion of wavefront (compare 6c)

Fig 8. At +200s. A transformation front, originating from A, has crossed X-X but not X-Y. More "dark island" features.

Fig 9. At +232s & 660°C. Transformation fronts from several origins sweep rapidly across the specimen.

The "wavefront" is briefly checked, but seems to cross austenite grain boundaries with ease. However, where the direction of the front is approximately parallel to the boundary, e.g. X-Y in fig 8, crossing to the neighbouring grain occurs less readily. The motion of the transformation fronts is as if they had a physical momentum in the direction of their movement, which does not transfer across boundaries hit at a shallow angle.

The black & white mottled appearance (fig 9) of the transformed structure is unexplained, but the ECCI set-up is extremely sensitive to any Z contrast, if present.

4 Conclusions

The converter plate is a practical method of imaging high temperature grain structures and would be easily capable of giving atomic number contrast at high temperature.

References

[1] Simkin B A Ben Simkin's Electron Channelling Contrast Imaging (ECCI) How-To [online] http://www.egr.msu.edu/~simkin/ECCI.html (at 26/08/03)

[2] Reimer L 1998 Scanning Electron Microscopy: Physics of Image Formation and Microanalysis, 2nd ed. (Heidelberg: Springer-Verlag)

A Technique for Real-Time, In Situ SEM Observation of Grain Growth at Elevated Temperatures

I.M. Fielden, J.M. Rodenburg

MRI, Sheffield Hallam University, Howard Street, Sheffield, S1 1WB, United Kingdom

I.Fielden@shu.ac.uk J.Rodenburg@shu.ac.uk

Keywords: Grain Growth, Kinetics, In Situ Techniques, Scanning Electron Microscopy (SEM), Hot Stage Microscopy, Phase Change

Abstract. We present a novel electron detector and technique permitting orientation contrast images to be generated using back-scattered electron signals. The detector is a modification of the converter plate. It is unaffected by Infra-Red and light photons and invulnerable to the effects of heat. Consequently, the detector is removed as the temperature limiting factor in elevated temperature SEM grain observations. The detector has been successfully applied to an environmental SEM (ESEM) operating in high vacuum mode and has produced good quality video image sequences of hot metal specimens with frame rates between 1 per second and 1 per 30 seconds (largely material dependent). Temperatures attained were up to 850°C, limited by the capability of the hot stage. Although developed for the ESEM the technique is applicable to any SEM provided that adequate measures are taken to manage contamination and heat effects on other microscope components. We have produced images and short, accelerated video sequences of recrystallisation and grain growth phenomena in steel, aluminium, copper and gold by the new technique. The technique has also successfully imaged phase transformations and high temperature behaviour of microelectronic materials.

Introduction

The introduction of the ESEM promised microscopists a new era of imaging hot specimens with few constraints. Regrettably, in practice imaging hot specimens was highly limiting from the perspective of the particular requirements of grain growth studies. This paper describes the techniques and tools developed to make grain orientation contrast hot stage microscopy possible and how they could potentially be applied to any hot-stage SEM.

The Problem

Grain growth studies by SEM have particular requirements, specifically the ability to image grain boundaries by SEM. This requires some kind of crystal orientation sensitive contrast mechanism. This requires that backscattered (or “forward scattered”) electrons be used, as only these electrons interact with the crystal structure of the specimen and hence are able to carry information from that structure.

The ESEM is nominally only capable of hot imaging when in ESEM mode and fitted with the hot-stage specific detector. Unfortunately, this detector is optimised for secondary electron imaging and is therefore unable to give grain orientation contrast. Backscattered electron detection capability is provided by a conventional solid-state backscatter detector. This solid-state detector suffers from the same limitations as all solid-state detectors - sensitivity to light/infra red and vulnerability to heat damage. Thus,

it is incapable of imaging specimens much in excess of 300°C, due to the electron signal becoming flooded out by spurious signal induced by infra-red photons arriving from the specimen.

The Solution

A technique is required to detect backscattered electrons, preferably over a large solid angle of collection. The equipment must be invulnerable to the effects of heat and photon radiation, yet sensitive enough to discriminate the relatively weak contrast between differently oriented crystals. The converter plate was originally developed by Moll et. al. [1] and Reimer et. al [2] and operates by placing a plate coated with a high secondary electron yield material in a position where it will be struck by backscattered electrons from the specimen. The backscattered electrons striking the plate will generate additional secondary electrons (SE3 in Fig. 1), which can be detected by a conventional SE detector in the normal way or by some other SE detector optimised for the purpose. This conversion technique operates irrespective of photon radiation and temperature and the plate and coating are easily made from thermally robust materials.

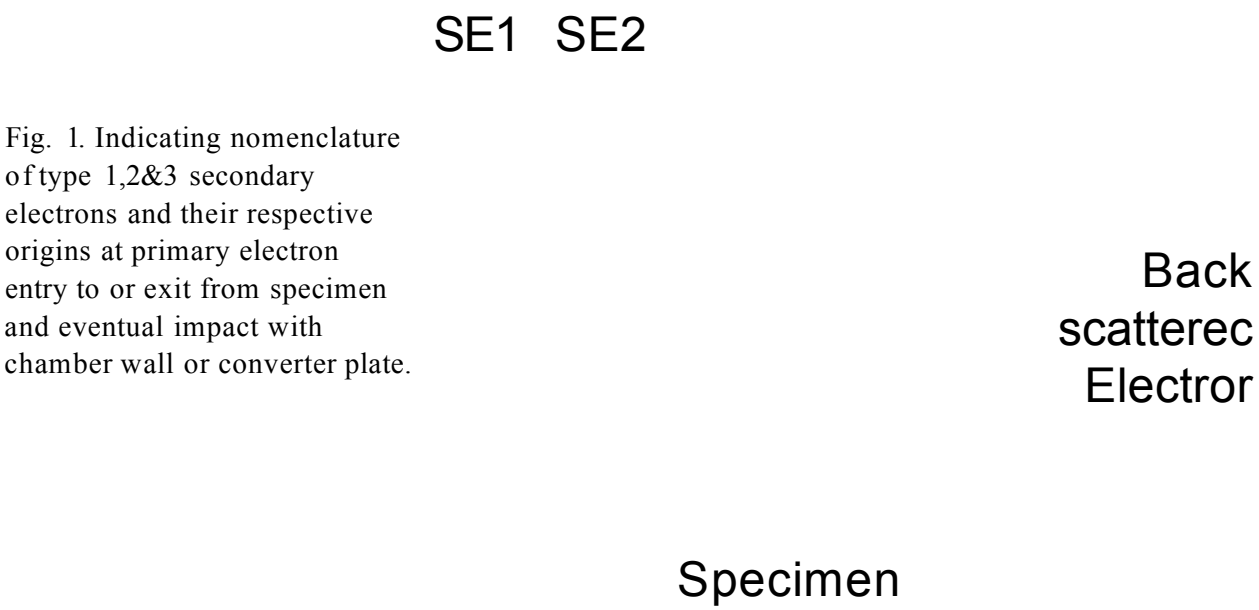

Fig. 1. Indicating nomenclature of type 1,2&3 secondary electrons and their respective origins at primary electron entry to or exit from specimen and eventual impact with chamber wall or converter plate.

Grain Orientation Contrast

Grain orientation contrast is generated by electron channelling effects and is a naturally weak contrast mechanism. A significant proportion of electrons entering a crystal as part of an electron beam will be backscattered, typically in the order of some tens of %. This proportion, $r\backslash$ is the backscattering coefficient and is determined primarily by incoming electron energy and the atomic number of the material (hence atomic number contrast). The value of $r\backslash$ is modified by other factors such as the angle between the incoming beam and the local surface (giving topographic contrast) and the angle between the incoming beam and certain critical zone axes in the specimen crystal (giving orientation contrast). The maximum possible change in $r\backslash$ across all the possible orientations of a target crystal lattice is referred to as Arp This varies with material and incoming electron energy. When expressed as a percentage relative to the bulk value of $r\backslash$, i.e. (Arj/r|)%, typical values for

most materials lie in the range 1-5% [3]. This change is small with respect to the changes in r| that will arise from atomic number or topography effects, hence it is vital to have a smooth surfaced and chemically homogenous material if these stronger contrast mechanisms are not to mask the channelling contrast information.

This small proportion of information carrying electrons, perhaps 2% of the total backscattered yield (itself perhaps 25%) would correspond to 0.5% of the total beam current. Clearly, maintaining a signal-to-noise ratio high enough to detect such subtle variation requires both high-efficiency detection and a high beam current, if scan times are to be reasonably fast.

The Specimen. In addition to the requirement that the specimen be flat and homogenous in order to minimise the unwanted strong contrast of topography and atomic number, it must be borne in mind that electron channelling occurs in the near-surface layers of the specimen (a few nm) and will be disrupted or suppressed by plastic deformation or contamination. These effects can be partially offset by increasing the probe energy, thus increasing the depth in which channelling effects occur. However, *Ar*\ decreases with increasing probe energy, limiting the benefits of this strategy. Preparation by means of electropolishing or ion polishing is strongly recommended by the literature, however the author has had success with combinations of conventional polishing followed by fine oxide polishing and/or attack-polishing using fine oxide with simultaneous attack by chemical etchant. It is possible that as the heating will tend to anneal out residual stresses, that the orientation contrast is easier to achieve on a hot-stage. It is notable that image quality often improves with increasing temperature, though this effect is observed at temperatures above well above those at which full stress-relief would be expected.

Optimisation

The plate can be interposed between the specimen and the SE detector to shield the detector from photon radiation (Fig. 2). The plate can also be made to function as a useful heat shield for other components of the microscope.

Fig. 2.
Schematic of converter plate

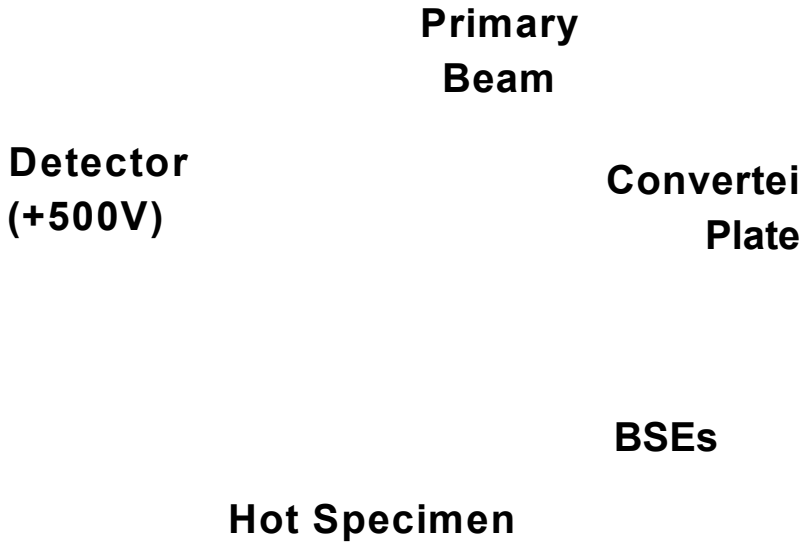

Maximising detection efficiency requires maximising the solid angle that the plate subtends at the specimen – the ideal is a hemispherical "plate", covering all possible angles at which an electron could exit the specimen [4]. In practice a hole must be provided for the beam and for electrons to pass through to the SE detector.

The coating material of the plate must give a high SE yield from the low energy loss backscattered electrons, as channelled electrons normally fall into this category. Metal coated converter plates give proportionately lower yield from higher energy electrons, (disappointing results were generated by aluminium and gold coated plates) so insulator coatings were chosen. Magnesia is recommended by the literature, diamond-like carbon was also tried, but showed no clear advantage over the Magnesia.

It must be remembered that the converter plate is not the only source of secondary electrons in the microscope. The specimen continues to emit its usual strong SE1+SE2 signal, so it is desirable – though not essential – to suppress these signals. Such suppression can be achieved by biasing the specimen and/or by placing a biased grid or electrode between the specimen and the detector. In normal SEM operation such biasing is a relatively simple matter, however, in practice the hotstage hardware is likely to complicate the process.

Results

The converter plate, fitted to a Phillips/FEI XL30 ESEM-FEG has yielded images from hot specimens of steel, aluminium, gold and electronic material. The frame rates have varied, mostly with different materials. At an image resolution of approximately 500 by 700 pixels (any higher is wasted by the NTSC video format) frame rates as low as 1 per second have been used successfully with gold and steel specimens. Aluminium requires the longest frame time of any material so far investigated at about 30 seconds per frame. Results from an investigation of carbon steel are being presented at this conference [5]. In this work a video sequence has been generated of a steel specimen being heated in situ and imaged at a frame rate of 4 seconds per frame, this frame rate has proved adequate to clearly show the dynamic behaviour of many of the phenomena of grain growth.

Summary

The converter plate has proved itself capable of imaging hot specimens in situ at temperatures up to 850°C (limited by the heater capacity) and of giving moving image sequences of those hot specimens with "real-time" frame rates typically in the order of 1-10 seconds per frame. An example can be downloaded from http://www.shu.ac.uk/schools/research/mri/instr/esem/hot-steel.htm.

References

[1] S.H. Moll, F. Healey, B. Sullivan and W. Johnson: A high efficiency, nondirectional backscattered electron detection mode for SEM. SEM 1978/I (SEM Inc., AMF O'Hare USA 1978) p. 303

[2] L. Reimer, and B. Vollbert: Detector System for backscattered electrons by conversion to secondary electrons. Scanning 2, 238 (1979).

[3] L. Reimer: *Scanning Electron Microscopy: Physics of Image Formation and Microanalysis* (2nd ed). (Springer-Verlag, Berlin 1998) p. 359

[4] B.A. Simkin: Ben Simkin's Electron Channeling Contrast Imaging (ECCI) How-To. (online) Available at: http://www.egr.msu.edu/~simkin/ECCI.html modified 2003, accessed 29 January 2004

[5] I.M. Fielden: Results From In-Situ, Real-Time SEM Observations of Grain Growth in Polycrystalline Metals (elsewhere in this conference proceeding)

Citation &
Copyright (to be inserted by the publisher)

Appendix 3

Results From In-Situ, Real-Time SEM Observations of Grain Growth in Polycrystalline Metal

IM Fielden

MRI, Sheffield Hallam University, Howard Street, Sheffield, S1 1WB, United Kingdom

I.Fielden@shu.ac.uk

Keywords: Grain Growth, Kinetics, In-Situ Techniques, Scanning Electron Microscopy (SEM), Steels

Abstract. The development of the converter plate detector has allowed the generation of real-time, in-situ image sequences of evolving microstructures in model and industrial polycrystalline metals. The principal metals investigated were steel, aluminium and gold. The raw video results allow a number of qualitative statements to be made about grain growth behaviour in these systems and some simplistic quantitative statements. However, the sheer volume and variety of data available in the time-stream of micrographs presents its own problems in identifying and extracting the information most useful for rigorous characterisation of the behaviour of a dynamically evolving microstructure. We present and discuss our approach to the analysis of this data and results of that analysis.

Introduction

All techniques for modelling growth of grains currently suffer one drawback - lack of experimental data with which to compare the models' output and process of grain network evolution. This is hardly surprising given that much of the most interesting information can only be captured while specimens are very hot and thus not readily compatible with sensitive instruments. Recently Fielden et al. [1,2] have adapted the converter plate [3] such that it can produce backscattered electron images giving grain-to-grain orientation contrast from hot specimens (1000K and more). A suitably equipped SEM can produce these images in real time, ideal for recording as a video stream.

Specimen

The specimen is a simple, commercial near-eutectoid plain carbon steel, 0.61% carbon by mass with manganese (0.54%), silicon (0.21%) and no other deliberate additions. In order to ensure an extremely fine grained initial austenite and a consequent strong driving force for grain growth, we have used a heavily cold-drawn wire. It was hoped that, with straining hot stages costly and incapable of high strain rates, the material might provide an accessible model for industrial hot working of metals. It was anticipated that the highly distorted structure of the cold drawn wire would transform to a very fine grained austenite, which would be initially pinned by the very fine carbides, but would rapidly and suddenly become "unlocked" by the dissolution of the carbides. Such a transformation might suddenly create a mobile/unstable fine grained austenite. This is in fact what we observe. Such a structure may be reasonably representative of hot working just above the transformation temperature, in which transient large strains, such as hammer blows or roll passes, might reasonably be expected to create just such a fine-grained suddenly-mobile/unstable structure at a similar temperature. During the experiment, the specimen is heated steadily from about 725°C to about 850°C over a period of about 900sec, and held at that temperature for a further 900sec.

Time. Time is measured in seconds from T=0, the first visible evidence of transformation. However, the accompanying video does not run in real time. Video time is given as min:sec (the

format in which most players will display it) from the start of the accompanying video, which runs 20X faster than real time. T=0 occurs at 0:10 (video), thus 1:10 (video) is 1200sec real time.

Data

The data produced is conventional monochrome video, in this case following the 525 line/30 frames per second NTSC standard. This is recorded as "DV" digital video for later processing and analysis. Processing is necessary for two reasons. Firstly the events occurring in the specimen are rarely rapid enough for convenient presentation to an audience or for the human eye to gain an overall sense of how events progress - the video (or sections of it) must be viewed at a variety of speeds and in reverse as well as forwards. Secondly the contrast produced by the electron channelling mechanism is intrinsically weak, so digital contrast enhancement is desirable.

Grain Tracing. Boundaries can be identified by eye in the SEM images. Efforts have been made to identify and characterise the grain boundaries and triple points by software. However, the limited contrast, in combination with the low resolution of video and somewhat noisy images have so far frustrated these efforts. Refinements to the converter plate may improve contrast in future.

Stills (fig 1) are taken from the processed video stream at suitable intervals, and grain/twin boundaries manually traced (fig 2) using conventional graphics software and a digital tablet. "Missing" grain boundaries are common at very early stages of the structure evolution, but rapidly become rare as development progresses. The low contrast makes some boundaries very difficult to identify in the still image, thus it is important to refer to both the still and moving images when tracing, as a low contrast boundary catches the eye much more readily when moving than in a still frame. By cross-referencing between still and moving images, identification of boundaries has proved quite reliable, though somewhat laborious.

Fig 1. T=1300 sec (1:15)

Fig 2. As Fig 1, with grain trace & grains marked with their graph symbols (see below).

Measurement of position is by reference to an invariant point - a non-metallic inclusion near the centre of the field. The specimen drifts in the image, due to expansion of the stage and disturbance of the beam due to the heating current, thus simple measurement with respect to the image frame is insufficient. Monitoring of the position of a single image feature (e.g. a triple point) is less laborious than performing a full grain trace, thus allowing more time points to be checked in such an analysis.

Data Analysis - Grains. The traced networks allow relatively easy measurement of key parameters of some selected grains, e.g. area, longest dimension (L), dimension at 90° to L (W), and hence approximate aspect ratio. Measurements are complicated by the fact that some grains

(especially the most active) grow beyond the field of view, or the specimen drifts to give that result.

Six crystallites were selected and measured at intervals of 100s (5sec video). These are identified by their symbols _,ρ,σ,↓,+,X (one does not survive to be visible in fig 2).

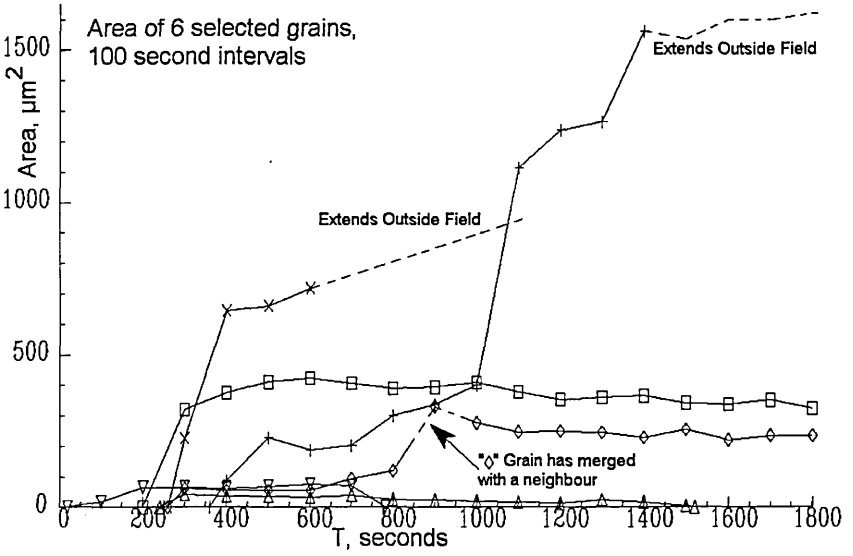

Fig 3. Grain Areas

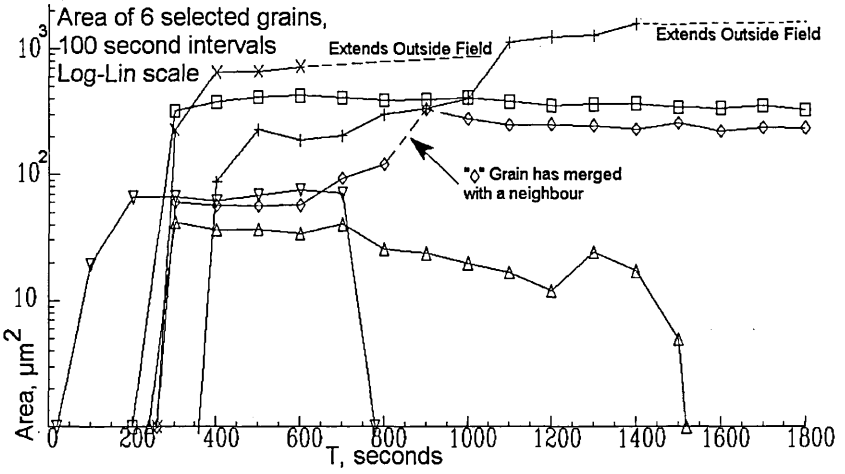

Fig 4. As Fig 3, log scale to show detailed behaviour of smaller grains.

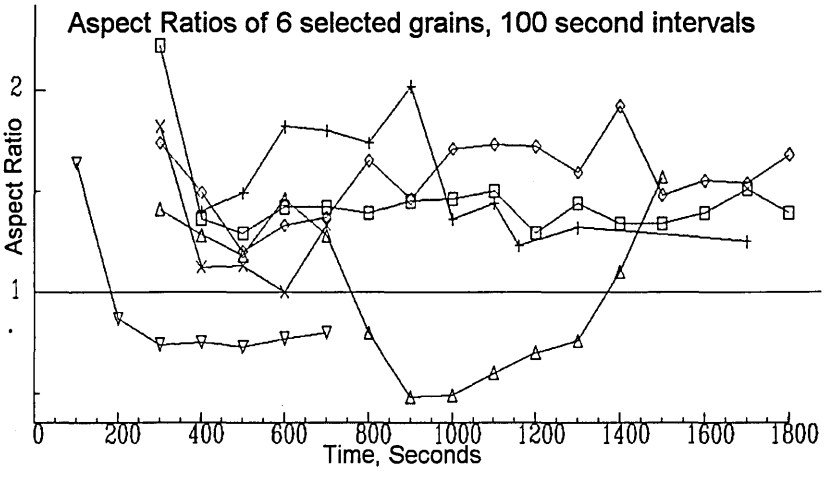

Fig 5. Aspect ratios. Measured as (L) –longest dimension : (W) –largest dimension at ≈90° to L. The large dimension closest in direction to the original L remains denoted as L, thus the ratio can fall below 1.0 over time.

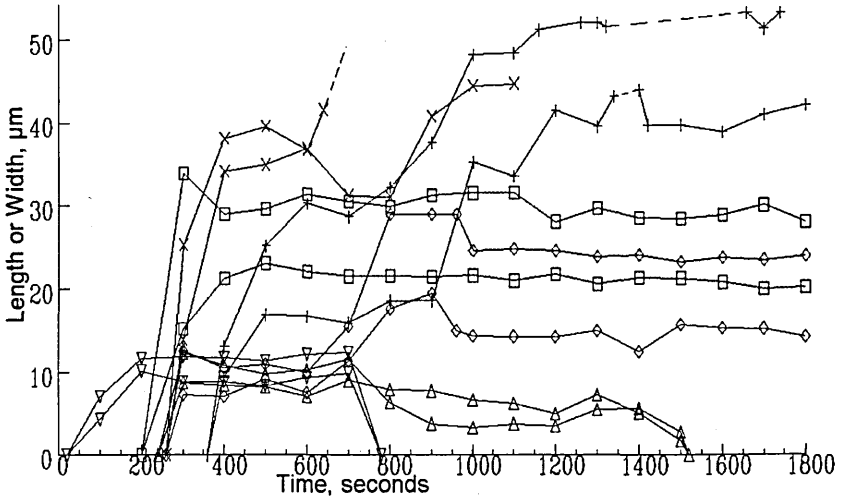

Fig 6. Length & Width of 6 grains monitored over time.

Figs 3-6 show highly discontinuous growth behaviour, a clear link between size and survival and that survival seems to correlate with a highly productive initial growth spurt. It is interesting to note that +, the largest crystallite at 1800sec is also the last to form, nucleated when the growth of X comes to a halt against a pre-existing grain (which + rapidly consumes between 0:28 and 0:38). It appears likely that +, X (and 0) are not truly separate grains, but a twin system (fig7). It is also interesting that of the monitored grains, σ, the first to form, is also the first to vanish.

Another notable behaviour is boundaries and triple points locally reversing their motion (reflected in negative slopes in the L and W values, e.g grain + in Fig 6). This rarely corresponds to a loss of grain area (figs 3,4) in which for instance + shows only very shallow negative slope segments.

As noted above, these figures yield qualitative information on grain behaviour, but little hard numerical data, other than successful crystallites tend towards an aspect ratio around 1:1.5. The inconsistent behaviour and sudden changes illustrated appear unpromising for simple mathematical analysis, though the situation may be better with a larger data set or a smaller time interval.

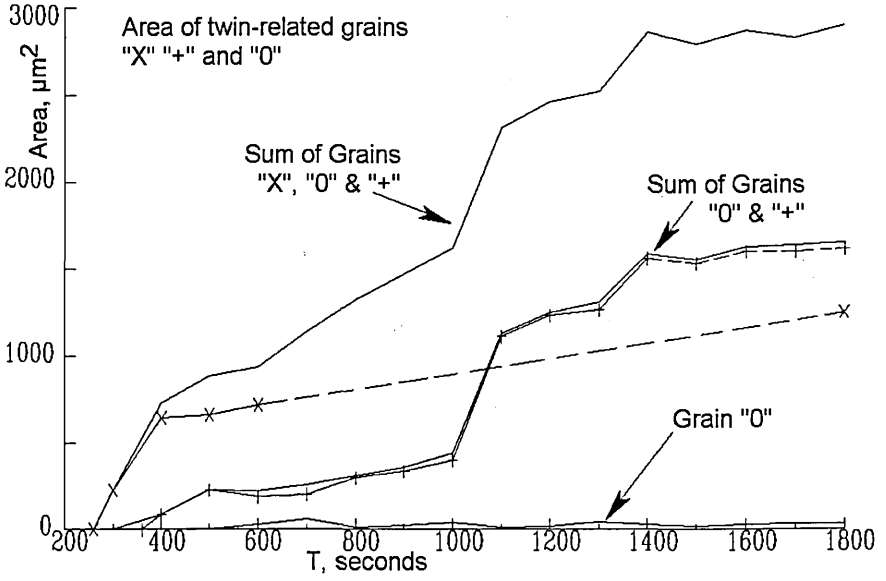

Fig 7. Grains X,+ and 0 analysed separately and as one. The significance of large twin-related grain areas (as opposed to needle shaped intrusions such as 0) and their treatment as separate grains (or not) is unclear.

Data Analysis – Points. The lower right triple point of X was tracked at 10sec intervals (0.5 sec video) across the field of view. When this point ceased to exist and neighbouring grain/twin, +, was nucleated, tracking continued with the corresponding point on that grain. This generated a stream of

2D co-ordinates relative to its starting point (arbitrarily (0,0)). The track is shown as Fig 8.

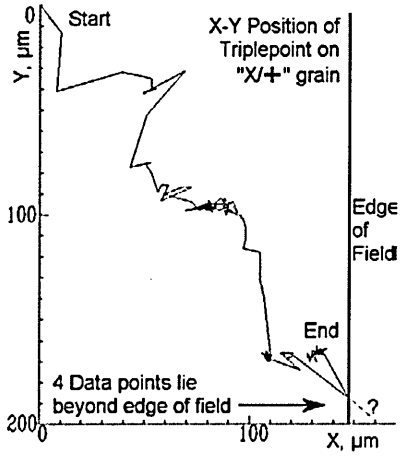

Fig 8. Track of triple point.

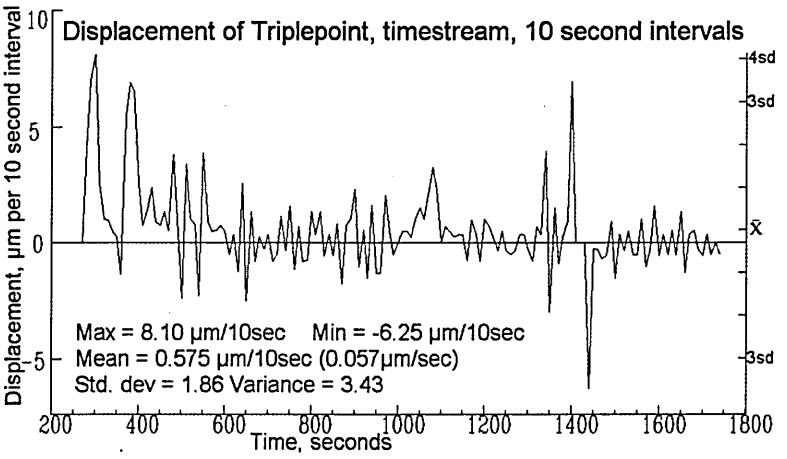

Fig 9. Triple point "speed" as timestream, with basic statistics.

The triple point positions shown in fig 8, clearly illustrate discontinuous motion, particularly in high speed initial movement, with 3 dense clumps of positions indicating the triple point dwelling in near-stability at one place for some considerable time. This behaviour is reflected in the "speed" timestream, fig 9. The "speed" is more properly the displacement of the point at 10 second intervals, roughly rendered into 1 dimensional motion from 2 dimensional motion, by reference to its overall x≈y trend. The calculation was a simple Pythagoras $\Delta s=\sqrt{(\Delta x^2+\Delta y^2)}$. This result was then assigned a sign, as follows. If Δx & Δy are positive, assign Δs positive. If Δx & Δy are negative, assign Δs negative. If $|\Delta x|>|\Delta y|$ assign Δs the sign of Δx. If $|\Delta y|>|\Delta x|$ assign Δs the sign of Δy. If $|\Delta x|=|\Delta y|$, assign Δs the sign of Δy. As the triple point makes very few major moves that are at or near 90° to the x=y direction, the approximation seems to work fairly well.

The statistics on Fig 9 show that, as expected from fig 8, the "speed" distribution does not fit a normal distribution. 4% of its data points lie outside ±3 s.d., an order of magnitude higher than expected if the distribution were Gaussian.

Phase Portrait. Fig 10 is a simple phase portrait [4,5] of the timestream data shown in Fig 8. This was constructed very simply by plotting $(s_1,s_2)(s_2,s_3)\ldots(s_{[n]},s_{[n+1]})$. This type of timestream analysis is capable of showing the presence (or absence) of periodic and quasi-periodic effects by their effect on the size and shape of the cloud of data points on the plot. A large quantity of data is often required, usually more than in this "speed" timestream.

This plot shows a compact and roughly circular centre to the data cloud, which most likely corresponds to normally distributed motion and errors in measurement when the triple point is stationary or slow moving. This distribution clearly has a standard deviation less than the calculated s.d. for the whole set (shown by the circles). Overlaying this compact distribution is a complex, diffuse distribution of data points,

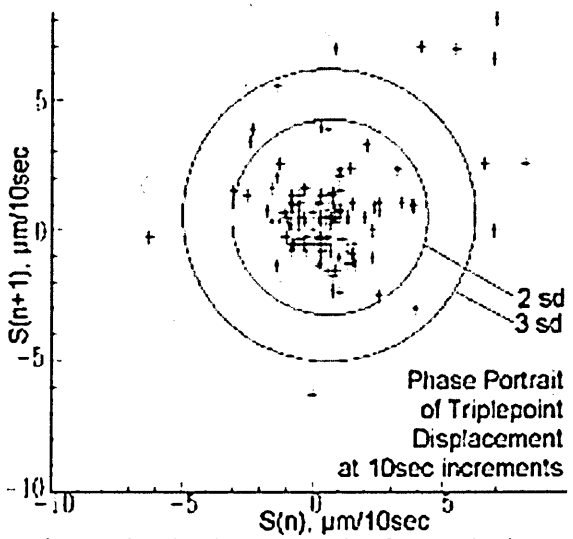

Fig10. Simple phase portrait of "speed" time stream, showing 2X & 3X standard deviation

corresponding to the large and rapid excursions of the triple point. With a much larger data set this distribution might yield some further insights into the kinetic behaviour of triple points.

The phase portrait and time stream do give some guidance for future experiment design. Clearly a larger data set is required, implying a longer experimental run, or hotter (more active grain growth) and with finer time resolution to generate more data points. The sharp spikes in the timestream suggest that a smaller time increment would probably be beneficial.

The central portion of the data cloud in the phase portrait is showing signs of dividing into a grid of points and of bunching at certain values ($\sqrt{2}$, $\sqrt{5}$, $\sqrt{10}$, $\sqrt{13}$ etc. corresponding to $\Delta x,\Delta y$ values of [1,1] [1,2] [1,3] [2,3] etc.). This indicates that the spatial measurement resolution at this magnification ($\approx$0.25μm per pixel) is just about adequate.

The trade offs to be made are obvious and invidious. Image resolution is limited by the NTSC video standard, thus it can be increased only by higher magnification. Higher magnification will give a shorter experimental run before features of interest move out of view, probably reducing the data gathered and dictating ultimately a trade of spatial resolution for time resolution/data volume.

Summary

The converter plate has delivered good qualitative insight into some of the processes of grain growth, but tools and techniques to easily extract volumes of quantitative data do not yet exist.

Video

A digital video file to accompany this paper will be at http://extra.shu.ac.uk/Fielden/REX-GG2

Acknowledgements

This work was supported by an EPSRC "Industrial CASE" award, sponsored by The Sheffield Universities' Materials Forum. The author wishes to thank Vikki Fielden for image processing, text tweaking and measuring co-ordinates of many triple points, Len Reynolds of Institute of Spring Technology for an introduction to phase portraits and timestream analysis and my PhD supervisors, particularly John Rodenburg and Jess Cawley, for their support and guidance.

References

[1] I.M. Fielden, J. Cawley, J.M. Rodenburg: *Backscattered SEM Imaging of High Temperature Samples for Grain Growth Studies in Metals.* **In** *Electron Microscopy and Analysis 2003: Proceedings of the Institute of Physics Electron Microscopy and Analysis Group Conference, 3-5 September 2003* (eds. S McVitie and D McComb) (IOP Publishing, Bristol 2004) p.181

[2] I.M. Fielden, J.M. Rodenburg: *A Technique for Real-Time, In-Situ SEM Observation of Grain Growth at Elevated Temperatures* (elsewhere in this conference proceeding)

[3] L. Reimer: *Scanning Electron Microscopy: Physics of Image Formation and Microanalysis* (2nd ed). (Springer-Verlag, Berlin 1998) p.188

[4] N. H. Packard, J. P. Crutchfield, J. D. Farmer, R. S. Shaw: *Geometry from a time series*. Phys. Rev. Lett. 1980 **45**: p.712

[5] F. Takens: *Detecting strange attractors in turbulence.* **In** *Dynamical systems and Turbulence,* (eds. D. A. Rand and L. S. Young) (Springer-Verlag, Berlin 1981) p.366

APPENDIX 4
VIDEO RESULTS
IN VARIOUS DIGITAL FORMATS

The videos referred to in the text are contained on the discs on this and the subsequent pages. The three videos are presented in a variety of file formats and on a variety of disc formats, to give future readers an improved chance of finding a format that remains usable. See the individual disc labels for details of their contents.

The three videos are
1 – Aluminium (rough edit)
2 – Steel (presentation version, grain growth & cooling transformation)
3 – Steel-full experiment (rough edit, several heat/cool cycles)

Each is presented in a variety of different digital formats. These differ only in the degree of data compression that has been applied. The largest sized file is of course the highest video quality and is the recommended version. Others are included for convenience and maximum compatibility.

It is recommended to copy the appropriate file to your computer before playing it, especially if using the large ".AVI" type files. This is because many CD drives cannot transfer data fast enough to give a smooth playback.